On the crosstalk between transmembrane and nucleotide binding domains of the ABC transport complex TAP

Dissertation
zur Erlangung des Doktorgrades
der Naturwissenschaften

vorgelegt beim Fachbereich
Biochemie, Chemie und Pharmazie
der Johann Wolfgang Goethe-Universität
in Frankfurt am Main

von
Giani Oancea
aus
Onesti, Rumänien

Frankfurt am Main, 2008

(D30)

vom Fachbereich Biochemie, Chemie und Pharmazie der

Johann Wolfgang Goethe-Universität als Dissertation angenommen.

Dekan: Prof. Dr. Dieter Steinhilber

1. Gutachter: Prof. Dr. Robert Tampé
2. Gutachter: Prof. Dr. Bernd Ludwig

Datum der Disputation: 2009-03-25

Teile der vorliegenden Arbeit wurden veröffentlicht in:

Herget M*, **Oancea G***, Schrodt S, Karas M, Tampé R, Abele R
Mechanism of substrate sensing and signal transmission within an ABC
transporter: use of a Trojan horse strategy.
J Biol Chem. 2007 Feb 9;282(6):3871-80.
* Both authors contributed equally to this work.

Oancea G, O'Mara M L, Bennett W F D, Tieleman D P, Abele R, Tampé R
Structural arrangement of the transmission interface in the ABC transporter TAP critical for
antigen binding and translocation.
PNAS 2009 Mar 18 [Epub ahead of print].

Deutsche Zusammenfassung

TAP („transporter associated with antigen processing") spielt eine zentrale Rolle in der MHC („major histocompatibility complex") I abhängigen Antigenprozessierung. Dabei transportiert TAP proteasomale Degradationsprodukte vom Zytosol ins Lumen des Endoplasmatischen Retikulums (ER). Dort werden die antigenen Peptide auf MHC I Moleküle geladen. Anschließend werden peptidbeladene-MHC Moleküle an die Zelloberfläche transportiert, um ihre antigene Fracht zytotoxischen T-Lymphozyten zu präsentieren. Erkennen diese zytotoxischen T-Zellen via dem T-Zellrezeptor virale oder onkogene Proteinfragmente, führt dies zur Elimination der virusinfizierten oder transformierten Zelle.

TAP gehört der Familie der ABC („ATP binding cassette") Transporter an, die die Energie der ATP Hydrolyse ausnutzen, um Substrate über Membrane zu transportieren. TAP bildet einen Heterodimer bestehend aus TAP1 und TAP2. Jede Untereinheit baut sich aus einer N-terminalen Transmembrandomäne (TMD) und einer C-terminalen Nukleotidbindungsdomäne (NBD) auf. Die TMDs bilden die Translokationspore und die Peptidbindungstasche. Die NBDs binden und hydrolysieren ATP, was den Peptidtransport über die Membran antreibt. Die Transmembrandomänen bestehen jeweils aus 10 Transmembranhelizes, wobei die sechs C-terminalen Transmembranhelizes in Kombination mit der Nukleotidbindungsdomäne jeder Untereinheit den Kernkomplex formen, welcher für den Peptidtransport ausreichend ist. Wie aus einem Homologiemodell von TAP basierend auf der Röntgenkristallstruktur des bakteriellen ABC-Exporters Sav1866 hervorgeht, sind die Transmembranhelizes auf der extrazellulären Seite durch kurze Schleifen–helikale α verbunden. Die zytosolischen Schleifen (CL) dagegen stellen Verlängerungen der Transmembranhelizes dar, die durch eine ca. 10 Aminosäure umfassende, parallel zur Membranebene liegende Kopplungshelix (CH) verbunden sind. Interessanterweise bilden diese CLs sowohl Kontakte mit der NBD der eigenen (*cis*-Interaktion) als auch mit der gegenüberliegenden Untereinheit (*trans*-Interaktion). In den NBDs sind vor allem der Q-Schleife wie auch der für ABC-Exporter einzigartige X-Schleife in diese Interdomäneninteraktion involviert. In biochemischen Studien konnte gezeigt werden, dass

I

die TMDs und NDBs während des Transportvorgangs in einer gekoppelten Art und Weise zusammenarbeiten.

Die zentrale Frage im ABC-Transporterfeld beschäftigt sich momentan damit, die Bedeutung dieser Interaktionsschnittstelle aufzuklären und strukturelle Änderungen dieser Schnittstelle im Verlauf des Transportvorgangs aufzuklären.

Die Ziele meiner Doktorarbeit waren (i) den Mechanismus zu entschlüsseln, wie die Anwesenheit von gebundenem Peptid in der Peptidbindungstasche an die NBDs übermittelt wird. (ii) Desweiteren sollte die Bedeutung dieser Transmissionsschnittstelle aufgeklärt werden und (iii) weiterhin strukturelle Veränderungen während des Transportzyklus untersucht werden.

Mit Hilfe eine kleinen, chemischen Protease kovalent an Peptidliganden von TAP gebunden, konnte eine bisher nicht beschriebene Interaktionsstelle detektiert werde. Um die physikalische Interaktion dieses in der CL1 von TAP1 gelegen Bereichs mit dem Peptid nachzuweisen, wurden durch gezielte Mutagenes einzelne Cysteine in cysteinloses TAP eingeführt und zusammen mit wt TAP2 mit dem Baculovirusexpressionssystem in Insektenzellen exprimiert. Die eingeführten Cysteine hatten keinen Einfluss auf die Faltung von TAP, da alle TAP-Varianten in vergleichbaren Mengen exprimiert wurden und die Peptidbindung durch diese Mutationen nicht beeinflusst wurde. Allerdings interferierten Cysteinsubstitutionen der am stärksten konservierten Aminosäurenreste in diesem Bereich (G282C, I284C und R287C) sehr stark mit dem Peptidtransport. Die Entkopplung zwischen Peptidbindung und Transport in diesen Mutanten legt nahe, dass diese Region in CL1 von TAP1 eine Art Transmitterfunktion einnimmt, indem sie den Beladungszustand der Peptidbindungstasche in der TMD an die NBD übermittelt. Die physikalische Nähe des Peptids zu diesem Transmitter konnte mittels oxidativer Quervernetzung von Cysteinen in dieser Region mit einem Cystein des gebunden Peptids nachgewiesen werden. Neben der Position 288 stehen allerdings schwächer die Positionen 284, 285 und 286 in TAP1 in Kontakt mit dem gebundenen Peptid. Durch Zugabe von ATP wird die Wechselwirkung mit der Position 285 unterbrochen, was auf eine strukturelle Flexibilität von TAP in diesem

Bereich hindeutet. Position 288 dagegen steht sowohl in Anwesenheit sowie in Abwesenheit von Nukleotiden (ATP, ADP, AMP-PNP, ATPγS) in Kontakt mit dem gebundenen Peptid. Allerdings ging diese Interaktion in Anwesenheit von ADP-AlFx, welches den Übergangszustand der Hydrolyse fixiert, verloren. Zusammenfassend zeigen diese Ergebnisse, dass der neu identifizierte Bereich als Peptidsensor wirkt, der sich im Verlauf des Transportzyklus strukturell reorganisiert und somit als Transmitter zwischen TMD und NBD fungiert.

Um den molekularen Aufbau des CL1 zu entschlüsseln, wurde ein minimal invasiver Ansatz gewählt, bei dem die Zugänglichkeit von einzel eingeführten Cysteinen in diesem Bereich mittels thiolspezifischer Fluoreszenzfarbstoffen mit unterschiedlicher Hydrophobizität analysiert wurde. Die N-terminalen Postionen von CL1 (Q277C, G282C, N283C und I284C) zeigten eine hohe Markierungseffizienz für den hydrophilen Farbstoff Iodacetamidofluorescein, den amphiphilen Farbstoff BODIPYmaleimid sowie den hydrophoben Fluoreszenzfarbstoff Coumarinmaleimid, sodass diese Region exponiert zu schein sein. Der C-terminale Bereich von CL1 dagegen (M285C, S286C, R287C und V288C) zeigte nur mit Coumarinmaleimid eine hohe Markierungseffizienz, was darauf hinweist, dass diese Seitenketten in einer hydrophoben Umgebung sich befinden.

Um auch kleinste strukturelle Änderungen der CL1 während des Transportvorgangs zu identifizieren, wurden Markierungskinetiken mittels BODIPYmaleimid im nukleotidfreien, im ATP gebundenen sowie im posthydrolytischen Zustand bestimmt. So ist zum Beispiel die Markierungsratenkonstante der Mutante I284C im nukleotidfreien Zustand 100-mal schneller als im ATP-gebundenen Zustand und 36-mal schneller als in Gegenwart von ADP. Betrachtet man die Ratenkonstante der Markierung, so konnten die CL1-Mutanten in vier Gruppen unterteilt werden:

i.   Seitenketten mit einer langsamen Markierungskinetik für alle getesteten Bedingungen (N283C, R287C, V288C)

ii.   Seitenketten mit eine schnelleren Markierungskinetik im nukleotidfreien Zustand als im ATP-gebundenen Zustand (I284C, M285C, S286C)

iii.   Seitenketten mit eine schnelleren Markierungskinetik in Gegenwart von ATP als im nukleotidfreien Zustand (G282C)

iv.   Seitenketten mit eine schnelleren Markierungskinetik im nukleotidfreien Zustand oder in Gegenwart von ADP als im ATP-gebundenen Zustand (Q277C)

Neben der Ratenkonstante wurden die einzelnen Mutanten auch nach der Markierungseffizienz klassifiziert, wobei diese nicht direkt mit den Ratenkonstanten korreliert:

i.   Seitenketten mit der höchsten Markierungseffizienz im ATP gebundenen Zustand (Q277C)

ii.   Seitenketten mit der höchsten Markierungseffizienz im ADP gebundenen Zustand (N283C, R287C, V288C)

iii.   Seitenketten mit der höchsten Markierungseffizienz im nukleotidfreien Zustand (G282C)

iv.   Seitenketten mit ähnlicher Markierungseffizienz in allen untersuchten Zuständen (I284C, M285C, S286C)

Die signifikanten nukleotidabhängigen Unterschiede sowohl der Markierungseffizienzen als auch der Markierungskinetiken belegen die Vermutung, dass die Struktur dieses Peptidsensor in CL1 in einer nukleotidabhängigen Art und Weise verändert wird. Somit ist CL1 sowohl an der Signaltransduktion von der TMD zur NBD als auch in die entgegengesetzte Richtung beteiligt.

Um den Effekt der Fluoreszenzmarkierung des CL1 in TAP1 auf die Funktionalität des Peptidtransportkomplexes zu adressieren, wurden alle Einzelcysteinmutanten mit

BODIPYmaleimid markiert. Während alle Mutanten eine reduzierte Transportaktivität durch die Fluorophormarkierung aufwiesen, blieb die Peptidbindung unverändert. Somit entkoppelte diese kovalente Modifikation die Peptidbindung vom Transport, indem die Signalübertragung zwischen TMD und NBD gestört wurde.

Um die Funktion dieser Transmissionsschnittstelle weiter zu studieren und die Bedeutung der *trans*-Interaktion in einem heterodimeren ABC-Halbtransporter zu untersuchen, wurde das konserviert Glutamat im X-Schleife von TAP2 durch verschiedene Aminosäuren ersetzt. Da all diese X-Schleife Mutanten keinen Einfluss auf die Peptidbindung hatten, ist dieser Bereich in TAP2 weder für die Membraninsertion noch für die Heterodimerisierung von Bedeutung. Allerdings zeigten alle Mutanten eine verringerte Transportaktivität. TAP Komplex mit der E602C Variante wiesen eine um 50% verringerte Transportrate auf. Mutationen zu Aspartat oder Alanin reduzierten den Transport um 80% und die Einführung eines Arginins an Position 602 führt zum völligen Verlust des Peptidtransports. Daraus geht hervor, dass dem hoch konservierte Glutamat des X-Schleifen eine Schlüsselrolle in der Translokation zukommt, ohne einen Einfluss auf die Peptidbindung zu haben.

Um Seitenketten in TAP1 zu identifizieren, welche mit dem X-Schleife in TAP2 in *trans* interagieren, wurden mit Hilfe des Homologiemodells des Kern-TAP-Komplexes 24 Aminosäuren in CL1 und CL2 von TAP1 identifiziert, die E602 in TAP2 umgeben. All diese Einzelcysteinmutanten von TAP1 wurden zusammen mit der E602C Mutante von TAP2 exprimiert. Keine der CL1-Mutationen beeinflussten die Peptidbindung. Dagegen interferierten alle CL1-Mutanten ausser Q277C mit dem Peptidtransport. In CL2 ergab sich allerdings ein ganz anderes Bild. Nur die R378C Substitution verringerte signifikant Peptidbindung und in Folge dessen Peptidtransporter. Zusätzlich hatte die Mutation P375C einen staken negativen Effekt auf den Peptidtransport ohne jedoch die Peptidbindung zu beeinträchtigen. Daraus kann geschlossen werden, dass CL2 nur eine geringe Bedeutung für die Signaltransduktion zwischen TMD und NBD hat.

Zur Verifizierung der aus röntgenkristallographischen Strukturen vorhergesagten *trans*-Interaktion zwischen zytosolischen Schleifen und dem X-Schleife in der NBD, wurden mit Hilfe der Cysteinmutanten Quervernetzungsexperimente durchgeführt. Dabei zeigte sich, dass CL1 sowie CL2 von TAP1 mit dem X-Schleife in TAP2 interagieren und damit auch in einem heterodimeren ABC-Exporter eine *trans*-Interaktion zwischen TMD und NBD besteht. Die Quervernetzung zwischen CL2 und dem X-Schleife arretiert TAP in einer Konformation, in der Peptide nicht mehr binden können. Die Quervernetzung zwischen CL1 und dem X-Schleife dagegen beeinträchtigt die Peptidbindung nicht, sondern inhibiert ausschließlich den Transport. Diese Fixierung verhindert somit strukturelle Änderungen im TAP Komplex, sodass die Kommunikation zwischen den Domänen verhindert wird.

Basierend auf diesen Ergebnissen kann festgestellt werden, dass das Zusammenspiel der TMDs und NBDs in TAP ein hoch komplexer und dynamischer Prozeß darstellt. Eingeleitet durch die Peptidbindung, welche mittels des Peptidsensors an die NBD signalisiert wird, kommt es in Gegenwart von ATP zur Dimerisierung der NBDs. Diese Dimerisierung löst weitere konformationelle Änderungen in den TMDs aus, wodurch es zur Peptidtranslokation kommen kann. Durch die ATP-Hydrolyse wird der Transporter wieder in den Grundzustand versetzt. Den zytosolischen Schleifen (CL1 und CL2) kommt dabei eine zentrale Rolle in der Signalübertragung zwischen den Domänen zu. Desweiteren sind sie auch an der Peptidbindung und Qualtitätskontrolle beteiligt.

Summary

By translocating proteasomal degradation products into the endoplasmic reticulum (ER) for loading of major histocompatibility complex (MHC) class I molecules, the ATP binding cassette (ABC) transporter associated with antigen processing (TAP) plays a pivotal role in the adaptive immunity against infected or malignantly transformed cells. A key question regarding the transport mechanism is how the inter-domain communication and conformational dynamics of the TAP complex are connected during the peptide transport.

To identify residues involved in this processes, we evolved a Trojan horse strategy in which a small artificial protease is inserted into antigenic epitopes. After binding, the TAP backbone in contact is cleaved, allowing the peptide sensor site to be mapped by mass spectrometry. Within this study, the peptide sensor and transmission interface have been identified. This region aligns with the cytosolic loop 1 (CL1) of Sav1866 and MsbA. Based on a number of experimental data and the homology to the bacterial ABC exporter Sav1866, we constructed a 3D structural model of the core TAP complex. According to this model, the CL1 and CL2 of TAP1 are extended cytosolic loops connecting the transmembrane helices (TMH) 2 and 3, and TMH4 and 5 respectively, and contact both nucleotide binding domains (NBDs) of the opposite subunit. In contrast to exporters, the cytosolic loop (named L-loop) of BtuCD importer is much shorter, and contacts only one NBD.

The data confirm that the CL1 of TAP1 functions as signal transducer in ABC exporters, because it does not interfere with substrate binding but with substrate transport. The peptide contact site identified herein is restructured during the ATP hydrolysis cycle. Importantly, TAP showed a structural change trapped in the ATP hydrolysis transition state, because direct contact between peptide and CL1 is abolished. By cysteine scanning, the most conserved residues within CL1 were identified, which disrupted the tight coupling between peptide binding and transport. Together with Val-288, these residues are essential in sensing the bound peptide and inter-domain signal transmission.

To characterize the molecular architecture of CL1, a convenient and minimally perturbing approach was used, which combined cysteine substitution in the CL1 region and determination of accessibility to thiol specific compounds with different properties. These studies revealed that the N-terminal region of CL1 has a good accessibility for hydrophilic (iodoacetamidofluorescein, IAF) and amphiphilic probes (BODIPY maleimide, BM), whereas

the C-terminal region is accessible for hydrophobic probe (coumarin maleimide, CM). Kinetic studies of fluorescence labeling suggest that this region displayed a different accessibility to probes when the protein undergoes distinct conformations (e. g. nucleotide free state), thereby reflecting conformational transitions. Fluorescence labeling with BM induces a lost of peptide transport, whereas the peptide binding remains unaffected. These results indicate that covalent modifications of the CL1 residues influenced the inter-domain communication between transmembrane domain (TMD) and NBD.

The X-loop is a recently discovered motif in the NBD of ABC exporters, which stays in close contact to the CLs. Moreover, because the X-loop precedes the ABC signature motif, it probably responds to ATP binding and hydrolysis and may transmit conformational changes to the CLs. By substitution of the highly conserved Glu-602 of TAP2 with residues that have different chemical properties, it was shown for the first time that the X-loop is a functional important element, which plays an key role in coupling substrate binding to downstream events in the transport cycle. We further verified domain swapping in the TAP complex by cysteine cross-linking. The TAP complex can be reversibly arrested either in a binding or translocation incompetent state by cross-linking of the X-loop to CL1 or CL2, respectively. These results resolve the structural arrangement of the transmission interface and point to different functions of the cytosolic loops in substrate recognition, signaling and transport.

Contents

List of Figures

List of Tables

1.   Introduction

1.1   MHC class I antigen presentation pathway

Higher eukaryotic organisms must defend themselves against invaders and malignant cells to survive. Therefore, the adaptive immune system has evolved to protect the organism against pathogens. The adaptive immune system, developed in jawed vertebrates, allows for specific recognition and elimination of antigens that are abundant in body fluids or within cells (Flajnik and Kasahara, 2001). The recognition and elimination of mutated or infected cells are performed by the cellular immune system, which can be subdivided into the class I major histocompatibility complex (MHC) and the class II MHC pathways. MHC class I molecules are present on the surface of nearly all nucleated cells, whereas class II molecules are restricted to the cells of the immune system, such as dendritic cells, macrophages and B-cells.

A main task of the MHC class I-dependent pathway of antigen processing is the selection of highly abundant and high-affinity peptides for MHC class I loading and presentation to the immune system. Endogenous proteins are constantly degraded by the 20S/26S proteasome, a multicatalytic protease complex in the cytosol (Rock *et al.,* 1994; Coux *et al.,* 1996; Baumeister *et al.,* 1998; Früh and Yang, 1999; York *et al.,* 1999). The contribution of the 20S proteasome for the generation of antigenic peptides is further strengthened by the observation that proteasomal subunits, LMP2 and LMP7 (low-molecular-mass polypeptides), are encoded within the MHC locus (Brown *et al.,* 1991; Glynne *et al.,* 1991; Martinez and Monaco, 1991). The catalytic core of the proteasome is a 20S (700 kDa) cylindrical particle composed of 28 subunits arranged in four heptameric rings. The outer rings are made up of seven α-subunits; the inner rings are composed of seven β-subunits. Whereas the α-subunits are thought to be primarily responsible for structural and regulatory functions, the β-subunits harbor the catalytic centers (Fenteany *et al.,* 1995; Löwe *et al.,* 1995; Seemüller *et al.,* 1995). Another form of the proteasome is the 26S (1.500 kDa) particle. It contains the 20S complex and additional subunits associated with regulation of its activity (Rechsteiner *et al.,* 1993; Peters*,* 1994). The proteasome produces peptides with a size distribution of 3-30 residues with an optimum of 6-11 residues (Ehring *et al.,* 1996; Kisselev *et al.,* 1999). This size corresponds in part to the size of antigenic peptides bound to MHC class I molecules. During interferon (IFN)-γ stimulation, the three active proteasomal β-subunits are replaced by LMP2 and LMP7 subunits to build up a so-called

1

"immunoproteasome" (Rock and Goldberg, 1999). Immunoproteasomes show a different cleavage pattern compared with the proteasomes, thereby generating more peptides with hydrophobic and basic C-termini (Rock and Goldberg, 1999), both of them are favored for uptake by transporter associated with antigen processing (TAP) into the endoplasmic reticulum (ER) and for optimal binding to MHC class I molecules (Buttgereit and Tampé, 2002). About one-third of newly synthesized proteins are rapidly degraded by proteasomes under physiological conditions (Schubert *et al.,* 2000; Turner and Varshavski, 2000). However, peptides are also generated, at least in part, by other proteases, such as the IFN-γ-inducible leucine aminopeptidase (Beninga *et al.,* 1998) or a giant cytosolic protease system, the tripeptidyl peptidase II (Glas *et al.,* 1998; Geier *et al.,* 1999). In addition, the remaining peptides are processed by cytosolic peptidases like the two aminopeptidases puromycin-sensitive aminopeptidase and bleomycin hydrolase (Stoltze *et al.,* 2000). Below the length of 15 amino acids, peptides are exclusively trimmed by tripeptidyl peptidase II, which displays both exo- and endopeptidase activity (Reits *et al.,* 2004), and are subsequently translocated into the ER lumen by TAP. After further trimming of the peptides by the ER-luminal aminopeptidases 1 and 2 (Saric *et al.,* 2002; Serwold *et al.,* 2002; Saveanu *et al.,* 2005) to a length of 8-11 residues (Falk *et al.,* 1991; York *et al.,* 2002), they are loaded onto MHC class I molecules, a complicated and tightly regulated process, which requires a macromolecular peptide-loading complex (PLC) comprised of TAP1, TAP2, tapasin, MHC class I heavy chain, β_2-microglobulin, calreticulin, and ERp57 (Ortmann *et al.,* 1997; Antoniou *et al.,* 2002). Following peptide binding, MHC-peptide complexes are released from the PLC and shuttled via the Golgi apparatus to the cell surface where they are scanned by cytotoxic T lymphocytes (CTL), which may trigger an adaptive immune response (Figure 1-1).

The chronic presentation of self-protein-derived peptides does not lead to a stimulation of T cells. During the development of the thymus, self-reactive T-cells are deleted. In case of malignant transformation or viral infection of the cells, an additional set of peptides is presented to the CTL. The intracellular pathways leading to the generation of peptides, their binding to MHC molecules, and presentation on the cell surface are called antigen processing and presentation (Buttgereit and Tampé, 2002). The recognition of MHC class I molecules as "self component" loaded with peptides from "non-self" proteins by CTL leads to apoptosis or lysis of malignant or infected cells. This is an essential process of the cellular immune response. The pathway of antigen presentation by the MHC class I complex is constitutively active in all nucleated cells and is upregulated by inflammatory cytokines. Interference with

this pathway has evolved as an effective strategy for pathogens to evade immune response, leading to chronic or latent infections.
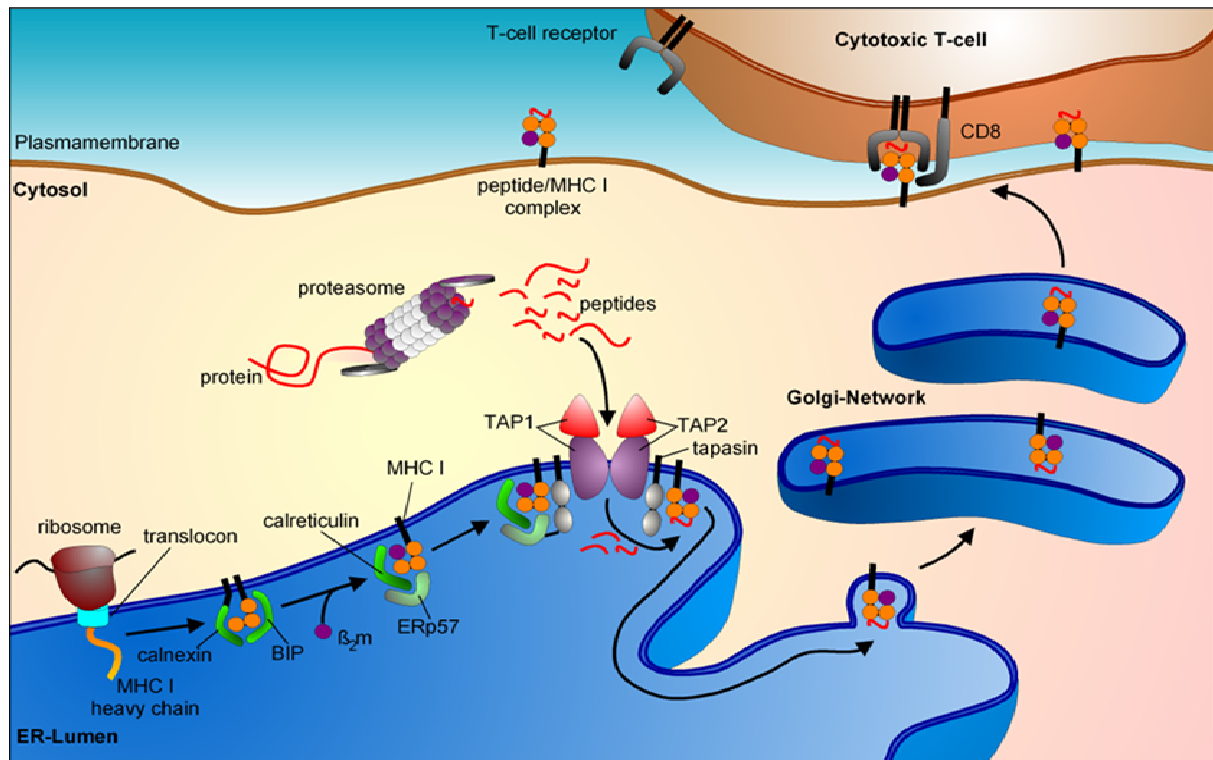
Figure 1-1. Antigen presentation pathway via MHC class I molecules.
The MHC I heavy chain is co-translationally translocated into the ER, where it folds and assembles with β_2-microglobulin assisted by the immunoglobulin binding protein (BiP) and calnexin. Subsequently, MHC class I molecules are recruited into a macromolecular peptide-loading complex (PLC) composed of calreticulin, ERp57, tapasin, TAP1 and TAP2. Peptides derived mainly by proteasomal degradation in the cytosol are translocated by TAP into the lumen of the ER, where they are loaded onto pre-assembled MHC class I molecules. Kinetically stable peptide-MHC complexes can escape the ER quality control and are transported via the Golgi to the cell surface. Binding of T-cell receptor and CD8 co-receptor to trimeric MHC class I molecules triggers the killing of the target cell (adapted from Schölz and Tampé, 2005).

TAP translocates peptides generated by the proteasome complex from the cytosol into the lumen of the ER. In the ER, peptides are loaded onto the newly synthesized MHC class I molecules. Deletion or mutation of TAP severely affects the translocation of peptides into the ER (Chen *et al.,* 1996; Seliger *et al.,* 2000; Seliger *et al.,* 2001; Yang *et al.,* 2003). Because binding of peptides stabilizes the MHC complex and induces subsequent export to the cell surface for presentation to T-cell receptors (Figure 1-1), any defect, which impairs the transport of peptides, results in reduced surface expression of MHC class I molecules. Despite the physical association of TAP and the MHC class I molecules, it was shown by inhibition of binding in cytosol after anti-peptide antibody application that possibly most TAP-transported peptides diffuse through the lumen of the ER before being loaded onto MHC class I molecules (Hilton *et al.,* 2001). The stable binding of peptides to class I heterodimers releases

the loaded MHC class I molecules from the assembly complex for transport to the cell surface via the Golgi apparatus and the *trans*-Golgi network.

1.2   Overview of ABC transporters

1.2.1   ABC transporters are ubiquitous and clinically important

ATP binding cassette (ABC) transporters are a large superfamily of integral membrane proteins that carry diverse substrates across cellular membranes. They are present in all organisms and contribute to various human diseases and to multidrug resistance in cancer cells. In bacteria, they catalyse the uptake of essential nutrients or the extrusion of, among others, toxic substances, thus contributing to drug and antibiotic resistance of pathogenic microbes (Holland *et al*., 2003). The human ABC transporters are classified by sequence homology into seven subfamilies, designated ABCA to ABCG (Dean *et al.,* 2001).

There are 48 ABC proteins in humans and mutations in many are at the root of genetic disorders including a bleeding disorder (Albrecht *et al*., 2005) and a number of eye (Martinez-Mir *et al*., 1998) and liver diseases (Jacquemin, 2000), all of which are caused by the failure to export a specific ligand across a lipid bilayer, as well as autoimmune diseases caused by genetic TAP defects (Table 1-1; Johnsen *et al.,* 1999; Dean *et al*., 2001; Holland *et al*., 2003). The normal function of some human ABC transporters is to secrete cytotoxic compounds (dietary cytotoxics and therapeutic drugs). These transporters (P-glycoprotein, BCRP, and MRP1) are highly expressed in the gut, liver and kidneys where they restrict the bioavailability of administred drugs. P-glycoprotein and BCRP in particular are also expressed in the epithelia of sensitive tissues (for example, the brain and placenta (Schinkel *et al.*, 1995; Jonker *et al*., 2000) and in stem cells (Zhou *et al*., 2001), where they perform a barrier function (Sarkadi *et al*., 2006). There are also a few atypical ABC proteins, which do not transport substrates, but they are either a channel for chloride ions such as the cystic fibrosis transmembrane regulator (CFTR; Tabcharani *et al.,* 1991), or function as a regulator of a potassium channel such as sulphonyl urea receptor (SUR; Inagaki *et al.,* 1995). Other atypical ABC proteins, which do not have transmembrane subunits, are involved in chromatin organization (Hirano, 2006), DNA repair, telomere maintenance (Hopfner *et al.,* 2000; Obmolova *et al.,* 2000), and mRNA trafficking through the nuclear pore (Kozak *et al.,* 2002).

Table 1-1. Clinically relevant and atypical ABC proteins (Linton, 2007).

ABC Protein	Pseudonym	Ligand(s)/Function	Associated Disease(s)
ABC1	ABCA1	Cholesterol	Tangier disease
ABCR	ABCA4	Retinal	Various eye diseases
TAP1/2	ABCB2/B3	Peptides	Autoimmune diseases
ABC7	ABCB7	Iron	Anemia and XLSA
MRP6	ABCC6	?	Pseudoxanthoma elasticum
ALD	ABCD1	vlcFA	Adrenoleukodystrophy
Sterolin1/2	ABCG5/G8	Sterols	Sitosterolemia
PGY3/MDR3	ABCB4	Phosphatidylcholine	Liver disease: PFIC3, OC
BSEP/SPGP	ABCB11	Bile acids	Liver disease: PFIC2
MRP2	ABCC2	Conjugated bilirubin	Liver disease: D-J syndrome
MDR1	ABCB1	Hydrophobic drugs	Failure of chemotherapy
BCRP/MXR	ABCG2	Hydrophobic drugs	
MRP1	ABCC1	Conjugated drugs	
MRP4	ABCC4	Conjugated nucleosides	
		Atypical ABC proteins	
CFTR	ABCC7	Chloride ion channel	Cystic fibrosis
SUR	ABCC8	Regulation of K_{IR} channel	PHHI
SMC1-6		Chromosome maintenance	
RAD50		DNA, telomere repair	
Elf1p		mRNA trafficking	

XLSA, X-linked sideroblastomic anemia; PFIC, progressive familial intrahepatic cholestasis; OC, obstetric cholestasis; D-J, Dubin-Johnson syndrome; PHHI, persistent hyperinsulinemic hypoglycemia of infancy.

1.2.2   Architecture of ABC proteins

ABC transporters share a basic domain organization (Figure 1-2). Two transmembrane domains (TMDs) provide a passageway for the substrate, while two cytoplasmic nucleotide binding domains (NBDs) bind and hydrolyze ATP, providing the energy needed for active transport (Higgins, 1992). In ABC importers, TMDs and NBDs are produced as separate polypeptide chains, whereas in bacterial exporters, one TMD is fused to a NBD, generating a "half-transporter" that can form a homodimer or a heterodimer to generate the complete, functional ABC transporter. Many eukaryotic ABC exporters are "full-transporters" that feature all four domains in a single polypeptide chain. Archaea and bacteria contain importers and exporters, whereas eukaryotes contain only exporters (Beismann-Driemeyer and Tampé, 2004). Crystal structures of numerous cytoplasmic NBDs have been determined at high resolution and have provided insight into the ATP hydrolysis mechanism (for review see

Davidson and Chen, 2004). However, direct visualization of transmembrane domains is required to understand key features such as substrate acquisition and translocation. A key problem in obtaining high-resolution structures of full transporters consists of difficulties in producing, purifying and crystallizing dynamic membrane proteins. Crystal structures of seven complete ABC transporters have recently been determined, providing the molecular basis for understanding the transport reaction. Five of the structures are of ABC importers: the vitamin B12 transporter BtuCD from *Escherichia coli* (Locher *et al.,* 2002), the putative metal-chelate transporter HI1470/71 from *Haemophilus influenzae* (Pinkett *et al.,* 2007), the molybdate/tungstate transporter ModBC from *Archaeoglobus fulgidus*, determined in complex with its cognate-binding protein ModA (Hollenstein *et al.,* 2007), the maltose transporter MalFGK$_2$ from *Escherichia coli* determined in complex with the maltose-binding protein, maltose and ATP (Oldham *et al.,* 2007), and the methionine transporter MetNI from *Escherichia coli* (Kadaba *et al.,* 2008). Currently there are four structures of ABC exporters: the Sav1866 protein from *Staphylococcus aureus,* determined in ATP-bound state (Dawson and Locher, 2006), and the MsbA from *Escherichia coli*, *Vibrio cholerae* and *Salmonella typhimurium* trapped in different conformations, two nucleotide bound structures and two in the absence of nucleotide (Ward *et al*., 2007). Analyzing the basic architectural features of ABC transporters as revealed by these recent structures and the large amount of biochemical and functional data obtained so far, a conserved engine and transmission machinery common to all ABC transporters has been suggested. According to this model a molecular mechanism has been proposed by which binding of ATP flips the TMDs of ABC transporters into an outward-facing conformation, whereas dissociation of the hydrolysis products ADP and phosphate returns them to an inward-facing conformation (Dawson *et al.,* 2007).
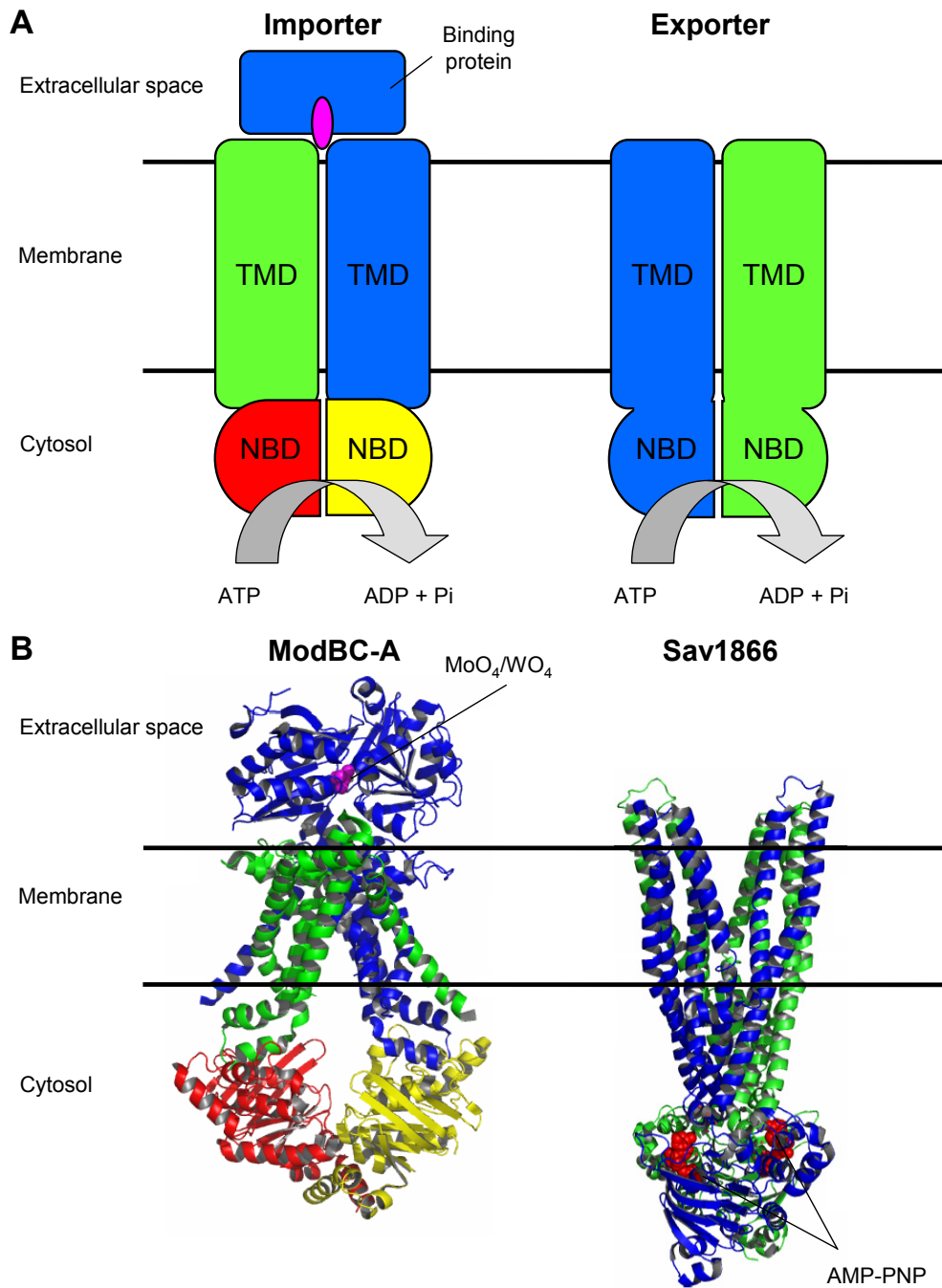
Figure 1-2. Domain organization and structure of two bacterial transporters.
(A) Schematic representation of domain organization. Both, ABC importers and exporters contain two TMDs and two NBDs. In importers, these are separate subunits, whereas the ABC transporters of eukaryotes are built up of either one (TMD-NBD)$_2$ fusion protein ("full-length transporters") or two TMD-NBD fusion proteins ("half transporters"). (B) Structures of ModBC-A and Sav1866. The ABC importer ModBC (left; PDB Accession Number: 2ONK) consists of two copies of the ModB subunit (TMD) and two copies of the ModC subunit (NBD), whereas the ABC exporter Sav1866 (right; Accession Number: 2HYD) is a homodimer with the stoichiometry (Sav1866)$_2$. Note that the TMDs of Sav1866 extend significantly into the cytoplasmic space, which is not observed for importers. ABC importers such as ModBC require an external binding protein (in this case ModA) that captures the transport substrate and delivers it to ModBC. ModBC-A and Sav1866 have been crystallized in distinct functional states: whereas ModBC-A was visualized in the nucleotide-free state, the structure of Sav1866 reflects the ATP-bound state. The nucleotide-free state of ModBC-A is coupled to an inward-facing conformation of the TMDs, whereas the ATP-bound state of Sav1866 is coupled to an outward-facing conformation. These two conformations are likely to be present in all ABC transporters and provide the structural basis of ATP-driven, unidirectional substrate transport (Dawson *et al.,* 2007).

7

1.2.3   Harnessing the power of ATP: structure and arrangement of the NBDs

The NBDs are the motor domains of ABC transporters. They are highly conserved, sharing over 25% sequence homology irrespective of whether the sequence is of prokaryotic or eukaryotic origin. They convert the chemical energy of ATP hydrolysis into mechanical work, which is realized in conformational changes within the TMDs. The NBDs are between 200 and 300 amino acids in length and contain a number of characteristic motifs found in all ABC proteins. The most prominent motifs are the Walker A and B motifs as well as the C loop (ABC signature). The Walker A motif has the consensus sequence GxxGxGKS/T (x = any amino acid) and the Walker B motif the consensus sequence $\varphi\varphi\varphi\varphi D$ (φ = any hydrophobic amino acid). Walker A and B motifs are 5-9 amino acid long and are separated from each other by 90-120 amino acids (Walker *et al.,* 1982). The C-loop is located between the Walker A and B motifs and has the consensus sequence LSGGQ. In contrast to the Walker A and B motifs, which are also present in other ATP- and GTP-binding proteins, the C-loop is exclusively found in ABC proteins, though trimeric G proteins contain a related motif (GGQR/K/Q) (Manavalan *et al.,* 1995). Other conserved amino acids and motifs present in NBDs include the glutamate residue C-terminal to the Walker B motif which acts as the general or catalytic base (Moody *et al.,* 2002; Smith *et al.,* 2002), the Q-loop which contains a conserved glutamine that contacts the γ-phosphate of ATP via a water molecule (Hung *et al.,* 1998), the Pro-loop which contains a conserved proline and together with Q-loop connects the arm I and arm II of the NBDs (Schmitt *et al.,* 2003), as well as the D-, H-, and X-loop (Figure 1-3). The D-loop is located within the NBD-NBD dimer interface, has the consensus sequence SALD, and interacts with the highly conserved histidine of the H-loop at the dimer interface providing an explanation of the mechanism for communication between monomers (Smith *et al.,* 2002; Chen *et al.,* 2003; Zaitseva *et al.,* 2005). The highly conserved histidine of the H-loop not only participates in ATP hydrolysis, but also forms essential hydrogen bonds in the so-called catalytic diad together with the conserved glutamate (Zaitseva *et al.,* 2005). The X-loop, which contains a short sequence TEVGERG conserved in ABC export proteins only, has an apparent function in communication between the intracellular loops of the TMDs with the NBDs (Dawson and Locher, 2006).

All NBDs adopt a similar fold that consists of two subdomains (arms). Arm I (catalytic domain) is an F1-ATPase-like domain and contains the Walker A and B motifs. The α-helical arm II (signaling domain), which is specific for ABC proteins, is thought to act as the signaling domain. Arm II lies perpendicular to the catalytic arm I and contains the Q-, X-,

and C-loop (Abele and Tampé, 2004). The hinge region connecting arm I and arm II is located between the Q-loop and the Pro-loop (Hung *et al.,* 1998; Schmitt *et al.,* 2003). Both, their general fold and the arrangement of the NBDs in ABC transporters are conserved. The arrangement is called "head-to-tail" or "Rad50-like" after the structure of the Rad50 protein in which it was first visualized (Hopfner *et al.,* 2000). The key feature is that the two NBDs present their conserved sequence motifs at the shared interface. Within an NBD-NBD dimer, two ATP molecules are bound. The binding of a single ATP molecule is mainly accomplished by residues from the Walker A and Walker B motifs, the Q-loop, and the H-loop of one NBD and of residues from the C-loop of the second NBD (Figure 1-3B). Since the ATPase site of each NBD is complemented by residues from the second NBD within an NBD dimer, the function of the second NBD is to shield the nucleotide from the solvent and to fix the γ-phosphate of the ATP (Beismann-Driemeyer and Tampé, 2004). The counterion of ATP (usually Mg^{2+}, Na^{+} in the MJ0796 (E171Q) mutant) interacts with the conserved S/T residue from the Walker A motif, the Q-loop glutamine, and the β- and γ-phosphates of ATP. These interactions are proposed to help tether the two NBDs together (Smith *et al.,* 2002).
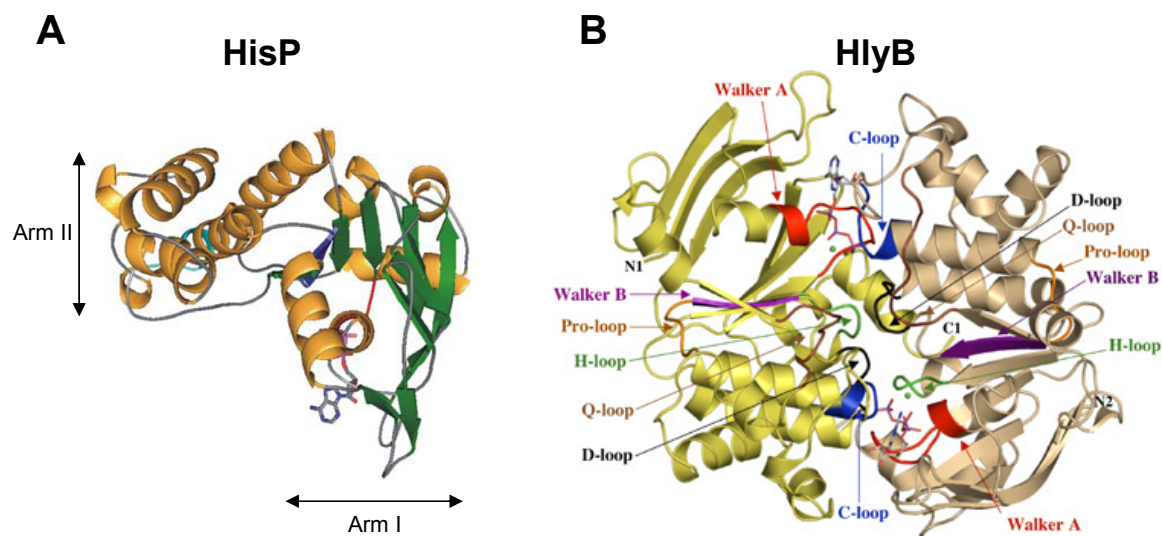
Figure 1-3. Structures of nucleotide binding domain of ABC transporters.
(A) Structure of HisP monomer (Hung *et al.,* 1998). The arm I contains the Walker A and Walker B motifs. Arm II contains mainly α-helices. α-helices are shown in orange and β-sheets in green. The location of conserved motifs are indicated by different colors: red (Walker A), blue (Walker B), cyan (C-loop). The bound ATP is in ball and stick representation. (B) Crystal structure of the HlyB-NBD H622A dimer with bound ATP/Mg^{2+} (Zaitseva *et al.,* 2005). ATP in stick representation and Mg^{2+} (green spheres) are sandwiched at the interface of the two HlyB-NBD monomers (shown in light tan and light yellow). N- and C-termini of the individual monomers are labeled. Conserved motifs are colored red (Walker A), brown (Q-loop), bleu (C-loop or ABC signature motif), magenta (Walker B), black (D-loop), and green (H-loop) and labeled accordingly.

The structures of the ATP-bound state of isolated NBDs and the NBDs of Sav1866 are very similar in structure and, indeed, show two ATP molecules (or non-hydrolysable analogues) sandwiched between the NBDs (Smith *et al.,* 2002; Zaitseva *et al.,* 2005; Dawson and Locher, 2006). Unlike the ATP-bound state, the nucleotide-free state seems to impose less stringent constraints on the NBDs. Common to the nucleotide-free structures is a substantial separation of the key motifs, leaving a gap that was also observed in the isolated NBD dimer (MalK subunits) from the maltose transporter (Chen *et al.,* 2003). Due to the high conservation of the NBDs of ABC transporters it is very likely that the mechanism of hydrolysis is similar in all ABC proteins. The catalytic cycle for ATP hydrolysis shown in Figure 1-4 represents a 'dual-mode' mechanism and is divided into distinct steps that involve different conserved sequence motifs as key players, acting to coordinate intramolecular movements (Zaitseva *et al.,* 2006).

(i)   In the first step ATP binding induces NBDs dimerization;

(ii)   In the next step a rigid-body movement of the helical domain, employing the Q- and Pro-loop as hinges, occurs;

(iii)   These conformational changes are transmitted to the TMDs and result in a rearrangement of the membrane helices. The dimer is formed, and this results in full displacement of the substrate binding site to the periplasmic site. For exporters, the substrate is now released, and for importers this results in opening of the binding protein, and binding of the substrate to the binding site in the TMDs.

(iv)   Hydrolysis of ATP destabilizes the dimer interface, and leads to dissociation of the dimer and TMDs rearrangement. This results in return of the transporter to its resting state.

For the importers the substrate is now transported to the other side of the membrane. Depending on the stability of the dimer after hydrolysis of the first ATP, the dimer can either dissociate immediately, or a second ATP molecule needs to be hydrolyzed to completely destabilize the dimer (van der Does and Tampé, 2004). In this model, one can assign distinct functions to the conserved motifs of NBDs: the Walker A and B motifs, as well as the ABC signature, the catalytic glutamate and H-loops are required for ATP binding and hydrolysis, whereas the Pro-, Q- and D-loops act as hinges and are likely central to NBD-NBD and NBD-TMD communication (Zaitseva *et al.,* 2006).
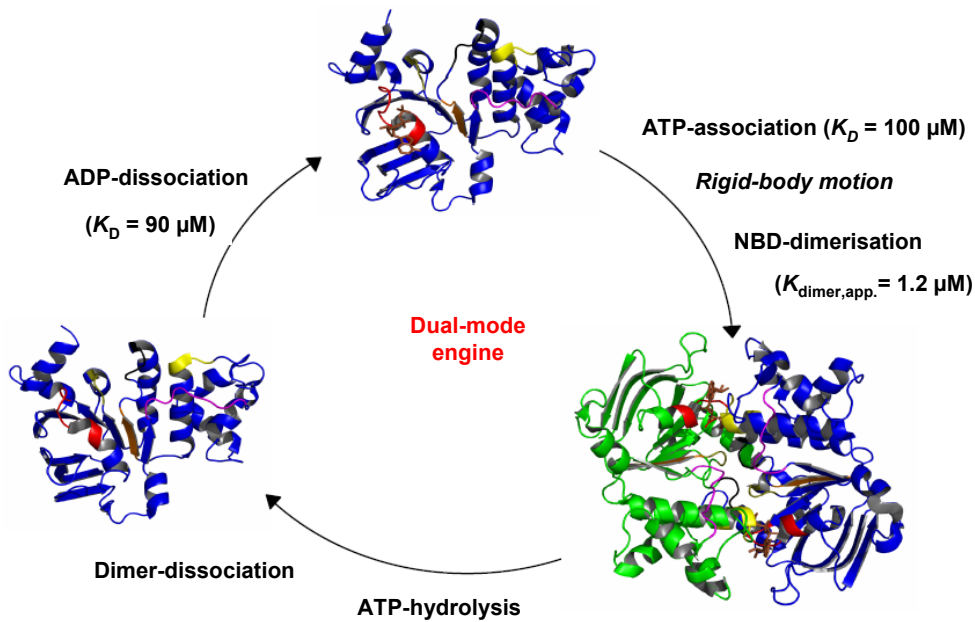
Figure 1-4. Catalytic cycle of the nucleotide binding domain (NBD) of Haemolysin B exporter (HlyB).
The crystal structures of the monomeric nucleotide-free (Schmitt *et al.,* 2003), ADP-bound and the dimeric ATP-bound NBD are shown (PDB Accession Numbers: 1MT0, 2FF7 and 1XEF). The conserved motifs Walker A (red), Walker B (orange), C-loop (yellow), Q-loop (magenta), D-loop (black), and H-loop (olive) are illustrated. ATP and ADP are shown as stick model (Zaitseva *et al.,* 2005).

1.2.4 Translocation pathways for diverse substrates: architectures of transmembrane domains

Unlike the NBDs, the membrane-spanning TMDs are highly diverse with respect to their primary sequences. This diversity likely reflects that of the substrate transported by the different ABC proteins. The determined crystal structures have revealed three unrelated transmembrane domain folds (Sav1866, ModBC, and those of BtuCD and HI1470/71, which are similar) (Dawson *et al.,* 2007).

ABC exporters contain a conserved core of 12 transmembrane helices (TM). Additional TM helices are found in several human homologues but are likely facilitating regulatory functions. For example, the human ABC transporter associated with antigen processing (TAP) has additional, N-terminal TM helices that are essential for the interaction with tapasin (Koch *et al.,* 2004). The crystal structure of Sav1866 is the first to reveal the conserved core structure of an ABC exporter (Dawson and Locher, 2006). The TM-helices extend beyond the membrane boundary and protrude far into the cytoplasm (Figure 1-2). Sav1866 exhibits a pronounced outward-facing conformation, with two wings, each consisting of six TM helices, which diverge towards the external side of the membrane. Each wing consists of TM1-TM2 from one TMD and TM3-TM6 from the other, which is in part a

consequence of the substantial twisting of the TMDs, a feature observed in ABC exporters only (Dawson *et al.,* 2007). The transmembrane segments are connected by long cellular and short extracellular loops (CLs and ECLs, respectively). The CLs extend the helical secondary structure beyond the lipid bilayer and protrude approximately 25 Å into the cytoplasm (Dawson and Locher, 2006). The TM helices of Sav1866 are arranged around a large, central cavity that is shielded from the cytoplasm but open to the extracellular space and to the outer leaflet of the lipid bilayer. The surface of this cavity is mostly hydrophilic and reflects a putative translocation pathway of the substrate.

In contrast to ABC exporters, the TMDs of ABC importers have many sizes and shapes. They feature a total of 10-20 TM helices, indicating a higher degree of structural diversity than the TMDs of exporters. For example, molybdate transporters of mesophilic organisms have 10 TM helices, whereas their counterparts from hyperthermophiles have 12 (Self *et al.,* 2001; Hollenstein *et al.,* 2007). The CLs of ABC importers are short with the NBDs close to the inner leaflet of the membrane, whereas the CLs of Sav1866 are much longer (Figure 1-2).

1.2.5   The translocation cycle: the ATP-switch model

The ATP-switch model involves repeated communication, in both directions, between the NBDs and TMDs (Abele and Tampé, 2004; Higgins and Linton, 2004; van der Does and Tampé, 2004). In the first step, ligand and nucleotide bind to the transporter independently from each other (van Endert *et al.,* 1994; Tomazin *et al.,* 1996). Ligand binding allows a putative NBD dimerization in the presence of ATP. In step 2, NBD dimerization induces a large conformational change in the TMDs sufficient to translocate the ligand (Hung *et al.,* 1998; Smith *et al.,* 2002; Chen *et al.,* 2003; Janas *et al.,* 2003). In this closed conformation, the bound nucleotides are sandwiched between the Walker A motifs (P-loops) and the LSGGQ motifs (C-signature), as depicted in the crystal structure of Sav1866 (Dawson and Locher, 2006). Compared to the nucleotide-free state of the import protein ModBC, ATP binding to the NBDs of Sav1866 causes the coupling helices approaching one another by 10-15 Å (Hollenstein *et al.,* 2007). This presumably triggers the flipping of the transmembrane helices from the inward-facing to the outward-facing conformation. In this state, importers may now accept substrates from their cognate binding proteins, whereas exporters probably release their substrate that has previously entered the translocation pore (Figure 1-5). If the substrate binding affinity is changed in this state, is controversially discussed. According to

functional data of LmrA of *Lactococcuis lactis*, the substrate-binding affinity is drastically decreased (van Veen *et al.,* 2000). In case of human TAP however, no changes in affinity were observed in the trapped transition state (Chen *et al.,* 2003b). Controverse results were obtained for P-glycoprotein (Ramachandra *et al.,* 1998; Qu *et al.,* 2003; Russell and Sharom, 2006). In step 3, ATP hydrolysis initiates NBD dissociation (Smith *et al.,* 2002; Zaitseva *et al.,* 2005). In the last step, P_i and ADP are released to complete the transport cycle and restore the protein to a high-affinity state for ligand (Smith *et al.,* 2002; Zaitseva *et al.,* 2006).

The ATP-switch model is the product of biochemical data interpreted in light of recent advances in structure determination of several ABC transporters. The model is divided into four steps (Figure 1-5), or four conformational changes; the first associated with the binding of ligand, then three that make use of the free energy available from protein-ATP and protein-protein interactions associated with ATP binding, ATP hydrolysis, and ADP·Pi release.
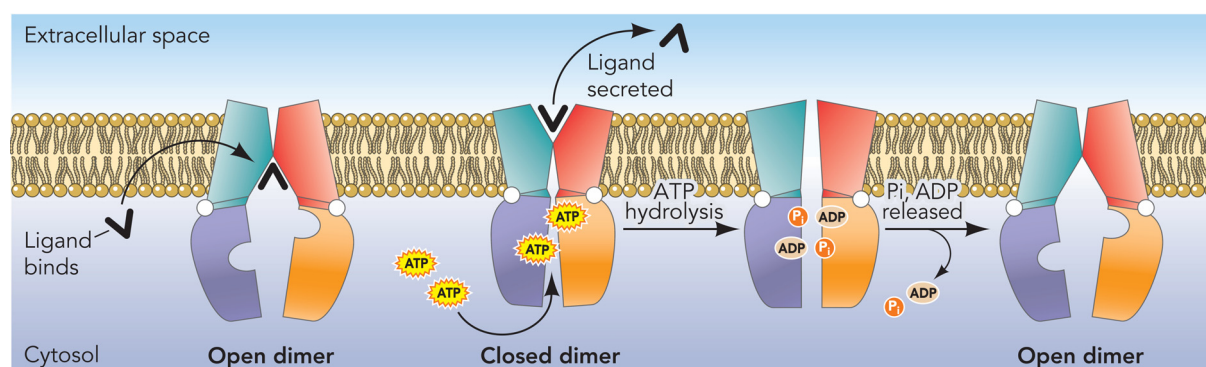
Figure 1-5. Model of the ATP-switch mechanism of ABC transporters.
Ligand binding to a high-affinity pocket formed by the TMDs induces a conformational change in the NBDs. Two molecules of ATP bind to the NBDs. The energy released by the formation of the closed NBD dimer causes conformational change in the TMDs. ATP hydrolysis triggers dissociation of the closed NBD dimer resulting in further conformational changes in the TMDs. Finally, phosphate and ADP release restores the transporter to the open NBD dimer conformation ready for the subsequent cycle (Abele and Tampé, 2004; Linton, 2007).

1.2.6 Coupling helices: an architecturally conserved motif transmits conformational changes

Based on the biochemical and structural data of ABC proteins a putative model of transmission interface has been proposed. According to this model, binding and hydrolysis of ATP induce conformational changes in the NBDs that are transmitted to the TMDs via non-covalent interactions (Dawson *et al.,* 2007). The TMD-NBD interface therefore serves as a putative 'transmission interface' that couples the changes at the NBDs to distinct conformations of the TMDs. The crystal structures of ABC transporters reveal that in the

NBDs, predominantly residues around the Q-loops contribute to the transmission interface. However, the TMDs of these transporters, despite their unrelated architectures, all feature strikingly similar short α-helices located in cytoplasmic loops between transmembrane segments. These helices show several contacts to the NBDs, and therefore they have been labeled 'coupling helices' (CH), which highlights their probable function (Dawson and Locher, 2006).

In the bacterial exporter Sav1866 the TMDs contribute to this interface mainly through the cellular loops CL1 and CL2. Both CLs contain short helices oriented roughly parallel to the membrane plane and providing the bulk of the contacts (Figure 1-6) (Dawson and Locher, 2006). These coupling helices can putatively modulate mechanistically crucial conformational changes. The CLs of Sav1866 reach across and contact both NBDs of the opposite subunit, therefore they are domain-swapped, a characteristic observed also in various enzymes (Liu and Eisenberg, 2002; Dawson and Locher, 2006). Domain swapping is not apparent in bacterial ABC importers. In contrast, the TMDs of the ABC importer BtuCD contact only one NBD, resulting in a large gap at the centre of the four protein domains (Locher *et al.,* 2002). However, there are also similarities with ABC importers. On the part of the NBDs, the contact surface with the TMD is primarily lined with residues around the Q-loop (Schneider and Hunke, 1998), as was also observed in BtuCD (Locher *et al.,* 2002). One prominent exception include the conserved residue Glu-473, which interacts with both CLs and is part of a previously unrecognized, short sequence motif (TEVGERG) that appears conserved in ABC export proteins only (Dawson and Locher, 2006). This newly identified sequence (called X-loop) functions in coupling the CLs. Because the X-loops precede the ABC signature motifs, they probably respond to ATP binding and hydrolysis and may transmit conformational changes to the CLs.
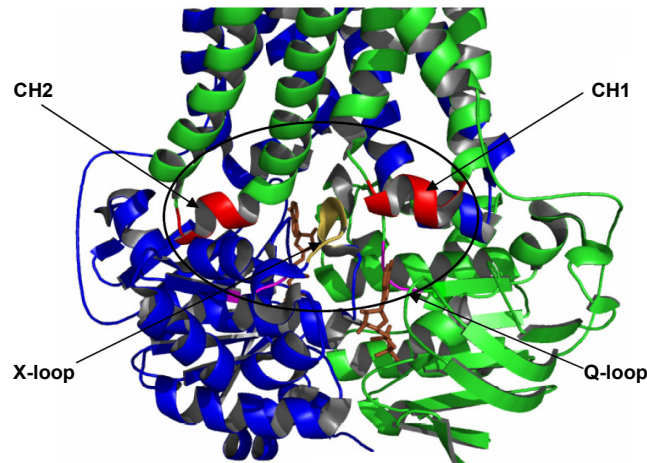
Figure 1-6. The putative TMD-NBD transmission interface.
Close-up view of Sav1866 (PDB Accession Number: 2HYD). The homodimeric protein has the subunits coloured green and blue, as ribbon representation. The coupling helices (CHs) of the green subunit are coloured red, the Q-loop of both subunits is coloured in magenta, and the X-loop of the blue subunit is shown in yellow. Bound ADP (brown) is in stick-model representation (Dawson and Locher, 2006).

1.3   Transporter associated with antigen processing

The first indication of peptide transporters was discovered from the studies of various mutant cell lines deficient in cell surface expression of MHC class I molecules, even though the expression levels of MHC class I heavy chain and β2m are normal (DeMars *et al.,* 1985). The genes responsible for these defective phenotypes are *tap1* and *tap2* located in the MHC class II locus of human chromosome 6 (Trowsdale *et al.,* 1991). Transfection of these cell lines with cDNA of TAP1 and TAP2 could restore cell surfaces expression of the MHC class I molecules (Powis *et al.,* 1991; Spies and DeMars, 1991; Attaya *et al.,* 1992; Spies *et al.,* 1992). Heterologous expression of TAP1 and TAP2 in insect cells and yeast showed a functional peptide translocation in the absence of factors of the adaptive immune system (Meyer *et al.,* 1994; Urlinger *et al.,* 1997).

1.3.1   Structural organization of TAP

The most recent annotation of the human genome sequence revealed 48 genes for ABC proteins, which were grouped into seven subclasses, from ABCA to ABCG (see: http//nutrigene.4t.com/humanabc.htm; Holland *et al.,* 2003). The transporter associated with antigen processing (TAP) belongs to the subfamily B of ATP-binding cassette (ABC) transporters and is a central component in the major histocompatibility complex (MHC) class I dependent antigen presentation pathway. TAP translocates peptides derived mainly from

proteasomal degradation from the cytosol into the lumen of the endoplasmic reticulum (ER), where these peptides are loaded onto MHC class I molecules (Figure 1-1). The transport of substrates across membrane is driven by ATP hydrolysis (Higgins, 1992; Schmitt and Tampé, 2002; Davidson and Chen, 2004). Stable peptide-MHC complexes traffic to the cell surface to present their antigenic cargo to CD8^{+}-cytotoxic T-lymphocytes. The recognition of viral or tumor antigens leads to an efficient elimination of the infected or malignant cell.

TAP1 was proposed to contain 808 aa in the initial reports (Trowsdale *et al.,* 1990). Human TAP forms a heterodimer consisting of TAP1 (748 aa) and TAP2 (686 aa) (Kelly *et al.,* 1992). Both subunits are essential and sufficient for peptide transport (Powis *et al.,* 1991; Spies and DeMars, 1991; Meyer *et al.,* 1994). TAP is localized in the ER and *cis*-Golgi (Kelly *et al.,* 1992; Kleijmeer *et al.,* 1992), although neither an ER-targeting sequence nor an ER-retention signal has been identified. Each subunit contains a transmembrane domain (TMD), followed by a cytosolic nucleotide binding domain (NBD) (Figure 1-7). The TMDs comprise the peptide binding pocket and the translocation pathway for the substrate. On the basis of sequence alignments with other ABC transporters of the subfamily B in combination with hydrophobicity plots, 10 and 9 TMs have been predicted for human TAP1 and TAP2, respectively (Tampé *et al.,* 1997; Lankat-Buttgereit and Tampé, 1999). Recently, the topological organization of transmembrane segments of TAP1 within a functional transport complex has been elucidated for the first time. Based on these results, it has been concluded that the transporter core is formed by 6 + 6 TMs, which is common for most ABC transporters (Schrodt *et al.,* 2006). In addition to the 6 + 6 TM core, TAP1 and TAP2 comprise an extra N-terminal domain that is essential for assembly of the peptide-loading complex mediated by the adapter protein tapasin (Koch *et al.,* 2004). Importantly, TAP1 and TAP2 lacking the first predicted four and three transmembrane helices, respectively, are targeted to the ER membrane and assemble into a fully functional heterodimeric transport complex, demonstrating that the extra N-terminal domains of both subunits are not required for peptide binding and transport (Koch *et al.,* 2004; Koch *et al.,* 2005). Topological investigations of these unique N-terminal domains of TAP1 and TAP2 revealed that the N-terminus of both subunits is located in the cytosol (Schrodt *et al.,* 2006; Baldauf *et al.,* manuscript in preparation). Because the N-terminus and the C-terminal nucleotide binding domain are both located in the cytosol, it can be suggested that TAP1 and TAP2 have an even number of transmembrane helices.

The peptide-binding site of human TAP is contributed by the transmembrane domains of both subunits (Androlewicz *et al.,* 1993; Androlewicz *et al.,* 1994). Mapped by photo-

16

crosslinking experiments, the cytosolic loops between TM4 and TM5 and a C-terminal stretch of approximately 15 amino acids after TM6 are shown to be involved in peptide binding (Nijenhuis and Hämmerling, 1996; Nijenhuis *et al.*, 1996). Deletion of some of these amino acids in the TAP1 region resulted in loss of peptide transport (Ritz *et al.*, 2001). The NBDs containing the highly conserved Walker A/B motifs and the C-loop (ABC signature) energise peptide transport by ATP binding and hydrolysis. The NBD sequences of TAP1 and TAP2 show a variation of the canonical C-loop sequence. TAP2 shows a degenerative C-loop sequence (LAAGQ). TAP chimera with exchanged C-loops (LSGGQ) preserved transport activity as wild type, whereas the TAP complexes with two degenerative LAAGQ motifs had the lowest transport rate. These mutational studies demonstrate that the ABC signature motifs control the ATPase activity as well as the peptide transport of TAP (Chen *et al.*, 2004).
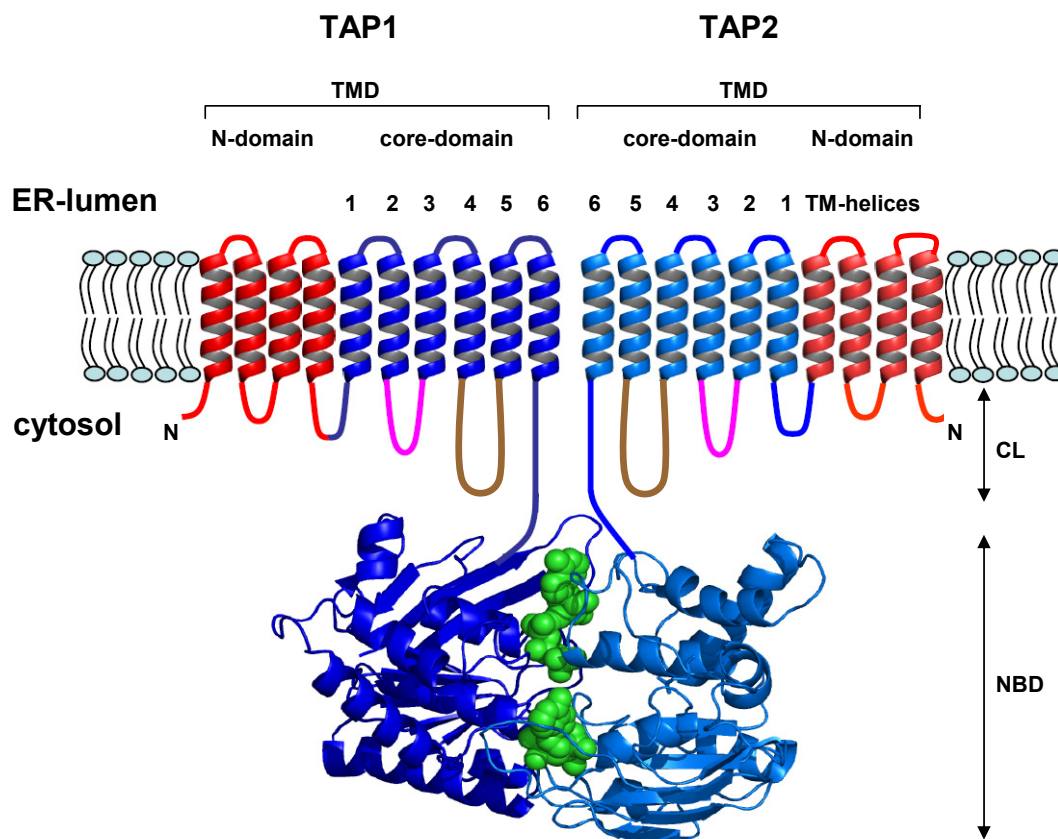
Figure 1-7. Schematic model of the TAP complex.
TAP forms a heterodimer composed of TAP1 and TAP2. Each subunit comprises an N-terminal transmembrane domain (red) and a C-terminal cytosolic NBD (blue, as ribbon representation). The transmembrane domain can be subdivided into a six helices containing core-domain (blue), which forms the peptide binding pocket and the translocation pore across the membrane, and an NH_2-terminal extension of four helices for TAP1 and TAP2, respectively. The CL1 and CL2 of both subunits are illustrated in magenta and brown, respectively. The NBDs in the cytosol are depicted in the ribbon diagram and show an ATP (green) bound dimer from MJ0796 (PDB Accession Number: 1L2T). The figure was modeled by using PyMOL (www.pymol.org).

1.3.2   Peptide specificity and transport of TAP

A prerequisite for peptide transport is peptide binding to TAP. This step is ATP independent (Androlewicz and Cresswell, 1994; van Endert *et al.,* 1994). In contrast, peptide transport strictly requires ATP hydrolysis (Neefjes *et al.,* 1993). Derived from the topological model of TAP (Figure 1-7), the peptide binding regions include the cytosolic loops between TM-helix 4 and 5 as well as an extension of 15 amino acids following TM-helix 6 in TAP1 as well as in TAP2 (Nijenhuis and Hämmerling, 1996). Peptides with 8-16 residues were found to be optimal for binding to TAP (van Endert *et al.,* 1994). Interestingly, peptides which are sterically restricted by long and bulky side chains or even labeled with large fluorophores are bound and even transported by TAP (Uebel *et al.,* 1995; Gromme *et al.,* 1997; Neumann and Tampé, 1999).

In addition to the peptide size, also the amino acid sequence determines the efficiency of translocation by TAP. To resolve the recognition principle and the substrate-binding motif in a systematic approach, complex peptide libraries were applied (Uebel *et al.,* 1997). In this method, the affinity of a randomized peptide mixture with one residue in common was compared with a totally randomized peptide library. Systematically, the influence of each amino acid on the affinity for TAP could be determined unbiased on the sequence context of the peptide. Besides free N- and C-termini, the first three N-terminal amino residues and the C-terminal amino acid are important for TAP recognition. At the C-terminus, human TAP favors peptides with hydrophobic or basic amino acids (Figure 1-8A). Strikingly, this is also a preferred anchor residue for MHC class I binding. Notably, upon stimulation by INF-γ, immunoproteasomes preferentially generate peptides with hydrophobic and basic C-terminal residues. The knowledge that the C-terminal peptide specificity of immunoproteasome, MHC class I and TAP are identical (Figure 1-8B), suggests a coevolution between the cleavage selectivity of the immunoproteasome and the binding specificity of TAP and MHC class I (Abele and Tampé, 2004). Remarkably, the T-cell receptors mainly contact the residues of antigenic peptides apart from the anchor residues where TAP shows the lowest specificity (Garboczi *et al.,* 1996; Garcia *et al.,* 1996). Peptides which are longer than 8-11 amino acids, will be N-terminal degraded by the ER-aminopeptidases ERAP1/2 (Serwold *et al.,* 2002). The sequence in between both ends of the peptides presented to the T cell receptor are highly promiscuous with respect to TAP and MCH I binding. This ensures that a limited set of peptide transporter and MHC I molecules can offer a maximal peptide diversity, protecting the organism against pathogens (Abele and Tampé, 2004). In conclusion, TAP binds peptides

through the two termini and transports peptides with maximal sequence diversity of the center residues for T-cell recognition (Figure 1-8B).

Peptide binding is composed of a fast, diffusion-controlled peptide association, followed by a slow structural rearrangement, which includes ~25% of the residues of TAP as shown by kinetic and thermodynamic studies (Neumann and Tampé, 1999; Neumann *et al.,* 2002). An essential question in the ABC proteins family is how the allosteric interaction between substrate binding, ATP hydrolysis and substrate translocation implies a crosstalk between the NBDs and substrate binding pocket? By developing an enrichment and reconstitution protocol for TAP, it was possible to restore the function in proteoliposomes and to examine the specific ATPase activity (Gorbulev *et al.,* 2001). Nucleotide hydrolysis was found to be strictly dependent on binding of peptides and on crosstalk with the peptide-binding and the translocation sites. The strict correlation between peptide binding and stimulation of ATP hydrolysis may be a strategy to avoid 'wasting' ATP without transport of peptides (Lankat-Buttgereit and Tampé, 2003). A further indication of the tight coupling between ATP hydrolysis and peptide transport is the observation that sterically restricted peptides, which cannot be transported by TAP, do not induce ATP hydrolysis. Maximal ATPase activity of TAP was found to be independent of substrate affinity, because peptides with different K_d values for the transporter exhibited the same V_{max} values (Gorbulev *et al.,* 2001). The two NBDs of the functional TAP complex can both interact with ATP, even if TAP1 or TAP2 are expressed separately (Müller *et al.,* 1994; Wang *et al.,* 1994). However, alone, the NBDs are unable to hydrolyze ATP. Thus, communication between the NBDs and TMDs, leading to a conformational change of the NBDs by peptide binding to TAP, seems to be a requirement to activate ATPase function. Furthermore, TAP function is dependent on the presence of both NBDs since disruption of one NBD leads to loss of transport (Chen *et al.,* 1996).

A

B
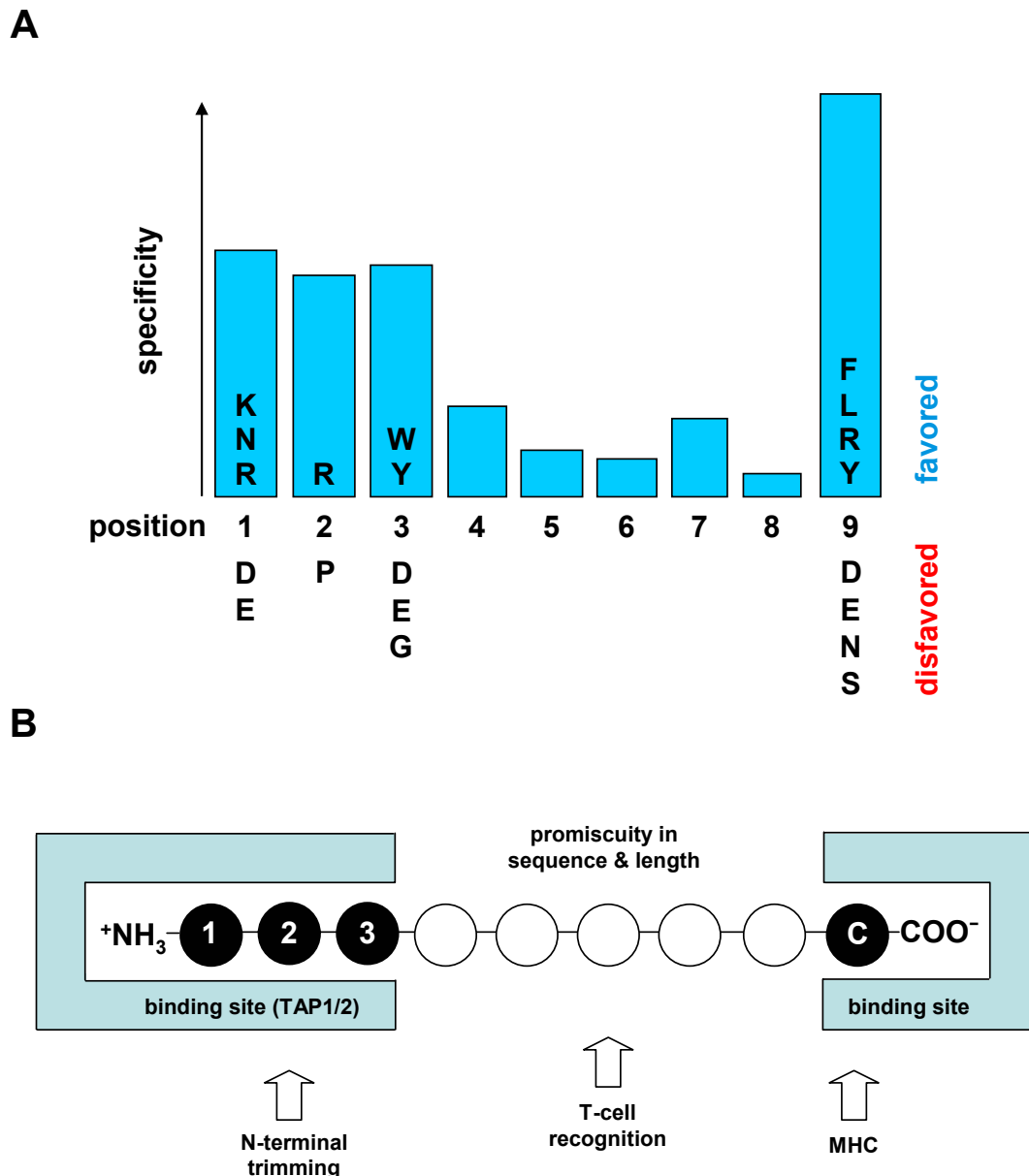
Figure 1-8. Peptide specificity of human TAP.
(A) TAP selectivity is illustrated for positions of the peptide. Favored (upper) and disfavored residues (lower) are given at the individual positions as elucidated using combinatorial peptide libraries. (B) Model of the peptide-binding pocket including residues utilized for MHC I binding and T-cell recognition (Abele and Tampé, 1999).

1.3.3   Functional nonequivalence of the two motor domains of TAP

By functional reconstitution of TAP, it has been demonstrated that peptide binding is tightly coupled to ATP hydrolysis (Gorbulev *et al.,* 2001). The contribution of both subunits in ATP hydrolysis was shown by nucleotide trapping and photo-cross-linking experiments (Chen *et al.,* 2004). The ATPase activity of both subunits was stimulated in the presence of peptide in the same way, suggesting an equal contribution of both NBDs for peptide transport.

However, based on mutational studies, the non-equivalence of both subunits was derived. Chimeric TAP complexes with two identical NBDs showed a drastically reduced transport activity whereas TAP with exchanged NBDs was fully active (Arora *et al.,* 2001; Daumke and Knittler, 2001). Furthermore, loss of transport was observed after mutation of the conserved lysine in the Walker A motif of TAP2 (ATP-binding site II), whereas the same exchange in TAP1 (ATP-binding site I) resulted in an only slightly decreased transport activity (Karttunen *et al.,* 2001; Lapinski *et al.,* 2001; Saveanu *et al.,* 2001). Site I is defined as the ATP-binding pocket composed of residues of the Walker A and B motifs of TAP1 and the C-loop of TAP2. Therefore, site II seems to be the canonical ATP-binding site, whereas site I is degenerate, also reflected by sequence comparison. In TAP1, the highly conserved glutamate ('catalytic base') and the histidine of the H-loop are replaced by aspartate and glutamine, respectively. Furthermore, the C-loop in TAP2, which contacts the γ-phosphate of ATP bound to site I, is degenerate to LAAGQ compared to the canonical signature motif LSGGQ. It is assumed that the highly conserved serin regulate the ATPase activity as shown for other ABC transporters (Hoof *et al.,* 1994; Browne *et al.,* 1996). TAP chimeras with two canonical C-loops showed highest transport rate compared to chimeras with two degenerate C-loops showing lowest transport rate, demonstrating that the ABC signature motifs control peptide transport efficiency (Chen *et al.,* 2004). Markedly, mutations of the leucine or glycine in TAP1 (LSGGQ) fully abolished peptide transport, whereas equivalent mutations in TAP2 still showed residual transport activity (Chen *et al.,* 2004). In summary, the functional asymmetry of both TAP subunits suggests an sequential catalytic site model for ATP hydrolysis where NBD2 (site II) first hydrolyzes ATP due to the canonical ABC transporter sequences before ATP hydrolysis and phosphate release occurs at NBD1, the degenerate site (van der Does and Tampé, 2004).

1.4   Objective

Peptide binding induces a large conformational change comprising 25% of all TAP residues, which could be the trigger for ATP hydrolysis and subsequently peptide transport (Neumann *et al.,* 2002). Remarkably, peptides with very bulky side-chains, which bind to TAP but are not transported, do not induce ATP hydrolysis (Gorbulev *et al.,* 2001). Thus, a key question regarding the mechanism of TAP is what senses the quality of incoming peptides and transmits it to the motor domain? Regarding the mechanism of TAP and how the TMD-NBD crosstalk during the catalytic cycle, the following questions were addressed:

1.   Which role plays CL1 (TAP1) in the substrate sensing and signal transmission?

2.   How is the molecular architecture of CL1 organized?

3.   How is the spatiotemporal communication coordinated between distinct events in the TMDs and NBDs?

To address these questions three strategies were applied. One strategy comprised the establishment of a TAP-cleavage assay by modifying the peptide epitope by a small chemical protease. Based on this, final evidence of a peptide sensor and transducer region was supposed to be provided by a cysteine-scanning approach and thiol-specific cross-linking. A second strategy involved the cysteine accessibility using fluorescence labeling. Furthermore, fluorescence labeling kinetics provided evidence of a direct correlation between covalent modification of CL1 and TMD-NBD signaling. Finally, the inter-domain communication and a dynamic transmission interface between TMD-NBD were found by using a cysteine cross-linking approach combined with functional assays. Based on these results, the CLs have different functions in substrate recognition, signaling and transport binding.

2.   Materials

2.1   Chemicals

Table 2-1. Chemical list.

Chemicals	Company
Aluminium chloride ($AlCl_3$)	Sigma-Aldrich
Acrylamide 30% (w/v)	National Diagnostics
Adenosine-5'-diphosphate (ADP)	Fluka Chemie
Adenosine-5'-triphosphate (ATP)	Fluka Chemie
AEBSF hydrochloride	Merck
Agarose	BioWhittaker
AmpLigase	Epicentre
Ampicillin	PAA laboratories
Ammonium peroxydisulfate (APS)	Roth
Aprotinin	Merck
Apyrase	Sigma-Aldrich
5-Bromo-3-indolyl-D-galactoside (bluo-gal)	Sigma-Aldrich
1,8-bis-Maleimidotriethylene glycol [BM(PEO)$_3$]	Pierce
10x Bacteriophage T4 polynucleotide kinase buffer	Fermentas
Bacteriophage T4 polynucleotide kinase	Fermentas
Bacto agar	Roth
BaculoGold Transfection Kit	BD Bioscience Pharmingen
BCA-Kit	Pierce
Benzamidine hydrochloride	Calbiochem
BODIPY maleimide (BM)	Invitrogen
Bovine serum albumin (BSA)	Sigma-Aldrich
Bromphenol blue	Roth
Calf intestine alkine phosphatase (CIAP)	Fermentas
Calcium chloride ($CaCl_2$)	Roth
Chloramine T	Riedel-de Haen
Concanavalin A sepharose	Sigma-Aldrich
Coumarin maleimide (CM)	Invitrogen
Copper sulfate ($CuSO_4$)	Fluka
Digitonin	Calbiochem
Dimethylsulfoxide (DMSO)	Fluka
N,N-Dimethylformamide (DMF)	Fluka
Dinucleotide-5'-triphosphate (dNTP)	Fermentas

Disodium hydrogen phosphate (Na_2HPO_4)	Roth
1,4-dithiothreitol (DTT)	Roth
Dowex 1 x 8 anion exchange	Sigma-Aldrich
Dynabeads® M-280	Dynal Biotech
Enhanced ChemiLuminescence System (ECL)	Amersham Pharmacia
1,2-Ethanediyl-bis-methanethiosulfonate (MTS-2-MTS)	Toronto Chemicals
Ethylendiamine-tetraacetic acid (EDTA)	Roth
N-Ethylmaleimide (NEM)	Fluka
Fetal calf serum (FCS)	Sigma-Aldrich
FluoroStar fluorometer	BMG Labtechnologies
Tetradecylphosphocholine (FC-14)	Anatrace
Fungizone	Invitrogen
Glycerol	Roth
Glucose	Roth
N-(2-Hydroxyethyl)-piperazine-N'-2-ethansulfonic acid	Roth
trans-4-Hydroxycinnamic acid (p-Coumaric acid)	Sigma-Aldrich
Igepal (NP-40)	Sigma-Aldrich
Iodoacetamidofluorescein (IAF)	Invitrogen
Isopropyl-β-D-thiogalactopyranoside (IPTG)	BTS-BioTech Trade & Service
K-acetate	Roth
Kanamycin (Km)	PAA Laboratories
Potassium chlorid (KCl)	Roth
Leupeptin	Merck
10x Ligation buffer	Fermentas
β-mercaptoethanol (β-ME)	Roth
Methanol	Roth
Methyl-α-D-mannopyranoside	Sigma-Aldrich
Mangnesium chloride ($MgCl_2$)	Roth
Micro BCA protein assay reagent kit	Pierce
Manganese chloride ($MnCl_2$)	Roth
3-(N-morpholino)propanesulfonic acid (MOPS)	Roth
MultiScreen plates with glass fibre filter, pore size 1.0 μm	Millipore
MN Mini kit	Macherey-Nagel
Sodium chloride (NaCl)	Roth
Sodium hydroxide (NaOH)	Roth
Neutral red	Invitrogen

Ni-NTA beads	Qiagen
Nucleospin plasmid kit	Macherey-Nagel
Oligos	MWG Biotech
PCR buffer (10x, with 20 mM $MgCl_2$)	Fermentas
PCR Purification Kit	Qiagen
Penicillin/Streptomycin (100x)	PAA Laboratories
Pepstatin A	Merck
1,5-Pentanediyl-bis-methanethiosulfonate (MTS-5-MTS)	Toronto Chemicals
Pfu DNA Polymerase	Fermentas
1,10-Phenanthroline	Sigma-Aldrich
Phenylmethanesulfonyl fluoride (PMSF)	Fluka
Pluronic F-69 (10%)	Invitrogen
Polyethylenimine cellulose plates	Merck
Polyethylimine (PEI)	Roth
Potassium dihydrogen phosphate (KH_2PO_4)	Roth
PVDF membrane	Schleicher-Schuell Bioscience
QIAquick gel extraction kit	Qiagen
QIAquick spin PCR purification kit	Qiagen
Rubidium chloride (RbCl)	Roth
Restriction enzymes	Fermentas
RNase A	Macherey-Nagel
Saponin	Sigma-Aldrich
SF900II medium	Invitrogen
Skim milk powder	Roth
Sodium azide (NaN_3)	Roth
Sodium disulfite ($Na_2S_2O_5$)	Merck
Sodium dodecyl sulfate (SDS)	Roth
Sodium fluoride (NaF)	Fluka
Sodium iodide ($Na^{125}I$)	Amersham Pharmacia
Sodium luminol	Roth
T4 DNA ligase	Fermentas
10x Y+ Tango buffer	Fermentas
10x *Taq* PCR buffer	Fermentas
Taq polymerase	Invitrogen
Tetracycline	PAA Laboratories
N,N,N`,N`-Tetramethylethylendiamine (TEMED)	Sigma-Aldrich
Transfection buffers A and B	BD Bioscience

Tris-acetate   Roth

Triton X-100   Roth

Tryptone   Roth

Yeast extract   Roth

2.2   Peptides

Table 2-2. Peptides used in this work.

Peptides	Sequence	Notes
C4F	RRYC(Ψ)KSTEL	(Ψ) cysteine labeled with iodoacetamidofluorescein
R9LQK	RRYQKSTEL	
R9LQK radioactive	RRY(^{125}I)QKSTEL	(^{125}I) tyrosine labeled with radioactive Na^{125}I
R9NST	RRYQNSTEL	

2.3   Antibodies

Table 2-3. Antibodies used in this study.

Antibodies	Protein	Type	Recognition site
148.3	TAP1	monoclonal	CYWAMVQAPADAPE
1P1	TAP1	polyclonal	GRLTDWILQDGSA
1P2	TAP1	polyclonal	ETEFFQQNQTGNIMSR
1P3	TAP1	polyclonal	TVRSFANEEGEAQKFR
1P4	TAP1	polyclonal	SEKIFEYLDRTPR
435.3	TAP2	monoclonal	DVSFAYP
2P1	TAP2	polyclonal	RVIDILGGDFD
2P2	TAP2	polyclonal	RIREQLFSSLL
2P3	TAP2	polyclonal	EAVGGLQTVRSFGAEE
2P4	TAP2	polyclonal	VGAAEKVFSYMDRQPN

2.4   Vector maps

2.4.1   pGEM-3Z

Figure 2-1. pGEM-3Z vector promoter and multiple cloning region sequence.
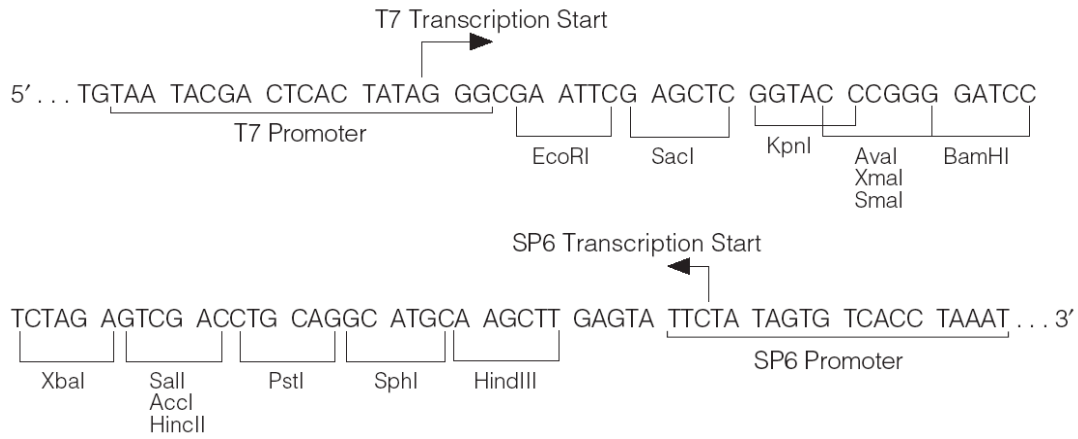
Figure 2-2. pGEM-3Z_TAP1_Cys-less vector circle map and sequence reference points.
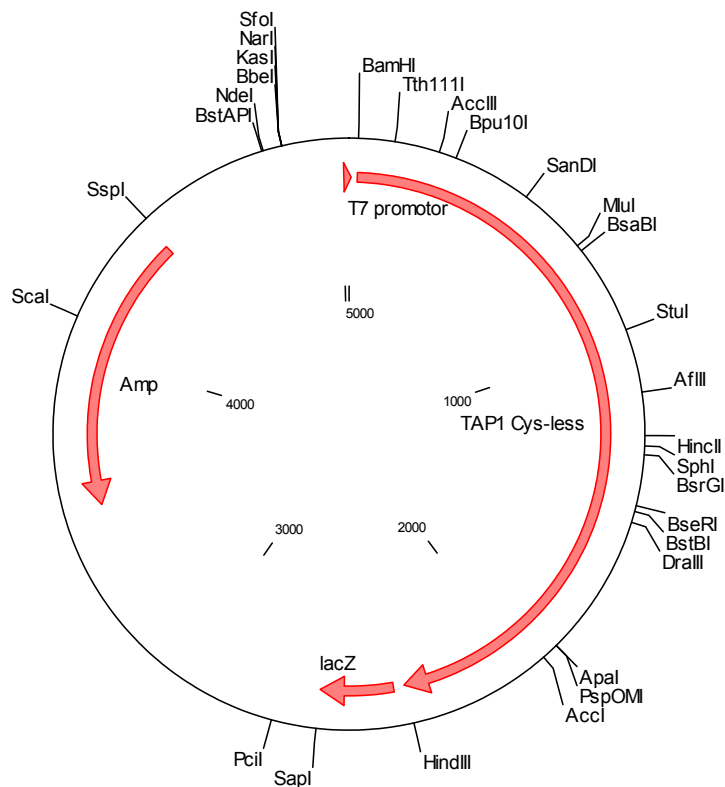
Figure 2-3. DNA sequence of TAP1_Cys-less (start 26, end 2338).

```
   1  gggcgaattc gagctcggta cccgg**gga**tc catggcttcc tccagatccc ctgctcctag
  61  aggctccaga tctctgcctg gcgcttccct ggcttggctg ggcaccgtcc tgctgctgct
 121  ggctgactgg gtcctgctga gaaccgctct gcctagaatc ttctccctgc tggtccctac
 181  cgccctgcct ctgctgagag tctgggctgt cggcctgtcc agatgggctg tcctgtggct
 241  gggtgcttcc ggagtcctga gagctaccgt cggctccaag tccgaaaacg ctggcgctca
 301  gggctggctg gctgctctga gcctctggc cgctgctctg gcctggcct tgccaggtct
 361  ggctctgttc agagaactga tctcctgggg cgctcccggg tccgctgact ccaccagact
 421  gctgcactgg ggctcccatc caaccgcttt cgtcgtctcc tacgctgctg ccctgcctgc
 481  tgccgccctg tggcacaagc tgggttccct gtgggtccca ggcggtcagg cggctccgg
 541  caaccctgtg agaagactgc tgggctccct gggttccgaa accagaagac tgtccctgtt
 601  cctggtcctg gtcgtcctgt cctctctggg cgaaatggct atccctttct tcaccggcag
 661  actgaccgac tggattctgc aggatggctc cgctgacacc ttcacgcgta acttaaccct
 721  gatgtccatc ctgaccatcg cttccgctgt cctggaattc gtcggcgacg gcatctacaa
 781  caacaccatg ggccacgtcc actcccacct gcagggcgaa gtcttcggtg ccgtcctgag
 841  acaggaaacc gaattcttcc agcagaacca gaccggcaac atcatgtcca gagtcaccga
 901  agatacgtcc accctgtctg actccctgtc cgaaaacctg tccctgttcc tgtggtacct
 961  ggtcagaggc ctggccctgc tgggcatcat gctgtggggc tccgtctccc tgactatggt
1021  gaccctgatc accctgcctc tgctgttcct gctgcctaag aaggtcggca agtggtacca
1081  gctgctggaa gtccaggtca gagaatccct ggctaagtcc tcccaggtcg ctatcgaagc
1141  cttaagtgct atgcctaccg tcagatcctt cgctaacgaa gaaggcgaag ctcagaagtt
1201  cagagaaaag ctgcaggaaa tcaagaccct gaaccagaag gaagctgtcg cttacgctgt
1261  caactcctgg accacctcca tctccggcat gctgctgaaa gtcggtatcc tgtacatcgg
1321  cggccaactg gtgacctccg cgctgtgag ctctggcaac ctggtcacct tcgtcctgta
1381  ccagatgcag ttcacccagg ccgtcgaagt cctgctgtcc atctacccta gagtccagaa
1441  ggctgtcggc tcctccgaaa agatcttcga atacctggac agaacccta gatccccacc
1501  tagtggcctg ctgacccctc tgcatctgga aggactggtc cagttccagg acgtctcctt
1561  cgcttaccct aacagacctg acgtgctggt cctgcagggt ctgaccttca ccctgagacc
1621  tggcgaagtc accgcactgg tcggccctaa cggctccggc aagtccaccg tcgctgctct
1681  gctgcagaac ctgtaccagc ctaccggcgg ccagctgctg ctggacggca gcctctgcc
1741  tcagtacgaa cacagatacc tgcacagaca ggtcgctgct gtcggccagg aacctcaggt
1801  cttcggcaga tctctgcagg aaaacatcgc ttacggcctg acccagaagc ctaccatgga
1861  agaaatcacc gccgccgctg tcaagtccgg ggcccactcc ttcatctccg gcctgcctca
1921  gggctacgac accgaagtag acgaagctgg ctctcagctg tccggcggcc agagacaggc
1981  tgtcgctctg gctagagccc tgatcagaaa gccttccgtc ctgatcctgg acgacgctac
2041  ctccgctctg gacgctaact cccagctgca agtcgaacaa ctgctgtacg aatcccctga
2101  aagatactcc agatccgtcc tgctgatcac ccagcacctg tccctggtcg aacaggctga
2161  ccacatcctg ttcctggaag gtggcgctat cagagaaggc ggcacccacc agcagctgat
2221  ggaaaagaag ggctcctact gggctatggt ccaggctcct gctgacgctc ctgaactggt
2281  ccctagaggc tccggtggac atcaccatca ccatcaccat caccatcact gaaag**ctt**ga
```

2.4.2   pPCR-Script

Figure 2-4. pPCR-Script vector promoter and multiple cloning site region (sequence shown 598-826).
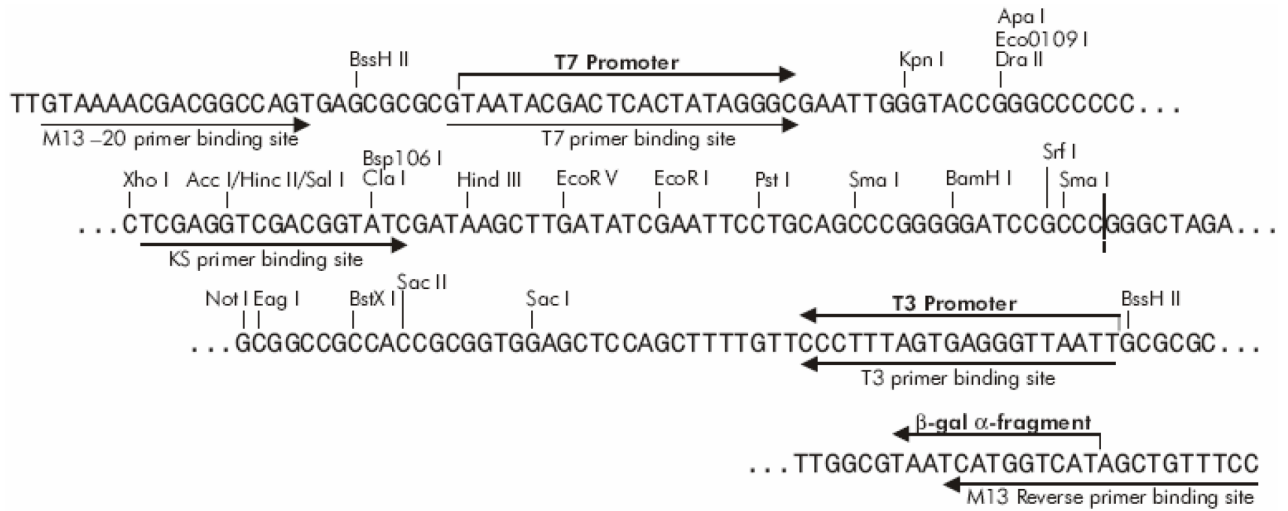
Figure 2-5. pPCR-Script_TAP2_C213 vector circle map and sequence reference points.
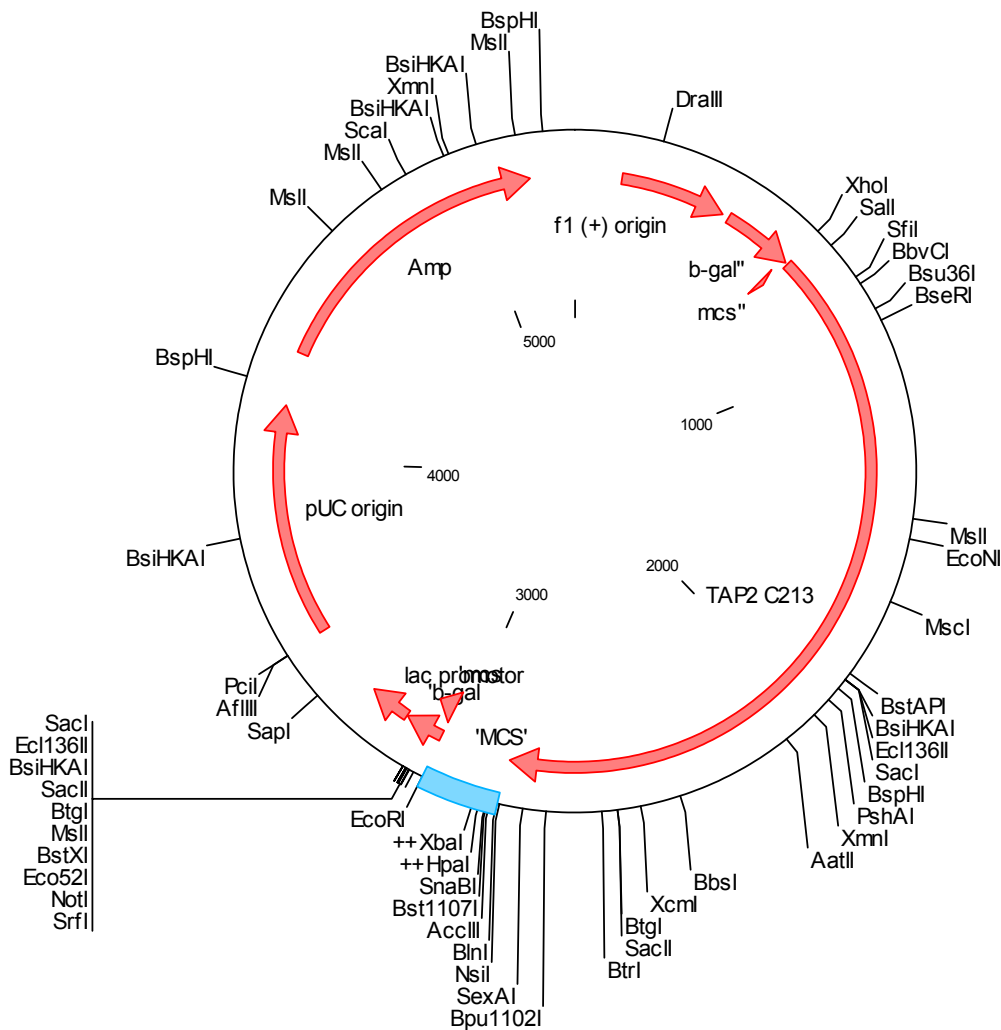
Figure 2-6. DNA sequence of TAP2_C213 (start 674, end 2839).

```
 661  gccccccctc gag**atg**agac tgcctgacct gagaccctgg acctctctgc tgctggtcga
 721  cgctgctctg ctgtggctgc tgcaaggtcc actgggtacc ctgctgccac aaggtctgcc
 781  tggtctgtgg ctggaaggca ccctgagact gggcggcctg tggggcctgc tgaagctgag
 841  gggcctgctg ggcttcgtcg gcactctgct gttgcctctg tccctggcta cccctctgac
 901  cgtctccctg agggctctgg tcgctggcgc ttccagggct cctcctgcta gagtcgcctc
 961  tgctccttgg tcttggctgt tggtcggcta cggcgctgct ggcctgtcct ggtccctgtg
1021  ggctgtcctg tcccctcctg cgctcagga aaaggaacaa gatcaggtca acaacaaggt
1081  cctgatgtgg cgtctgctta agctgtccag acctgacctg cctctgctgg tcgctgcttt
1141  cttcttcctg gtcctggccg tcctgggtga accctgatc ccacactact ccggcagagt
1201  catcgacatc ctgggcggcg acttcgaccc tcacgctttc gcttccgcta tcttcttcat
1261  ggccctgttc tccttcggtt cttccctgtc cgctggtgcc agaggcggtt gtttcaccta
1321  caccatgtcc agaatcaacc tgagaatcag agaacaactg ttttcctccc tgctgagaca
1381  ggacctgggc ttcttccagg aaaccaagac cggcgaactg aactccagac tgtcctccga
1441  caccaccctg atgtccaact ggctgccttt aaacgctaac gtcctgctga tccctggt
1501  caaggtcgtc ggcctgtacg gtttatgct gtctatctcc cctagactga ccctgctgtc
1561  cctgctgcac atgcctttca ccatcgctgc tgaaaaggtc tacaacacca gacaccagga
1621  agtcttaaga gaaatccagg acgctgtcgc tagagctggc caggtcgtca gagaagctgt
1681  cggcggcctg caaaccgtca gatccttcgg cgctgaagaa cacgaagtct ccagatacaa
1741  ggaagctctg aacagtcca gacagctgta ctggagaaga gacctggaaa gagccctgta
1801  cctgctggtc agaagagtcc tgcacctggg agtccagatg ctgatgctgt ccgtcggtct
1861  gcaacagatg caggacggcg agctcacaca gggctccctg ctgtccttca tgatctacca
1921  ggaatctgtc ggctcctacg tccagaccct ggtctacatc tacggcgaca tgctgtccaa
1981  cgtcggtgcc gccgagaagg ttttctccta catggacaga cagcctaacc tgccttcccc
2041  tggcaccctg gctcctacca ccctgcaagg agtcgtcaag ttccaggacg tctctttcgc
2101  ttaccctaac agacctgata ggcctgtcct gaagggcctg accttcaccc tgagacctgg
2161  cgaagtcacc gctctggtcg ccctaacgg ttctggcaag tccaccgtcg ctgctctgct
2221  gcagaacctg taccagccta ccggcggcca ggtcctgctg gacgaaaagc ctatctccca
2281  gtacgaacac cactacctgc actcccaggt cgtctccgtc ggccaggaac ctgtcctgtt
2341  ctccggctcc gtcagaaaca acatcgctta cggcctgcag tcctccgaag acgacaaggt
2401  catggctgct gctcaggctg ctcacgctga cgacttcatc caggaaatgg aacacggcat
2461  ctacaccgat gtcggcgaaa agggctccca actggctgct ggtcagaagc agagactggc
2521  tatcgctagg gctctggtca gagatccgcg ggtcctgatc ctggacgaag ctacctccgc
2581  tctggacgtg cagtccgaac aggctctgca ggactggaac tccagaggcg acagaaccgt
2641  cctggtcatc gctcacagac tgcagaccgt ccagagagcc caccagatcc tggtcctgca
2701  agaaggcaag ctgcagaagc tggctcagct gcaagagggc caggacctgt actccagact
2761  ggtccagcag agactgatgg acctggtccc tagaggctcc ggtggatctg cttggagaca
2821  tccacagttc ggtggt**tga**a
```

2.4.3   pFastBac1

Figure 2-7. pFastBac1 vector promoter and multiple cloning site region (sequence shown 3901-4400).
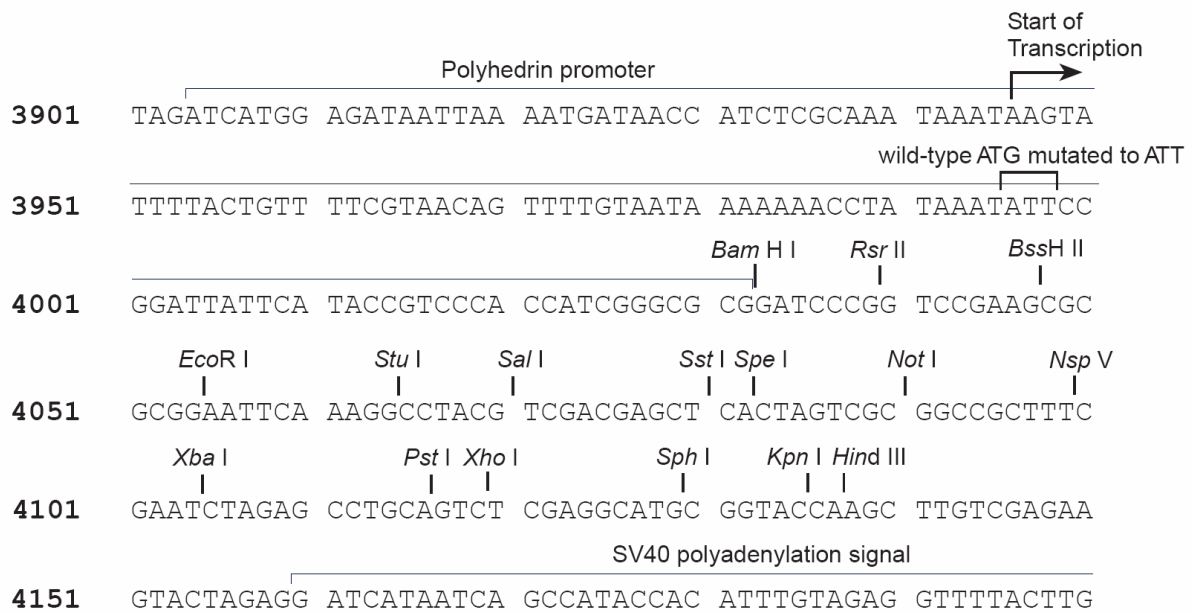
Figure 2-8. pFastBac1 vector circle map and sequence reference points.

31
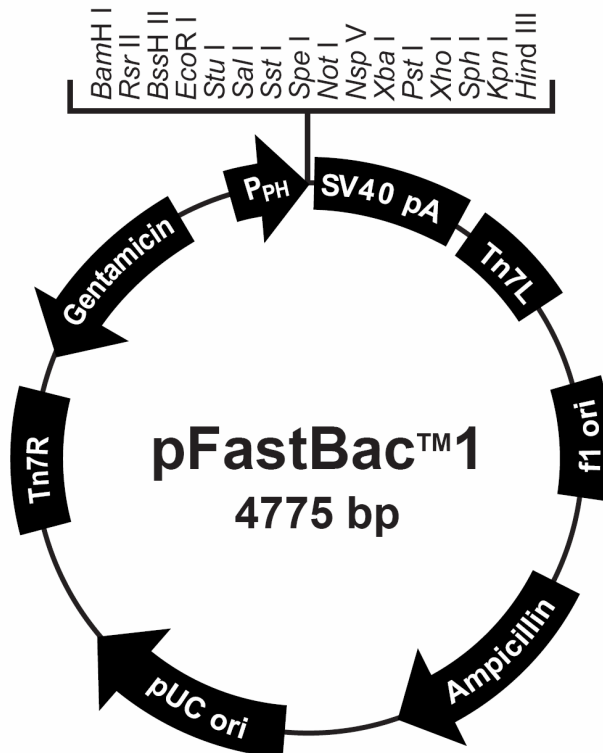
3.   Methods

3.1   Molecular cloning

3.1.1   *E. coli* culture

E. coli DH5α cells were grown in LB-medium (10 g trypton, 5 g yeast extract, 10 g NaCl per liter) at 37°C. If not indicated, 100 µg/ml ampicillin (final concentration) was added after autoclaving. *E. coli DH10Bac* was grown in LB-medium containing 50 µg/ml kanamycin and 10 µg/ml tetracycline.

3.1.2   Preparation of *E. coli DH*5α competent cells

Transformation buffer 1 (TFB-1)	**Transformation buffer 2 (TFB-2)**
30 mM K-acetate	10 mM MOPS
100 mM RbCl	10 mM RbCl
50 mM MnCl$_2$	75 mM CaCl$_2$
10 mM CaCl$_2$	15 % glycerol
15% glycerol	pH 6.8
pH 5.8	

The following protocol was used to prepare batches of competent bacteria that yield 5×10^6 to 2×10^7 transformed colonies/µg of supercoiled plasmid DNA. This efficiency of transformation is high enough to allow all routine cloning in plasmids to be performed with ease. Competent cells made by this procedure are preserved at -80°C, although there may be some deterioration in the efficiency of transformation during prolonged storage.

- Inoculate 5 ml of LB medium without ampicillin with 100 µl of *E. coli DH*5α cells.
- Incubate the culture overnight at 37°C.
- Inoculate 100 ml of LB medium with 5 ml from the previous overnight culture.
- Incubate the culture for 2-3 h until the $OD_{600} = 0.3 - 0.5$ at 37°C.
- Transfer the culture to ice, and keep it for 10 min on ice.
- Centrifuge the cells for 10 min at 2,000 x g, 4°C.
- Resuspend gently the pellets in 15 ml ice cold TFB-1 buffer.
- Incubate the cell suspension for 1 h at 4°C.
- Centrifuge the cell suspension for 10 min at 3,000 x g, 4°C.
- Resuspend gently the pellet in 4 ml of TFB-2 buffer.
- Split the competent cells in 100 µl aliquots and freeze them in liquid nitrogen.

- Store the cells at -80°C.

3.1.3   Preparation of *E. coli DH10Bac* competent cells

In order to prepare *E. coli DH10Bac* competent cells, the same procedure was applied as indicated at 3.1.2, except for LB-medium containing 50 µg/ml kanamycin and 10 µg/ml tetracyclin.

3.1.4   Transformation of Rb-competent *E. coli* cells

- Transfer an aliquot of competent cells (100 µl) to an ice bath, and allow it to thaw on ice.
- Add DNA (not more than 1 µg in a volume of 10 µl). Mix by gently swirling.
- The cells are incubated on ice for 30 min.
- Transfer the cells to 42°C for 90s.
- Allow the cells to recover for 1-2 min at 4°C.
- Add 500 µl of LB medium without antibiotic.
- Incubate the culture for 45 min at 37°C; the cells may be gently agitated (50 cycles/min or less in a rotary shaker).
- Transfer 100 µl of transformed competent cells onto agar LB plate containing the appropriate antibiotic (*e.g.* 100 µg/ml ampicillin).
- The rest of the cells (500 µl) are centrifuged at 20,000 x g for 30s at 25°C. Resuspend the cell pellet in 100 µl of LB medium without antibiotic.
- Transfer the cell suspension onto agar plate containing the appropriate antibiotic (*e.g.* 100 µg/ml ampicillin).

3.1.5   DNA isolation

To obtain highly purified plasmids for sequencing and restriction analysis, DNA was isolated by MN Mini kit (MACHEREY-NAGEL GmbH & Co. KG, Germany).

3.1.6   Oligonucleotide-directed mutagenesis (Ligase Chain Reaction)

Oligonucleotide-directed mutagenesis is used to introduce point mutations in a particular gene.

3.1.6.1 Primer phosphorylation

- Phosphorylation of oligonucleotide primers with bacteriophage T4 polynucleotide kinase.

Synthetic oligonucleotide	200 pmoles
10x bacteriophage T4 polynucleotide kinase buffer (Fermentas)	2 µl
10 mM ATP (Fermentas)	2 µl
bacteriophage T4 polynucleotide kinase (Fermentas)	4 units
H_2O	to 20 µl

- Incubate the reaction for 30 min at 37°C and then inactivate the polynucleotide kinase for 10 min at 70°C.

3.1.6.2 Ligase chain reaction (LCR)

- Anneal the phosphorylated mutagenic oligonucleotide primer to the double stranded plasmid DNA containing the target sequence.

Double-stranded template DNA (~200 ng)	0.5 pmoles
Phosphorylated mutagenic oligonucleotide	20 pmoles
10x PCR buffer (+20 mM $MgSO_4$) (Fermentas)	10 µl
2 mM dNTP (Fermentas)	10 µl
100 mM NAD (Fermentas)	1 µl
Pfu DNA polymerase (Fermentas)	2.5 units
AmpLigase (Epicentre)	5 units
H_2O	to 100 µl

- Perform the following LCR-program:

95°C	3 min	
95°C	1 min	
60°C*	1 min	30x (typical 2 min pro 1 kbp template)
65°C	10 min 30s	
65°C	10 min	
4°C	pause	

* annealing temperature is primer dependent, and should not exceed 65°C

3.1.6.2.1 PCR purification

The LCR-product is purified using the PCR Purification Kit (Qiagen).

3.1.6.2.2 Selection of mutants with *DpnI*

The products of the amplification reaction are treated with the restriction enzyme *DpnI*, which specifically cleaves fully methylated $G^{Me6}ATC$ sequences, but it will not digest DNA synthetized during the course of the LCR (Sambrook and Russell, 2001).

10x Y+ Tango buffer (Fermentas)	2 µl
Purified LCR product	19 µl
DpnI (Fermentas)	20 units
H_2O	to 23 µl

Incubate the reaction for 6 – 24 h at 37°C and then inactivate the restriction enzyme by heating for 20 min at 80°C.

3.1.6.2.3 Transformation of amplified product

In a sterile microfuge tube mix:

Restriction digest	10 µl
E.coli DH5α competent cells	100 µl

then perform the standard transformation into *E.coli DH5α* competent cells (see 3.1.4).

3.1.7   Directional cloning into plasmid vectors

Directional cloning requires that the plasmid vector is cleaved with two restriction enzymes that generate incompatible termini and that the fragment of DNA to be cloned carries termini that are compatible with those of the doubly cleaved vector (Sambrook and Russel, 2001). The present protocol describes the cloning procedure, as example, when termini are produced by restriction endonucleases *BamHI* and *HindIII*.

3.1.7.1 Target DNA restriction, isolation and purification

Tris-acetate EDTA buffer (TAE)
40 mM Tris-acetate
1 mM EDTA
pH 8.3

1. In a sterile microfuge tube mix:

- target DNA (2 – 4 µg)	3 µl
- *BamHI* (Fermentas)	20 units
- *HindIII* (Fermentas)	20 units
- 10x Y+ Tango buffer (Fermentas)	4 µl
- H_2O	40 µl

2. Incubate the reaction for 2 h at 37°C.

3. Run electrophoresis on 0.8% agarose in TAE buffer and visualize under UV light.

4. Excise the target band from the gel.

5. Purify the target DNA using the QIAquick Gel Extraction Kit (Qiagen), elute the DNA in 30 µl elution buffer (Qiagen) and visualize an aliquot on 0.8% agarose gel electrophoresis.

3.1.7.2 Vector DNA isolation and purification

1. In a sterile microfuge tube mix:

- vector DNA (2 – 4 µg)	5 µl
- *BamHI* (Fermentas)	20 units
- *HindIII* (Fermentas)	20 units
- 10x Y+ Tango buffer (Fermentas)	4 µl
- H$_2$O	40 µl

2. Incubate the reaction for 2 h at 37°C.

3. Run electrophoresis on 0.8% agarose in TAE buffer and visualize under UV light.

4. Excise the band from the gel, which represents the vector DNA.

5. Purify the vector DNA using the QIAquick Gel Extraction Kit (Qiagen), and visualize it on 0.8% agarose gel electrophoresis.

3.1.7.3 Ligation

1. In a sterile microfuge tube mix:

- 10x Ligation buffer (Fermentas)	1.5 µl
- T4 DNA ligase (Fermentas)	7.5 units
- target DNA	1 µl
- vector DNA	6 µl
- molar ratio between target : vector	1:6
- H$_2$O	ad to 15 µl

2. Incubate the reaction mixture overnight at 16°C or for 4 h at 20°C.

3. Inactivate the DNA ligase by incubating the reaction mixture for 20 min at 70°C.

4. Transform competent *E. coli DH5α* cells with ligation reaction.

3.1.8   Plasmid construction for generation of baculovirus

Point mutations were generated by ligase chain reaction using various mutagenic primers (Tables 3-1; 3-2) and the plasmids pGEM3Z_TAP1_cys-less and pPCR-Script_TAP2_C213 as templates (Figures 2-1 to 2-6). To validate the introduced mutations, the *tap1* and *tap2* genes were sequenced using sequencing primers (Tables 3-3; 3-4).

3.1.8.1 Generation of single cysteine mutants of the coupling helix 1 (TAP1)

When plasmid pGEM3Z_TAP1_cys-less was used for generation of baculovirus, the *tap1* gene containing the desired mutation was excised with the restriction enzymes *BamHI* and *HindIII* (Fermentas), and purified using the QIAquick Gel Extraction Kit (Qiagen). Subsequently, pFastBac1_TAP1_cys-less was digested with *BamHI* and *HindIII* and the linearized vector was purified. After ligation, the following mutants (TAP1) were obtained: Q277C, G282C, N283C, I284C, M285C, S286C, R287C, and V288C.

Alternatively, a fragment of *tap1* gene (437 bp) containing the desired mutation was excised with the restriction enzymes *BspTI* and *MluI* (Fermentas) and purified. Subsequently, the pFastBac1_TAP1_cys-less was digested with *BspTI* and *MluI* and the linearized vector was purified. After ligation, the following mutations were generated: T273C, E274C, F275C, Q278C, and N279C.

3.1.8.2 Generation of single cysteine mutants of the coupling helix 2 (TAP1)

A similar approach has been used, as described above with one modification. In this case the fragment of the *tap1* gene (322 bp) and pFastBac1_TAP1_cys-less were treated with the restriction enzymes *SphI* and *StuI* (Fermentas). After ligation, the following mutations were confirmed by sequencing: I368C, E369C, A370C, P375C, T376C, V377C, R378C, S379C, F380C, A381C, and N382C.

3.1.8.3 Generation of single cysteine mutant of the X-loop (TAP1)

A similar approach has been used, as described above with one modification. A fragment of the *tap1* gene (866 bp) containing the mutation E638C was excised with the restriction enzymes *Bsp119I* and *HindIII* (Fermentas) and purified. Subsequently, the pFastBac1_TAP1_cys-less was digested with *Bsp119I* and *HindIII* and the linearized vector was purified. After ligation, the introduced mutation was confirmed by sequencing (pFastBac1_TAP1_E638C).

3.1.8.4 Generation of single cysteine mutants of the X-loop (TAP2)

From previous studies in our group (unpublished data), it has been shown that Cys213 (TAP2) was essential in preserving the TAP function. Therefore, for generation of single cysteine mutants of X-loop (TAP2) the plasmid pPCR-Script_TAP2_C213 was used as template for LCR. Afterwards, a 500 bp fragment of the *tap2* gene containing the desired mutation was excised with the restriction enzymes *AjiI* and *AatII* (Fermentas) and purified. pFastBac1_TAP2_C213 was linearized with *AjiI* and *AatII* and purified. After ligation the following single cysteine mutations were confirmed by sequencing: E602C, E602R, E602D, and E602A.

Table 3-1. Primer sequences used for LCR. Single cysteines were introduced into the cysteine-less TAP1 and single cysteine TAP2 (C213) coding sequence by site-directed mutagenesis, employing the mutagenic oligonucleotides (in each case the cysteine codon is in bold underlined).

Primer	Sequence
TAP1 T273C	CGT CCT GAG ACA GGA A**TG C**GA ATT CTT CCA
TAP1 E274C	GAC AGG AAA CC**T GC**T TCT TCC AGC AGA AC
TAP1 F275C	AAC CGA ATT C**TG C**CA GCA GAA CCA GAC
TAP1 Q277C	CCG AAT TCT TCC AG**T GC**A ACC AGA CCG GC
TAP1 Q278C	GAA TTC TTC CAG **TGC** AAC CAG ACC GGC AAC AT
TAP1 N279C	TTC TTC CAG CAG **TGC** CAG ACC GGC AAC AT
TAP1 G282C	GCA GAA CCA GAC C**TG C**AA CAT CAT GTC C
TAP1 N283C	CAG AAC CAG ACC GGC **TGC** ATC ATG TCC AGA G
TAP1 I284C	GAC CGG CAA C**TG C**AT GTC CAG AG
TAP1 M285C	GAC CGG CAA CAT C**TG C**TC CAG AGT CAC CGA AG
TAP1 S286C	GGC AAC ATC ATG **TGT** AGA GTC ACC GAA GA
TAP1 R287C	GCA ACA TCA TGT CC**T GC**G TCA CCG AAG ATA C
TAP1 V288C	CGG CAA CAT CAT GTC CAG A**TG C**AC CGA AGA TAC G
TAP1 I368C	CCC AGG TCG CT**T GC**G AAG CCT TAA GTG
TAP1 E369C	CAG GTC GCT ATC **TGC** GCC TTA AGT GCT A
TAP1 A370C	GGT CGC TAT CGA A**TG C**TT AAG TGC TAT GCC
TAP1 P375C	GCC TTA AGT GCT ATG **TGT** ACC GTC AGA TCC
TAP1 T376C	GTG CTA TGC CT**T GC**G TCA GAT CCT TC
TAP1 V377C	TGC TAT GCC TAC C**TG C**AG ATC CTT CGC TAA
TAP1 R378C	TAT GCC TAC CGT C**TG C**TC CTT CGC TAA C
TAP1 S379C	CCT ACC GTC AGA **TGC** TTC GCT AAC GAA GA

TAP1 F380C	TAC CGT CAG ATC C**TG C**GC TAA CGA AGA AG
TAP1 A381C	CAG ATC CTT C**TG T**AA CGA AGA AGG CGA AGC TC
TAP1 N382C	AGA TCC TTC GCT **TGC** GAA GAA GGC GAA GCT C
TAP1 E638C	GAC ACC GAA GTA GAC **TGT** GCT GGC TCT CA
TAP1 R659C	GAC CCC TGA TC**T GT**A AGC CTT CCG TCC TG
TAP2 L3C	CTC GAG ATG AGA **TGT** CCT GAC CTG AGA
TAP2 T43C	TCT GTG GCT GGA AGG C**TG C**CT GAG ACT G

Table 3-2. Primer sequences used for LCR (E602, TAP2). The highly conserved E602 of X-loop (TAP2) has been mutated to C, R, A and D using the plasmid pPCR-Script_TAP2_ C213 as template, employing the mutagenic nucleotides (in each case the mutated codon is in bold underlined).

Primer	Sequence
TAP2 E602C	TAC ACC GAT GTC GGC **TGC** AAG GGC TCC CAA CTG
TAP2 E602R	CCG ATG TCG GC**A GA**A AGG GCT CCC AAC T
TAP2 E602A	TAC ACC GAT GTC GGC **GCT** AAG GGC TCC CAA CT
TAP2 E602D	CCG ATG TCG GC**G AT**A AGG GCT CCC AAC T

Table 3-3. Primers used for TAP1 sequencing.

Primer	Sequence
TAP1 Seq 0F	GTG CTG CAA GGC GAT TAA GT
TAP1 Seq 3F	CTG CTC TGG GCC TGG CC
TAP1 Seq 4F	GGG TTC CGA AAC CAG AAG AC
TAP1 Seq 5F	GTC AGA GGC CTG GCC CTG
TAP1 Seq 6F	TGC TAT GCC TAC CGT CAGAT
TAP1 Seq 8F	CAA GCC TCT GCC TCA GTA CG
TAP1 Seq 9F	GAC CTG GCG AAG TCA CC
TAP1 Seq 6R	AGC AGG CCA CTA GGT GG

Table 3-4. Primers used for TAP2 sequencing.

Primer	Sequence
TAP2 Seq 2F	GTA AAA CGA CGG GCA GTG AG
TAP2 Seq 9F	GAC CTG GCG AAG TCA CC
TAP2 Seq 2R	AGC AGG AGG AGC CCT GG
TAP2 Seq 12R	ACA AGC TTT CAA CCA CCG

3.1.9   Transposition in *DH10Bac*

SOC Medium

Tryptone	20 g
Yeast extract	5 g
NaCl	0.5 g
KCl	0.186 g
$MgCl_2$	10 mM
Glucose	20 mM
H_2O	to 1000 ml

LB Medium (Luria-Bertani)

Tryptone	10 g
Yeast extract	5 g
NaCl	10 g
Bacto agar	15 g
H_2O	to 1000 ml

100 µl of competent *DH10Bac* cells were thawed on ice. 6 µl (20 ng) of pFastBac1 from miniprep was added to the cells and the mixture was incubated for 30 min on ice. Then, the cells were heat-schocked for 45s at 42°C and immediately transferred to 4°C for 2 min. Then 900 µl of SOC medium was added and cells were subsequently incubated at 37°C for 4 h. Cells were then spinned down and diluted serially with SOC medium to 10^{-1}, 10^{-2} and 10^{-3}. 100 µl mixture of each dilution was plated onto LB agar plates containing 50 µg/ml kanamycin, 7 µg/ml gentamicin, 10 µg/ml tetracyclin, 100 µg/ml Bluo-gal and 40 µg/ml IPTG. Insertions of the mini-Tn7 into the mini-*att*Tn7 attachment site on the bacmid disrupt the expression of the LacZα peptide, so colonies containing the recombinant bacmid are white in a background of blue colonies that harbor the unaltered bacmid. Plates were incubated at 37°C for 48 h for development of blue-white colonies. The white colonies were selected for amplification to isolate the recombinant bacmids for transfection of insect cells.

3.1.9.1 Isolation of recombinant bacmid DNA (according to Invitrogen)

Solution-1-bacmid buffer   **Solution-2-bacmid buffer**
15 mM Tris-HCl (pH 8.0)   0.2 N NaOH
10 mM EDTA   1% (w/v) SDS
100 µg/ml RNase A (Macherey-Nagel)

LB Medium   **K-acetate buffer**

Tryptone	10 g	3 M K-acetate
Yeast extract	5 g	pH 5.5
NaCl	10 g	
H_2O	1000 ml	
pH 7.0		

- Inoculate a single, isolated bacterial colony in 2 ml of LB medium containing 50 µg/ml kanamycin, 7 µg/ml gentamicin, and 10 µg/ml tetracyclin. The culture is grown at 37°C overnight.

- Centrifuge 1.5 ml of bacterial culture for 1 min, at 14,000 x g, 4°C.

- Resuspend the cell pellet in 0.3 ml of Solution-1-bacmid buffer.

- Add 0.3 ml of Solution-2-bacmid buffer and mix gently. Incubate at room temperature for 5 min.

- Add slowly 0.3 ml of 3M K-acetate. Mix gently during addition. Incubate the sample on ice for 10 min.

- Centrifuge for 10 min at 14,000 x g.

- Mix the supernatant with 0.8 ml isopropanol. Invert the tube several times to mix and incubate on ice for 10 min.

- Centrifuge the sample for 15 min at 14,000 x g at room temperature.

- Add to the pellet 0.5 ml 70% ethanol. Invert the tube several times to wash the pellet.

- Centrifuge for 5 min at 14,000 x g at room temperature.

- Air dry the pellet for 5-10 min at room temperature.

- Dissolve the DNA pellet in 40 µl of 1 x AE buffer (Qiagen).

- Store the DNA at +4°C.

3.1.9.2 Analyzing recombinant bacmid DNA by PCR (according to Invitrogen)

In order to verify the presence of the gene of interest in the recombinant bacmid by PCR, the M13 forward and M13 reverse primers (Table 3-5) together with Taq polymerase (Invitrogen) were used. The bacmid containts M13 forward and M13 reverse priming sites flanking the mini-*att*Tn7 site within the *lacZα*-complementation region to facilitate PCR analysis.

Table 3-5. Primers used for analyzing recombinant bacmid DNA by PCR.

Primer	Sequence
M13 forward	GTT TTC CCA GTC ACG AC
M13 reverse	CAG GAA ACA GCT ATG AC

a)   For each sample, set up the following PCR reaction (50 µl):

Recombinant bacmid DNA (100 ng)	1 µl
10x Taq PCR buffer (Fermentas)	5 µl
10 mM dNTP (Fermentas)	1 µl
50 mM $MgCl_2$	1.5 µl
PCR primers (1.25 µl each 10 µM stock)	2.5 µl
H_2O	38.5 µl
Taq polymerase (5 units/µl) (Invitrogen)	2.5 units

b)   For amplification the following cycling parameters were used:

Step	Time	Temperature	Cycles
Initial denaturation	5 min	95°C	1
Denaturation	1 min	95°C	
Annealing	1 min	52°C	30
Extension	5 min	72°C	
Final extension	10 min	72°C	1

c)   Remove 10 µl from the reaction and analyze by agarose gel electrophoresis (0.8%).

3.2   Cell Culture

3.2.1   Monolayer culture of Sf9 insect cells

Spodoptera frugiperda (Sf9) monolayer culture was grown in SF900 II medium (Invitrogen) supplemented with 50 units/ml penicillin, 0.05 mg/ml streptomycin, 0.2% pluronic acid, 0.5 µg/ml fungizone and 5% fetal calf serum. Before passage, medium and floating cells from a confluent monolayer were discarded by aspiration. 10 ml of

supplemented SF900 II medium was added to 75 cm^2 flask. Cells were then detached from the surface by tapping the flask. 2.5 ml of cells were diluted into a new flask in 10 ml medium and incubated at 27°C.

3.2.2   Shaker culture of Sf9 insect cells

The culture flask was incubated at 27°C in less than 1/4 of the total flask volume until it reaches a cell density of 2×10^6 cells/ml. Then cells were diluted to 0.4×10^6 cells/ml with supplemented SF900 II medium and placed on a rotary shaker (60 rpm).

3.2.3   Transfection of Sf9 insect cells

2×10^6 Sf9 insect cells were seeded onto a 60 mm tissue plate. Initially cell density should be 50-70% confluent. Cells were incubated at 27°C for 1 h to allow them to attach firmly onto the plate. Then the culture medium was removed and 1 ml of transfection buffer A (BD Bioscience) was added to the plate. All areas of the plate should be covered by this buffer. 5 μg of bacmid DNA from mini-prep was mixed with 1 ml transfection buffer B (BD Bioscience). Subsequently the mixture was added to the plate drop by drop. After every two or three drops, the plate should be gently rotated to facilitate the mixing of buffer B with buffer A. Following incubation of the plate at 27°C for 4 h, the transfection solution was removed and 3 ml of fresh SF900 II medium (Invitrogen) was added. The plate was incubated at 27°C for 5-7 days before the recombinant virus (P1 stock) can be harvested.

3.2.4   Virus amplification

3 ml of P1 virus stock harvested from transfection generally have a titre of 1×10^7 pfu/ml. Viruses were amplified two times before going for infection of cells in large scale. 10 ml P2 virus stock was obtained by infecting 1.2×10^6 cells of monolayer in 75 cm^2 flask for 5 days with 1 ml P1 stock; after that, 25 ml of P3 can be harvested from infection of 3×10^7 cells with 3 ml in 175 cm^2 flask for 5 days. For large scale virus amplification, 6×10^8 cells in 500 ml were infected with 10 ml P3 stock; after 6-8 days the virus is harvested and stored at 4°C. Typically, 98% cells should be dead as determined by trypan blue staining.

3.2.5   Co-transfection of Sf9 insect cells with TAP1/TAP2 viruses

Phosphate-buffered saline (PBS)

137 mM NaCl
2.7 mM KCl
10 mM Na$_2$HPO$_4$
2 mM KH$_2$PO$_4$
H$_2$O 1000 ml
pH 7.4

100 ml of Sf9 insect cells were grown at 27°C in a Erlenmeyer flask to a density of 1.8 x 10^6 cells/ml. 5 ml of virus P4 stock (TAP1) and 10 ml of virus P4 stock (TAP2) were added and the culture was incubated for 48 h. Typically, 30% cells are dead at this time point. Subsequently the cells were harvested by centrifugation at 200 x g for 5 min. Cell pellets were washed with 20 ml PBS buffer once and were frozen at -20°C.

3.2.6   Determination of virus titer by plaque assay

Neutral red/PBS solution

1 vol 0.4% Neutral red (Invitrogen)
19 vol PBS

Sf9 cells (1 x 10^6 cells) were seeded into 35 mm petri dishes and incubated at room temperature for 2 h. Virus stock was serially diluted from 10^{-1}, 10^{-2}, to 10^{-7}. After removal of the medium from the culture, 100 µl of virus dilution was added, then the mixture was incubated at room temperature for 1h with gently agitation every 15 min. During incubation, the agarose solution was prepared by mixing 8 ml medium with 4 ml 3% low melting agarose (plus 120 µl X-gal 25 mg/ml in DMF). After this, the viral solution was removed and 2 ml of 1% agarose solution (40°C) was added onto each dish. When the agarose solidified, 1 ml of medium was overlaid on it. The dishes were kept at 27°C for 3-4 days and then stained with 1 ml Neutral Red/PBS solution. After incubation at 27°C in the dark for 2h, the liquid was removed. Incubation of inverted dishes overnight resulted in several white plaques in dark red background. Each plaque is generated by infection of Sf9 cells with an individual baculovirus particle, therefore the total amount of the virus can be determined.

3.3   General biochemical methods

3.3.1   SDS-PAGE

Sample buffer   **Running buffer**

150 mM Tris (pH 6.8)   25 mM Tris

6 % (w/v) SDS   192 mM glycine

30 % (v/v) glycerol   0.1% (w/v) SDS

0.3 % (w/v) bromophenol blue   pH 8.3

300 mM DTT

Stacking gel buffer   **Separating gel buffer**

500 mM Tris   1500 mM Tris

0.4% (w/v) SDS   0.4% (w/v) SDS

pH 6.8   pH 8.8

The acrylamide solution consists of 30% acrylamide and 0.8% N,N'-methylenebisacrylamide. Stock aliquots of 10% ammonium peroxydisulfate (APS) are prepared in H_2O and stored at -20°C. Before electrophoresis the proteins were denatured in sample buffer. Membrane proteins were incubated for 20 min at 65°C. The SDS electrophoresis was performed at 150 V for 1-1.5 h in running buffer for electrophoresis.

Table 3-6. Composition of stacking and running gel according to Laemmli (Laemmli, 1970) for 8 gels.

	Stacking gel 5%	Separating gel 7.5%	10%	12%
Acrylamide	6.8 ml	18 ml	24 ml	29 ml
Stacking gel buffer	5 ml	-	-	-
Running gel buffer	-	18 ml	18 ml	18 ml
H_2O	28 ml	36 ml	30 ml	25 ml
APS	320 μl	470 μl	470 μl	470 μl
TEMED	32 μl	40 μl	40 μl	40 μl

3.3.2   Immunoblotting

Transfer buffer   **Blocking buffer**

25 mM Tris-HCl   10 mM Tris-HCl pH 8.0

192 mM glycine   150 mM NaCl

20% methanol (v/v)   0.1% (v/v) Triton X-100

pH 8.2   7% (w/v) skim milk powder

                                                             0.1% (w/v) NaN_3

Tris-buffered saline with triton (TBS-T)   **Electrochemiluminescence buffer 1 (ECL-1)**

10 mM Tris-HCl   2.5 mM Sodium luminol

150 mM NaCl   0.4 mM Coumaric acid

0.1% (v/v) Triton X-100   100 mM Tris-HCl (pH 8.5)

pH 8.0

Electrochemiluminescence buffer 2 (ECL-2)

100 mM Tris-HCl (pH 8.5)

0.019% (v/v) H_2O_2

To transfer proteins from the gel onto nitrocellulose, a blotting sandwich was prepared with the following layers: 1) filter paper soaked in transfer buffer, 2) gel, 3) membrane soaked in transfer buffer (in the case of PVDF membrane, it should be soaked in methanol for 1 min previously), 4) filter paper soaked in transfer buffer. The sandwich was set onto a semidry blotting apparatus (Bio-Rad Laboratories GmbH, Germany) with the nitrocellulose/PVDF membrane facing the anode. The electroblotting was performed at constant current (100 mA per mini gel) for 90 min. For immunodetection, the membrane was blocked with blocking buffer for at least 30 min at room temperature or overnight at 4°C. The membrane was incubated at room temperature for 1 h with the primary antibody diluted in TBS-T buffer (1:20 dilution). After 3 times washing with TBS-T for 10 min, the membrane was incubated with horseradish peroxidase conjugated second antibody (1:30,000 dilution) for 1 h. Subsequently, the membrane was washed again 3 times and incubated with 10 ml ECL-1 buffer for 1 min, followed by 10 ml ECL-2 buffer for 1 min. The chemiluminescent signal was detected by a LumiImager (ROCHE).

3.4   Biochemical assays for TAP

3.4.1   Preparation of crude membranes

Phosphate buffered saline (PBS)   **Tris buffer**

137 mM NaCl   10 mM Tris-HCl

2.7 mM KCl   pH 7.5

10 mM Na_2HPO_4

2 mM KH_2PO_4

pH 7.4

Protease inhibitors mix

50 µg/ml AEBSF hydrochloride

1 µg/ml aprotinin

10 μg/ml leupeptin

5 μg/ml pepstatin A

150 μg/ml benzamidin

200 ml of Sf9 insect cells (1.8×10^6 cells/ml) were co-transfected with baculoviruses encoding for *tap1* and *tap2* genes at MOI (multiplicity of infection) of 5. After 48 h, the cells were harvested by centrifugation at 2,600 x g for 10 min, at 4°C and washed once with PBS containing 15% (v/v) glycerol plus 1 mM DTT. The pellets were frozen at -20°C for 1 h, followed by thawing on ice. Sf9 pellets were resuspended in 20 ml of Tris buffer and 1% protease inhibitors plus 1 mM DTT. After incubation on ice for 30 min, cells were then homogenized by a glass douncer and centrifuged at 200 x g for 4 min followed by 700 x g for 8 min at 4°C. The resulting supernatant was centrifuged at 154,000 x g in a Ti70 rotor for 30 min at 4°C. The pellet was resuspended in 4 ml PBS pH 7.4 plus 1 mM DTT, and aliquots were frozen in liquid nitrogen and stored at -80°C. Typically aliquots of 100 μl had a protein concentration of 5 mg/ml.

3.4.2   Peptide labeling with Na^{125}I

RRY(^{125}I)QKSTEL – radioactive labeled peptide

1 mg/ml chloramine T

0.17 mg/ml sodium disulfite ($Na_2S_2O_5$)

10% (v/v) bovine serum albumin (BSA)

Dowex 1x8 anion exchange

PBS buffer, pH 7.0

The chloramine T method, a chemical oxidation, covalently couples iodine to tyrosine residue (Hunter and Greenwood, 1964). The reaction was started by adding to 50 μl of 88 μM peptide, 10 μl Na^{125}I (100 μCi), and 10 μl chloramine T (1 mg/ml in PBS 7.0). After 5 min incubation at room temperature, the reaction was stopped by addition of 120 μl $Na_2S_2O_5$. Free iodine was removed by anion exchange chromatography using Dowex 1 x 8 material. Initially, Dowex (10 mg) was equilibrated in PBS buffer containing 0.2% dialyzed BSA and was washed 3 times with PBS buffer without BSA. The dowex suspension (250 μl) was added to the reaction mix, vortexed and incubated for 5 min at room temperature. The suspension was applied to an empty spin column and centrifuged for 30 sec at 500 x g. The flow-through contained the radiolabeled peptide in a concentration of 10 μM.

3.4.3   Peptide binding assay

3.4.3.1 Peptide binding assay (Centrifugation assay)

PBS buffer	**Binding buffer**
137 mM NaCl	PBS buffer
2.7 mM KCl	5 mM $MgCl_2$
8.1 mM Na_2HPO_4	pH 7.0
1.8 mM KH_2PO_4	
pH 7.0	

Lysis buffer	**RRYC(F)KSTEL (C4F) peptide**
PBS buffer	**RRYQKSTEL (R9LQK) peptide**
1% (w/v) SDS	
pH 7.0	

Crude membranes (100 µg total protein) were mixed with 500 nM iodoacetamidofluorescein labeled peptide (C4F) in binding buffer (total volume 150 µl). To determine unspecific binding control sample contained 400-fold excess of unlabeled peptide (R9LQK, 200 µM). After 15 min of incubation on ice, the crude membranes were washed twice with 400 µl binding buffer and centrifuged at 20,000 x g for 8 min. Afterwards, the pellets were resuspended in 300 µl of lysis buffer to solubilize the crude membranes as well as the peptides, and 250 µl lysate solution was added to the filter plate. Filter plate was incubated at room temperature for 15 min. Subsequently, the fluorescence emission of the solution was measured in the multi-well plate at 520 nm with the excitation wavelength at 470 nm using FluoroStar fluorometer (BMG Labtechnologies, GmbH, Germany). The C4F peptide was diluted in lysis buffer to a series of defined concentration (0, 10, 20, 40, 80 and 100 nM), which were used as standard.

3.4.3.2 Peptide binding assay (Filter assay)

Binding buffer	**RRY(^{125}I)QKSTEL- radioactive labeled peptide**
PBS buffer	
5 mM $MgCl_2$	
pH 7.4	

The filter assay was performed using a multiple filtration manifold (Multiscreen Assay System, Millipore) that is capable of handling 96 samples in parallel. The binding reaction took place in multi-well plates in which crude membranes (40 µg total protein)

were mixed with radioactive labeled peptide R9LQK at indicated concentration in binding buffer in a final volume of 50 µl. After incubation on ice for 15 min, the mixture was transferred onto a multiscreen filter (MultiScreen Plates with glass fibre filter, pore size 1.0 µm, Millipore), which was preincubated with 100 µl 0.3% polyethylimine. Unbound peptide was removed by washing with 100 µl ice-cold binding buffer twice. The filters were air-dried, and radioactivity was quantified by γ-counting. The amount of bound peptides were corrected for unspecific binding, which was determined in the presence of 400-fold molar excess of unlabeled peptide R9LQK. To determine the peptide dissociation constant, the data were fitted with Langmuir (1:1) binding equation:

$$B = B_{max} \times \frac{C}{K_d + C} \qquad \text{(Eq. 1)}$$

where B represents the bound peptide, B_{max} − maximal amount of bound peptide, C - concentration of peptide, and K_d − dissociation constant.

3.4.4   TAP concentration

Binding buffer   **RRY(^{125}I)QKSTEL- radioactive labeled peptide**
PBS buffer
5 mM MgCl$_2$
pH 7.4

The amount of TAP in crude membranes was considered to be equal to their active peptide-binding sites under saturation condition assuming one peptide-binding site per TAP complex. The crude membranes (15 µg protein) were incubated with 1 µM radiolabeled RRY(^{125}I)QKSTEL on ice for 15 min in 50 µl binding buffer. The mixture was loaded on the filter plates, which were then washed with binding buffer two times (details see 3.4.3.2). Afterwards, the radioactivity of filter plates was directly measured. In parallel, the radioactivity of 1 µl peptide (cpm/µl) was measured and the specific radioactivity of this peptide (cpm/mol) can be calculated. After counting the retained radioactivity of the filter plates, the total amount of the peptides (peptide-binding sites) was determined.

3.4.5   Protein concentration

Micro BCA Protein Assay Reagent Kit (Pierce)
Bovine serum albumin (BSA, Sigma-Aldrich)
FluoroStar fluorometer (BMG Labtechnologies)

The bicinchoninic acid assay (BCA) combines the reduction of Cu^{2+} to Cu^{1+} by protein in an alkaline medium with the highly sensitive and selective colorimetric detection of the cuprous cation (Cu^{1+}) by bicinchoninic acid. In the first step the chelation of copper with protein in an alkaline environment induces a blue colored complex. In the second step, BCA, a highly sensitive and selective colorimetric detection reagent reacts with the cuprous cation (Cu^{1+}) and forms a colored complex, whose absorbtion is measured at 594 nm. In this respect, 150 µl of sample or standard protein (BSA) is mixed with 150 µl BCA reagent in a 96 multiwell-plate and incubated for 60 min at 37°C. A calibration curve is generated using serial dilutions with BSA, and this is used to determine the protein concentration of the sample of interest.

3.4.6   Peptide transport

3.4.6.1 Peptide transport (semi-permeabilized cells)

Transport lysis buffer	Binding buffer
50 mM Tris-HCl	PBS buffer
150 mM NaCl	5 mM $MgCl_2$
5 mM KCl	pH 7.4
1 mM $CaCl_2$	
1 mM $MnCl_2$	
1% (v/v) Igepal (Sigma)	
pH 7.4	

To probe the TAP function, insect cells (2.5×10^6) were semipermeabilized with 0.05% saponin (Sigma) for 1 min at 25°C in 200 µl of binding buffer. After washing, the cells were resuspended in a volume of 100 µl of binding buffer containing ATP (10 mM). The transport reaction was initiated by adding 0.50 µM fluorescent peptide RRYQNSTC(Ψ)L (Ψ indicates iodoacetamidofluorescein coupled via a cysteine residue) for 3 min at 32°C and terminated with 1 ml ice cold binding buffer supplemented with 10 mM EDTA. After centrifugation, the cells were solubilized in 1 ml transport lysis buffer for 60 min on ice. N-core glycosylated and thus transported peptides were recovered with 60 µl concanavalin A (ConA)-Sepharose beads (Sigma-Aldrich) overnight at 4°C. After three times washing with 500 µl transport lysis buffer, the glycosylated peptides were eluted with 300 µl methyl-α-D-mannopyranoside (200 mM, Sigma) and quantified with a fluorescence plate reader ($\lambda_{ex/em}$ = 485/520 nm; Polarstar Galaxy, BMG Labtech). Background transport activity was measured in the presence of apyrase (1 unit, Sigma-Aldrich).

3.4.6.2 Peptide transport (crude membranes)

The peptide transport assay has been investigated using either radioactive labeled peptide [RRY(^{125}I)QNSTEL, where ^{125}I is covalently coupled to tyrosine residue] or iodoacetamidofluorescein labeled peptide (RRYQNSTC(Ψ)L, where Ψ indicates iodoacetamidofluorescein coupled via a cysteine residue. In the first case, the crude membranes (150 µg total protein) where incubated with 3 mM ATP in 50 µl binding buffer on ice for 1 min. The transport starts by adding 1 µM radioactive labeled peptide and incubating the reaction mixture for 3 min at 32°C. The reaction was stopped by adding 1 ml of ice-cold binding buffer supplemented with 10 mM EDTA. After centrifugation, the pellets were solubilized in 500 µl of transport lysis buffer by incubation for 30 min on ice. The insoluble material was removed by centrifugation, and the supernatant was incubated with 60 µl concanavalin A (ConA)-Sepharose (50%, w/v, Sigma-Aldrich) for 1h. After three washing steps with 500 µl transport lysis buffer, the radioactivity associated with ConA-Sepharose was quantified by γ-counting.

3.4.7   Immunoprecipitation

IP-lysis buffer	**IP-wash buffer**
20 mM Tris-HCl	20 mM Tris-HCl
150 mM NaCl	150 mM NaCl
5 mM MgCl$_2$	2 mM EDTA
1% (w/v) Digitonin	0.1% (w/v) Digitonin
pH 7.5	pH 7.5

The TAP complex was immunoprecipitated as a complex using Dynabeads$^®$M-280 Sheep anti-Mouse IgG magnetic beads (Dynal Biotech) bound with TAP2 antibody 435.3. Initially, 150 µl magnetic beads were washed three times with 1 ml IP-lysis buffer containing 0.1% (w/v) BSA. Subsequently, 1 ml of hybridoma supernatant (monoclonal antibody mAb. 435.3) was added and incubated for 2h at 4°C. After three washing steps with 1 ml IP-lysis buffer (0.1% BSA), the beads were equilibrated with 600 µl IP-lysis buffer containing 0.1% (w/v) digitonin.

TAP was solubilized in 1 ml IP-lysis buffer for 60 min at 4°C. After centrifugation for 45 min at 20,000 x g at 4°C, the solubilized membranes were added to the equilibrated magnetic beads and incubated for 2h at 4°C. After three washing steps with 1 ml IP-wash buffer, the beads were resuspended in SDS-sample buffer, and an aliquot was loaded on

10% SDS-PAGE. Precipitation of TAP1 and TAP2 was confirmed by immunoblotting with TAP1-(mAb 148.3) and TAP2-(mAb 435.3) antibodies, respectively.

3.4.8   AlF$_x$-trapping of the TAP complex

Trapping buffer
PBS buffer
5 mM ATP
3 mM MgCl$_2$
2.5 mM AlCl$_3$
250 mM NaF
pH 7.4

TAP-containing membranes (500 µg total protein) were pre-incubated with 1 µM RRYQKSTEL in 500 µl trapping buffer for 25 min at 27°C. Afterwards, membranes were washed in ice-cold trapping buffer, collected by centrifugation at 20,000 x g for 8 min at 4°C and resuspended in 100 µl PBS buffer supplemented with 3 mM MgCl$_2$ for oxidative cross-linking, peptide transport or peptide binding.

3.4.9   Cysteine accessibility using fluorescence labeling

Hepes buffer	**IP-lysis buffer**
50 mM Hepes	20 mM Tris-HCl
145 mM NaCl	145 mM NaCl
1 mM KCl	5 mM MgCl$_2$
pH 7.5	1% (w/v) Digitonin
	pH 7.5

TAP-containing crude membranes (500 µg total protein) were labeled with 50 µM of the thiol-specific probes 5-iodoacetamidofluorescein (5-IAF), BODIPY maleimide (BM) or coumarin maleimide (CM) (Invitrogen) for 3 min at 4°C in 100 µl HEPES buffer. The labeling reaction was stopped with β-mercaptoethanol (80 mM) and the membranes were washed once with 500 µl ice cold HEPES buffer and pelleted by centrifugation for 8 min, at 20,000 x g. After labeling, the TAP complex was solubilized with digitonin (1%) in 1 ml of IP-lysis buffer and purified via immunoprecipitation using Dynabeads M280-Sheep anti-mouse IgG (Dynal Biotech) coupled with TAP2-(mAb 435.3) antibody. Purification of TAP1 and TAP2 was confirmed by immunoblotting with TAP1-(mAb 148.3) and TAP2-(mAb 435.3) antibodies, respectively. Fluorescence labeling was monitored by in-gel fluorescence using the Lumi-Imager F1^{TM} (Roche Applied Science). Images of the gel were

quantified using densitometric analysis (Lumi-Imager Software). Cys-less TAP was used as a negative control in the labeling reaction.

3.4.10 Kinetics of fluorescence labeling

Hepes buffer
50 mM Hepes
145 mM NaCl
1 mM KCl
pH 7.0

TAP-containing crude membranes (60 µg total protein) were incubated with 3 mM ATP or ADP for 10 min at 4°C or 1 unit apyrase for 1 min at 32°C in 100 µl Hepes buffer. Afterwards, the membranes were labeled with BM (50 µM) at 4°C. The reaction was stopped with β-mercaptoethanol (80 mM) at different time points (1-30 min), then SDS-sample buffer (containing 300 mM DTT) was added, and the samples were loaded on SDS-PAGE (10%). For the 100% labeling, the sample was labeled with BM (50 µM) for 30 min at 4°C, then denatured in SDS (2%) for 10 min at room temperature, and additionally labeled with BM (100 µM) for 5 min. Fluorescence labeling was monitored by in-gel fluorescence (see 3.4.9). Fluorescence intensity of the TAP1 bands (normalized to TAP1 immunoblot signal) was expressed as a percentage of the denatured sample and plotted as a function of labeling time. The profiles were fitted using non-linear regression of the exponential association curve,

$$L = L_{max} \times (1 - e^{-kt}) \qquad \text{(Eq. 2)}$$

where L is the percent labeled, L_{max} is the maximum percent labeled, t is time (min), and k is the observed rate constant for labeling.

3.4.11 Influence of fluorescence labeling on the function of TAP

Hepes buffer
50 mM Hepes
145 mM NaCl
1 mM KCl
pH 7.0

TAP-containing crude membranes (500 µg total protein) were labeled with 50 µM BM for 10 min at 4°C in 100 µl Hepes buffer in the presence of 10 mM MgATP. The reaction was stopped with β-mercaptoethanol (80 mM) and subsequently the peptide

binding and ATP-dependent peptide transport were investigated. The non-labeled probe (100% activity) has been treated identical as described above except that the sample was incubated with 50 μM DMSO instead of BM.

3.4.12 Cysteine cross-linking of single cysteine mutants (radioactive)

Phosphate buffer saline (PBS)
137 mM NaCl
2.7 mM KCl
10 mM Na_2HPO_4
2 mM KH_2PO_4
pH 7.4

TAP-containing membranes (500 μg total protein) were incubated with 1.25 μM of radiolabeled peptide RRY(^{125}I)QKCTEL in 200 μl PBS for 15 min at 4°C. Experiments were performed in the presence or absence of competitor peptide (250 μM RRYQKSTEL). Chemical cross-linking was initiated by adding of BM[PEO]$_3$ (200 μM final). After incubation for 45 min at 4°C, the reaction was quenched with DTT (5 mM). Membranes were washed with 1 ml PBS buffer and collected by centrifugation at 20,000 x g for 8 min at 4°C. TAP was solubilized in 100 μl PBS buffer containing 35 mM Foscholine-14 (Anatrace) for 20 min at 4°C. Insoluble material was removed by centrifugation at 100,000 x g for 30 min at 4°C. The supernatant (100 μl) was incubated with 100 μl Ni-NTA beads (Qiagen) for 45 min at 4°C. For oxidative cross-linking, TAP-containing membranes and radiolabeled RRY(^{125}I)QKCTEL were incubated with CuPhe (1 mM CuSO$_4$/4 mM 1,10-phenanthroline) for 5 min at 4°C under the same conditions as described above. The reaction was stopped by addition of *N*-ethylmaleimide (10 mM) and purified as stated above. TAP was analyzed by SDS-PAGE (10%) and cross-linked products were detected by autoradiography with a Phosphorimager 445i (Molecular Dynamics).

3.4.13 Cysteine cross-linking of double cysteine mutants

100 mM CuSO$_4$
100 mM 1,10-phenanthroline
100 mM 1,2-Ethanediyl bismethanethiosulfonate (MTS-2-MTS)
100 mM 1,2-Pentanediyl bismethanethiosulfonate (MTS-5-MTS)

TAP-containing membranes (500 μg total protein) were washed once with 1 ml PBS buffer and collected by centrifugation at 20,000 x g for 8 min at 4°C. Afterwards, the

TAP-containing membranes (500 µg total protein) were washed once with 1 ml PBS buffer and collected by centrifugation at 20,000 x g for 8 min at 4°C. Afterwards, the oxidative cross-linking was initiated with copper phenanthroline (1 mM $CuSO_4$/4 mM 1,10-phenanthroline) in 100 µl of PBS buffer (pH 7.0) for 1 min at 4°C. The reaction was stopped by addition of 10 mM N-ethylmaleimide. Membranes were washed with 500 µl PBS buffer containing 10 mM EDTA and collected by centrifugation at 20,000 x g for 8 min at 4 °C. Membranes were resuspended in SDS-sample buffer containing 10 mM NEM and were analyzed by non-reducing SDS-PAGE (6%) and immunoblotting with TAP1-(mAb. 148.3) and TAP2-(mAb. 435.3) monoclonal antibodies. To reduce the disulfide bonds after cross-linking, 100 mM DTT were added in the sample buffer before electrophoresis.

3.4.14 Influence of cross-linking on the function of TAP

TAP-containing membranes (500 µg total protein) were washed once with 1 ml PBS buffer (pH 7.0) and collected by centrifugation at 20,000 x g for 8 min at 4°C. Afterwards, the oxidative cross-linking was initiated with or without CuPhen (1 mM $CuSO_4$/4 mM 1,10 phenanthroline) for 1 min at 4°C in 100 µl PBS buffer. Then, the membranes were incubated with or without 100 mM β-mercaptoethanol for 5 min at 4°C, washed twice with 1 ml PBS containing 10 mM EDTA, and the peptide binding (see 3.4.3.2) and peptide transport (see 3.4.6.2) were performed.

3.5   Molecular modeling

3.5.1   Homology modeling of the core TAP transport complex

The homology modeling of the core TAP transport complex has been performed by Megan L. O'Mara, W. F. Drew Bennett and D. Peter Tieleman (Department of Biological Sciences, University of Calgary, Canada). Each TAP1 and TAP2 half-transporter was modeled on the corresponding subunit of the ADP-bound *S. aureus* Sav1866 homodimer (2HYD.pdb) (Dawson and Locher, 2006). Although the Sav1866 structure was crystallized with ADP, the tight NBD dimer conformation and outwards-facing configuration of the TMDs is believed to represent the ATP-bound state. The Sav1866 conformation allowed us to develop a homology model of heterodimeric TAP complex in the ATP-bound state. We

aligned the amino acid sequence of human TAP1 and TAP2 with that of Sav1866 using

ClustalW2 (Thompson *et al.,* 1994). Secondary structure predictions (Rost *et al.,* 2003) and

experimental data on the membrane topology (Schrodt *et al.,* 2006) for the TAP1 and TAP2

TMHs corresponded to the Sav1866 based alignment. The alignment for TAP1 and TAP2,

respectively, against Sav1866 was 27% and 28%, although this varies markedly between the

TMDs and NBDs. The absolute sequence identity between TAP1 and Sav1866 is 20% for

the TMDs and 37% for the NBDs. For the alignment between TAP2 and Sav1866, the

sequence identity is 22% for the TMDs and 34% for the NBDs. When sequence similarity is

taken into account, these percentages become 61% and 56% for the TMDs, and 69% and

63% for the NBDs of TAP1 and TAP2, respectively. TAP1(173-741) and TAP2(141-686)

were modeled separately using MODELLER v9.3 (Sali and Blundell, 1993). The TAP1 and

TAP2 models were dimerized to reproduce the Sav1866 subunit interface and refined to

remove steric clashes (Guex and Peitsch, 1997). The models were inserted into a 1-

palmitoyl-2-oleoyl-phosphatidyl ethanolamine (POPE) lipid bilayer and the system was

solvated. Position restraints on the protein backbone conformation were relaxed over a 40-

ns period using the GROMACS 3.2.1 simulation package to give an energy minimized

TAP1/2 heterodimer. Additional MD simulations were not performed, as short timescale

simulations have been shown to increase the backbone disorder of homology models.

4.   Results

4.1   Role of the CL1 mutants (TAP1) in the substrate sensing and signal transmission

4.1.1   The CL1 is an important region of the TMD-NBD interface

As shown in earlier studies with purified and reconstituted TAP, the allosteric interaction between peptide binding, ATP hydrolysis and peptide translocation involves a dialogue between the NBDs and the substrate binding site in the TMDs (Gorbulev *et al.,* 2001). However, how this downstream mechanism functions at molecular level remains unknown. Based on the X-ray structures of ABC transporters, cytoplasmic loops in TMDs display the interface with the NBDs (Locher *et al.,* 2002; Dawson and Locher, 2006). In biochemical studies, the EAA motif in a cytoplasmic loop of the TMD, which is part of the L-loop found in BtuCD, and the Q-loop in the NBD were identified to be important for signal transduction between the TMDs and NBDs in ABC importers (Mourez *et al.,* 1997; Hunke *et al.,* 2000). The main contacts between the membrane spanning domain BtuC and the ABC-cassette BtuD are formed by the L-loop of BtuC and the Q-loop of BtuD of the vitamin B_{12} transporter (Locher *et al.,* 2002). The L-loop consists of two short helical stretches named L1 and L2 interrupted by a glycine residue. By sequence comparasion, this L-loop sequence, can be found in cytoplasmic loops of nearby all ABC transporters. Interesting the position of the L-loop is variable, depending on the ABC transporter.

The cytosolic loops of ABC exporters and importers are verry different. For example, in contrast to the ABC import proteins, the ABC exporters like MsbA and Sav1866 show an enlarged TMD-NBD interface comprising the large cytosolic loops CL1 and CL2 of the TMD and different regions in the NBD (Dawson and Locher, 2006). In order to define residues of the transmission interface in TAP, a 3D homology model of the core TAP complex based on the x-ray structure of Sav1866 has been constructed (Dawson and Locher, 2006; Figure 4-1A). The homology modeling of the core TAP transport complex has been performed by Megan L. O'Mara, W. F. Drew Bennett and D. Peter Tieleman (Department of Biological Sciences, University of Calgary, Canada). The final TAP model had a backbone root-mean-square deviation (RMSD) of 3.08 Å from the Sav1866 structure. The quality of the TAP1/2 model was assessed using WHATIF on local factors such as backbone conformations, bond lengths, side chain planarity, and overall packing quality and found to be of comparable quality to Sav1866. However, some caveats must be applied when using WHATIF for analysis of transmembrane proteins (O'Mara and Tieleman, 2007). Therefore, an additional

analysis of the Ramachandran plot using SPDBV (Guex and Peitsch, 1997) was used as an extra structural analysis method. The Ramachandran plot showed 99% of all TAP1/2 residues fell within favourable regions, increasing our confidence in the backbone geometry. The cytosolic loops of TAP and Sav1866 are of similar length and clearly distinct from the short cytosolic loops of ABC importers (Figure 4-1A). The constructed model is in full agreement with a number of experimental data, including the membrane topology, structure and function of a core transport complex, peptide-binding regions, and the sensor loop (Nijenhuis and Hämmerling, 1996; Koch *et al.,* 2004; Schrodt *et al.,* 2006; Herget *et al.,* 2007). The NBDs are close together with distances reflecting the ATP-bound state and the TMDs opened to the ER-luminal site, reflecting an outward-facing conformation. The cytosolic loops are composed of TMH-extended helices, which are connected by short coupling helices (CHs) in parallel orientation to the membrane plane (Figure 4-1A). Importantly, the X-loop of TAP occupies a central position, in which the conserved glutamate is surrounded by residues of CL1 and 2 of the opposite subunit (Figure 4-1A). The X-loop is localized in the α-helical domain of the NBD close to the C-loop, suggesting a role in transmitting conformational changes generated by ATP binding and hydrolysis. The sequence conservation of CL1 and 2 including the coupling helix 1, the identified peptide sensor and coupling helix 2, as well as the X-loop are illustrated in Figure 4-1B.
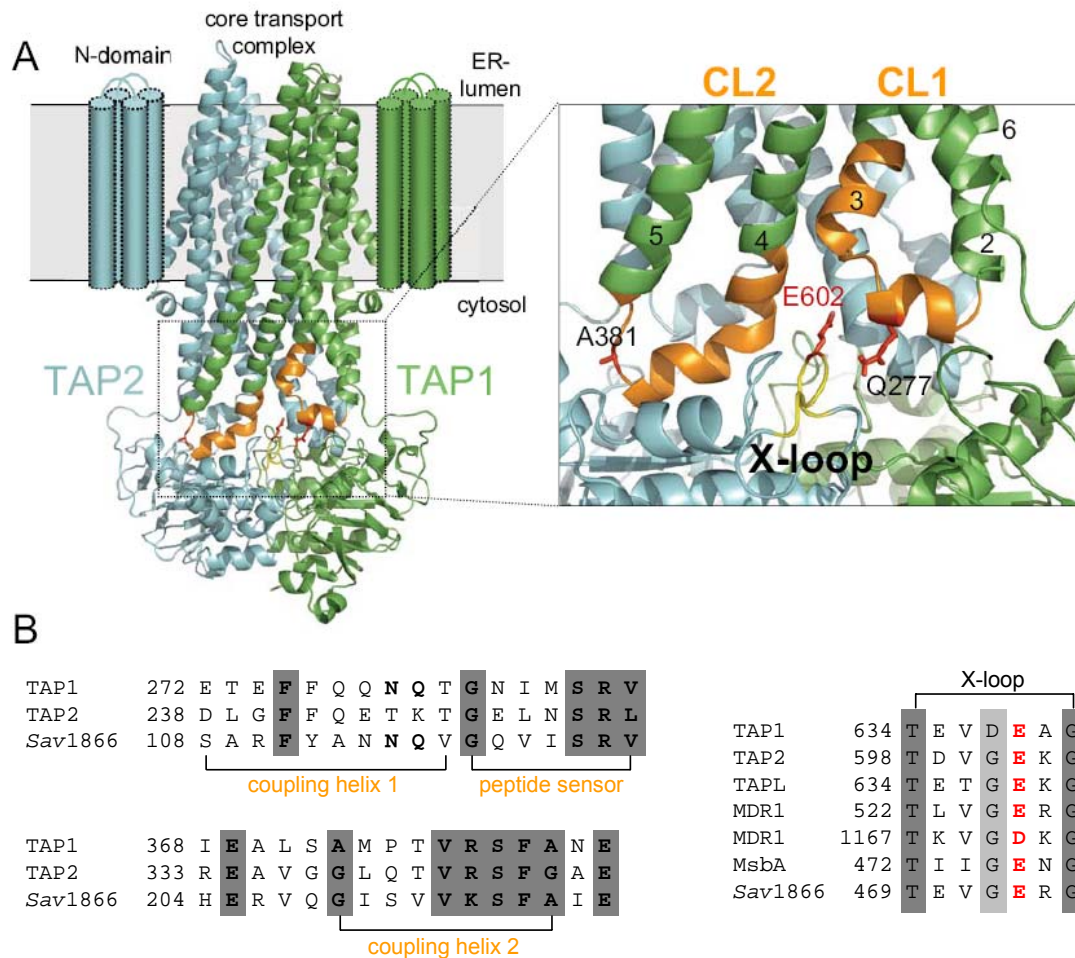
Figure 4-1. The TMD-NBD interface of the TAP complex. (A) 3D homology model of the core TAP complex composed of TAP1 (green) and TAP2 (cyan) based on the x-ray structure of Sav1866 (2HYD.pdb) (26). The homology modeling of the core TAP transport complex has been performed by Megan L. O'Mara, W. F. Drew Bennett and D. Peter Tieleman (Department of Biological Sciences, University of Calgary, Canada). The TMHs of the extra N-domain (TMD0) are indicated by cylinders. CL1 and CL2 are extensions between TMH2 and 3, and TMH4 and 5, respectively. The region of CL1 and CL2 in TAP1 investigated by cysteine scanning and cross-linking is colored in orange, the X-loop of TAP2 in yellow, respectively. The conserved glutamate (E602) in the X-loop and residues in CL1 and CL2 (Q277 and A381) are highlighted in red using a stick representation. A zoom-in of the transmission interface illustrates the close interaction of coupling helix 1 and 2 and the X-loop of TAP2. The extensions of the TMHs are indicated by numbers. (B) Multiple alignments of the transmission interface of different ABC exporters (Swiss-Prot accession numbers: Q03518/9, human TAP1/2 (ABCB2/3); Q9NP78, human TAPL (ABCB9); P08183, human MDL1 (ABCB1); P63359, *S. typhimurium* MsbA; Q99T13, *S. aureus* Sav1866) using ClustalW2 (http://www.clustalW.org). The coupling helix 1 and 2, the peptide sensor, and the X-loop are presented. Residues with high conservation are shaded dark grey and bold. The conserved glutamate of X-loop is labeled in red.

4.1.2   Expression of single cysteine CL1 mutants of TAP1

In order to investigate the contribution of the CL1 in the intramolecular crosstalk between TMD and NBD of TAP, cysteines were introduced in cys-less TAP construct. Recently, cysteine-less human TAP subunits were created, replacing all 19 cysteines in TAP1 and TAP2. Cysteine-less TAP1 and TAP2 are fully functional in respect of intracellular peptide transport and MHC class I antigen presentation (Heintke *et al.,* 2003). Based on the structure of BtuCD, where residues located in the L2 helix make contacts with the NBD, we have mutagenized all residues of the L2 helix of cysteine-less TAP1 to cysteine. Furthermore, the Q277 and the highly conserved G282 were replaced by cysteine. In our studies, all CL1 (TAP1) mutants were combined with a wild type counterpart (TAP2), which resulted in the following mutants: TAP1-Q277C/TAP2-wt, G282C/wt, N283C/wt, I284C/wt, M285C/wt, S286C/wt, R287C/wt, V288C/wt. All TAP1 and TAP2 constructs were cloned individually into one baculovirus, and co-expressed in Sf9 insect cells under the control of the polyhedrin promoter, respectively. Two days after infection (with an multiplicity of infection of 5), cells were harvested and crude membranes were prepared. As revealed by immunoblotting, all TAP1 mutants were expressed in crude membranes at comparable level to TAP C-less/wt (Figure 4-2).
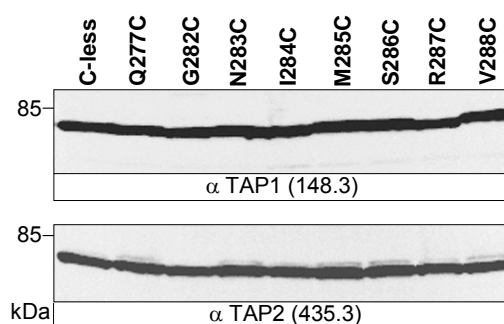
Figure 4-2. Expression of single cysteine CL1 mutants (TAP1).
Immunoblotting of crude membranes from Sf9 insect cells co-transfected with baculoviruses encoding TAP1 mutants and TAP2wt. The anti-TAP1 (148.3) and anti-TAP2 (435.3) monoclonal antibodies were used to detect TAP1 and TAP2 protein expression, respectively (Herget *et al.,* 2007).

4.1.3   Peptide binding of CL1 mutants

In order to investigate if the CL1 mutants are functionally active, we have examined first peptide binding at 4°C. Crude membranes containing TAP variants were incubated with increasing concentrations of radiolabeled R9LQK peptide. As shown in Figure 4-3, the data were fitted by the Langmuir (1:1) binding equation and the peptide dissociation constants K_d as well as the maximal peptide-binding capacity B_{max} were determined. All the constants are summarized in Table 4-1. The B_{max} values of each mutant show only 2 fold difference, indicating similar expression. The K_d values of all CL1 mutants are quite similar with TAP C-less/wt, demonstrating that the substitution of the CL1 residues with cysteines does not alter the peptide-binding affinity.

Table 4-1. Summary of peptide binding constants of single cysteine CL1 mutants (TAP1).

CL1 mutants (TAP1)	K_d (μM)	B_{max} (cpm/1000)
C-less/2wt	0.57 ± 0.17	40.41 ± 4.13
Q277C/2wt	0.61 ± 0.24	59.62 ± 8.12
G282C/2wt	0.77 ± 0.17	73.93 ± 7.36
N283C/2wt	1.31 ± 0.52	132.33 ± 22.81
I284C/2wt	0.58 ± 0.19	54.55 ± 8.59
M285C/2wt	0.51 ± 0.17	79.91 ± 12.34
S286C/2wt	1.04 ± 0.66	43.22 ± 12.63
R287C/2wt	1.67 ± 0.13	53.76 ± 2.51
V288C/2wt	0.57 ± 0.29	52.54 ± 13.16
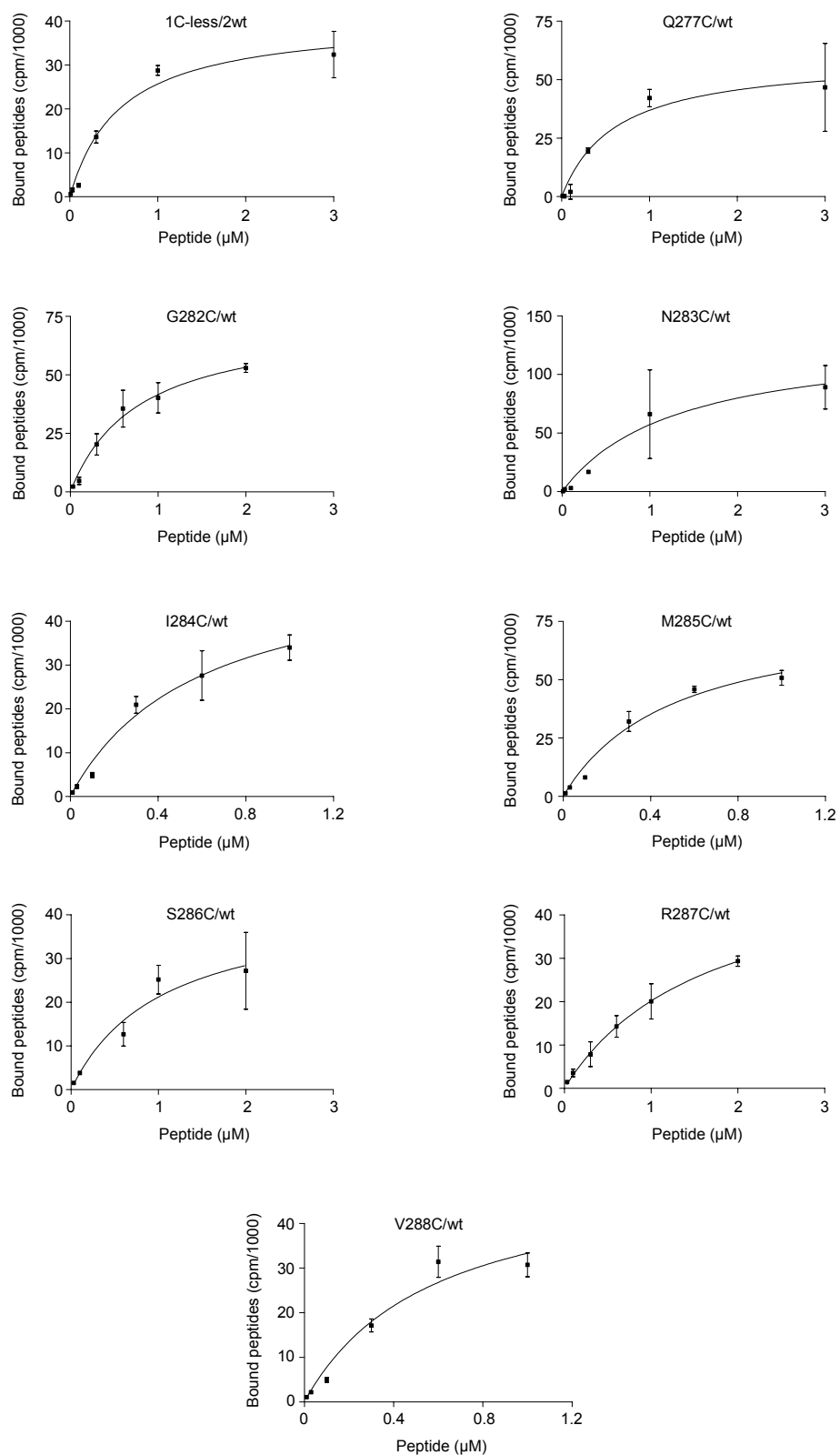
Figure 4-3. Peptide binding of CL1 mutants (TAP1).
Crude membranes (35 µg protein) of CL1 mutants were incubated with increasing concentrations of radiolabeled peptide R9LQK (15 min, 4°C). Free peptides were removed by washing and membrane-associated peptides were determined by γ-counting. Amount of specifically bound peptides is plotted against the peptide concentration and fitted by a Langmuir (1:1) binding equation. The peptide affinities and B_{max} values are summarized in table 4-1. Data resemble the mean of triplicate measurements. The error bars indicate the deviation of triplicate measurements.

4.1.4   Peptide transport of CL1 mutants

We next investigated the peptide transport activity of the CL1 mutants in whole cells using fluorescent peptide RRYQNSTC$^{(F)}$L. As shown in Figure 4-4, mutations of the most conserved residues within the sensor loop (Gly-282, Ile-284, and Arg-287) strongly decreased peptide transport. In these mutants, the coupling between peptide binding and transport is disrupted, indicating that this sensor site serves as a checkpoint in controlling downstream events.
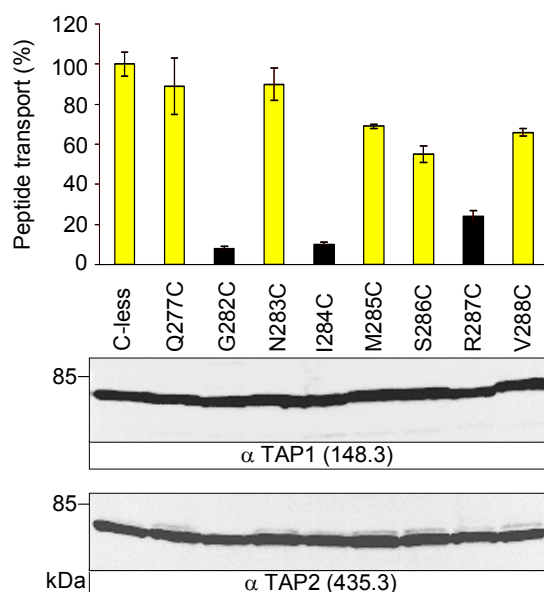
Figure 4-4. Peptide transport of single-cysteine CL1 mutants (TAP1).
ATP-dependent peptide transport of single cysteine TAP1 mutants was analyzed in semipermeabilized insect cells. The assay was performed with fluorescein-labeled peptide (0.50 µM, RRYQNSTC$^{(F)}$L) for 3 min at 32°C in the presence and absence of Mg-ATP (10 mM). N-core-glycosylated and therefore transported peptides were bound to ConA-beads and quantified by fluorescence detection after elution with methyl-α-D-mannopyranoside. The relative ATP-dependent transport efficiencies of the single-cysteine TAP constructs are plotted in comparision to that of TAP1 Cys-less/TAP2wt. The error bars indicate the deviation of three independent experiments (Herget *et al.,* 2007).

4.1.5   The sensor loop is in contact with the bound peptide

Recently, the peptide contact site was identified by mass spectrometry (Herget *et al.,* 2007). This contact site is located in the cytosolic loop 1 (CL1) between TM2 and TM3 of TAP1, and shares some degree of homology with CL1 of the bacterial multidrug exporter Sav1866 and the L-loop of the bacterial vitamin B_{12} importer. Based on the x-ray structure of these proteins these loops form the major contact between the transmembrane domain and the Q-loop as well as the α-helical subdomain of the nucleotide-binding domain as derived from distance measurements. To proof the direct contact of the sensor region with the bound peptide, a cross-linking approach was established with TAP1 mutants and radioactive labeled peptide RRYQKCTEL (C6-peptide), each containing a single cysteine. After binding of radio-labeled peptide to TAP, membranes were incubated with the thiol-specific cross-linker $BM[PEO]_3$. Cross-linking products were analyzed by SDS-PAGE and autoradiography. As shown in Figure 4-5A, specific cross-linking was detected only if a single cysteine (V288C) was placed at the peptide contact site identified by mass spectrometry. Background labeling was observed in the presence of an excess of the epitope, demonstrating the specificity of the cross-linking. No cross-linking was monitored for cysteine-less TAP1. TAP1 mutants with single cysteines placed in the NBD (R659C) did not show specific cross-linking (Figure 4-5A). To prove the direct contact of the sensor region with the bound peptide, also oxidative cross-linking of single cysteine TAP and peptides with copper phenanthroline was performed, which induces disulfide formation only if two cysteines are in very close proximity (Wu and Kaback, 1996). A 200-fold excess of non-labeled peptide, RRYQKSTEL, was used as competitor. As negative control, the construct TAP1 C-less/TAP2 wt was used in the cross-linking experiments. After quenching of free cysteines with NEM, cross-linking products were analyzed by non-reducing SDS-PAGE and autoradiography. Notably, the bound C6-peptide was cross-linked to the TAP1 contact site identified by mass spectrometry, including position 288 (Figure 4-5B). The cysteine-less and TAP1-R659C mutant did not show a specific cross-linking. In addition, the TAP1 mutants I284C, M285C ans S286C are cross-linked to a very small extend in the nucleotide free state (Figure 4-6A). Interestingly, in the ATP bound state the bound C6-peptide was cross-linked to the position 288. In addition, the TAP1 mutants I284C and S286C are cross-linked to a very small extend, but the mutant M285C is not cross-linked, suggesting a state dependent rearrangement of the sensor interface in TAP1 (Figure 4-6B). All other residues within the peptide sensor site are not in contact

with the bound peptide. Importantly, the crosslinking observed is TAP1 specific, since the

TAP1 C-less/TAP2 wt shows no crosslinking with the bound C6-peptide.

A

B
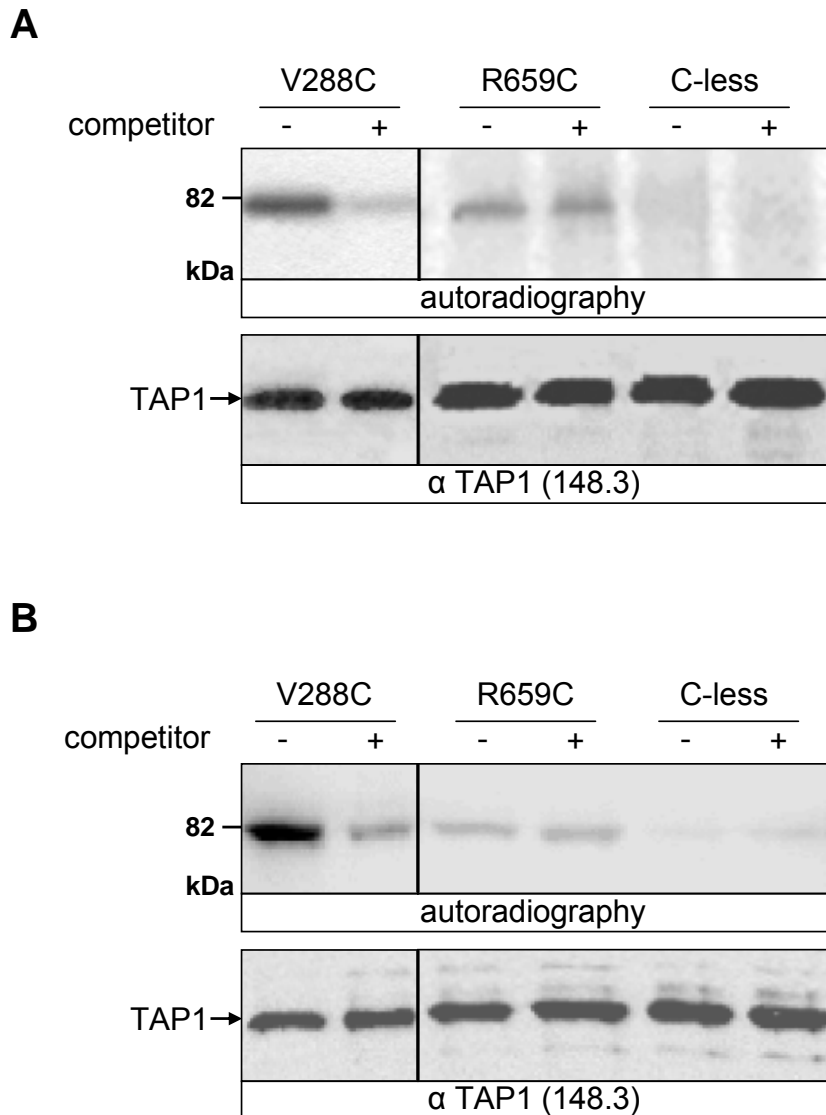
Figure 4-5. Bound peptides are in direct contact with the cytosolic loop 1 of TAP1.
(A) Site-specific thiol cross-linking with BM[PEO]$_3$. TAP-containing membranes (0.5 mg of total protein; TAP1 (single cysteine or cysteine-less) combined with TAP2 wt were preincubated with radio-labeled C6-peptide (1.25 µM) in the absence or presence of the peptide RRYQKSTEL (250 µM). Cross-linking was induced by adding 0.2 mM of BM[PEO]$_3$. After purification of TAP via metal affinity beads, cross-linked products were analyzed by reducing SDS-PAGE and autoradiography. (B) Oxidative cysteine cross-linking with copper phenanthroline. Experiments were performed as described in (A), except that membranes were incubated with copper phenanthroline (1mM) and SDS-PAGE was performed under non-reducing conditions. Equal amounts of TAP in each experiment were confirmed by immunoblotting (Herget *et al.,* 2007).

A

B
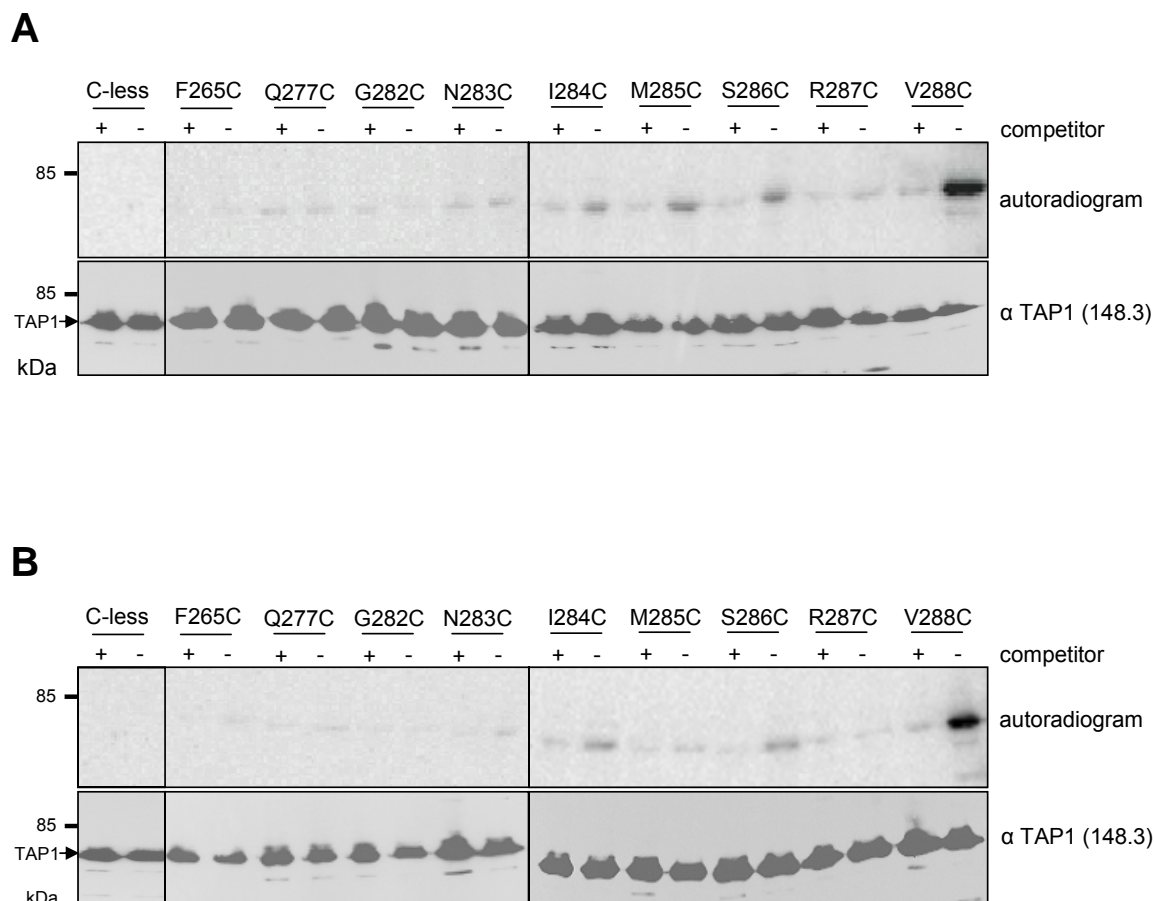
Figure 4-6. The C-terminal part of the CL1 is in contact with the bound peptide.
TAP-containing membranes (0.5 mg of total protein) were incubated with either 2 units apyrase (A) or 3 mM ATP (B). Afterward, radiolabeled C6-peptide (1.25 μM) was added in the absence or presence of the competitor peptide RRYQKSTEL (250 μM). Cross-linking was induced by adding copper phenanthroline (1 mM). After metal affinity capture of TAP, cross-linked products were analyzed by non-reducing SDS-PAGE (10%) and autoradiography. Equal amounts of TAP in each experiment were confirmed by immunoblotting (Herget *et al.,* 2007).

4.1.6   The peptide sensor interface is restructured in the transition state of the ATPase domains

Peptide transport by TAP is a multistep process composed of peptide binding, interdomain signal transmission, ATP binding/hydrolysis and peptide translocation. To elucidate structural changes in the peptide sensor and transmission interface, we examined the peptide-TAP1 contact site at various stages of the ATP hydrolysis cycle. We focused on the single cysteine mutant TAP1 (V288C)/TAP2 (wt), since this construct showed the strongest cross-linking with the bound C6-peptide in the ATP-bound and nucleotide free states (Figure 4-6A, B). To fix each single state, we performed this experiment at 4°C where ATP hydrolysis is absent. Apart from an ATP-bound, ADP-bound, and nucleotide-free state, a catalytic transition state can be arrested by aluminium fluoride (AlF_x). AlF_x is a potent ATPase inhibitor, which replaces the γ-phosphate of ATP and traps ADP stably in the ATP binding pocket of TAP (Chen *et al.,* 2003) and also other ATPases like P-glycoprotein (Sankaran *et al.,* 1997) or F1-type ATPases (Lunardi *et al.,* 1988). Derived from x-ray structures of myosin, this ADP-trapped state mimics the pentacovalent phosphorus transition state of ATP hydrolysis (Fisher *et al.,* 1995). In this state, peptide transport but not peptide binding by TAP is inhibited (Figure 4-7A and B). As shown in Figure 4-7C, cysteine cross-linking of the single cysteine peptides to residue 288 of TAP1 was observed in the presence of ADP or ATP. In addition, in the presence of the non-hydrolyzable ATP-analogues ATPγS and AMP-PNP, which do not energize peptide transport (Meyer *et al.,* 1994), peptide cross-linking occurred. Disulfide formation was most efficient in the absence of nucleotides. Strikingly, if the TAP complex was arrested in the translocation incompetent ADP•AlF_x state, no specific peptide contact to the peptide sensor site was observed. These results demonstrate a structural reorganization of the peptide sensor and transmission interface and an inter-domain cross-talk of the TMD and NBD during ATP hydrolysis.
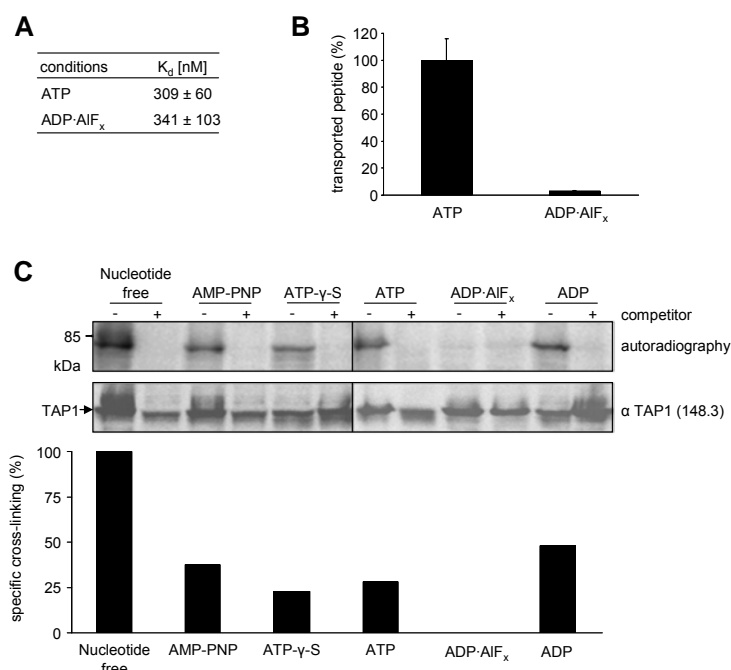
Figure 4-7. The peptide sensor loop is remodelled during the ATP hydrolysis cycle.
TAP-containing membranes were preincubated with 1 μM RRYQKSTEL and 5 mM ATP in the presence or absence of 2.5 mM AlF$_x$ for 25 min at 27°C. Afterwards, membranes were washed once. (A) Peptide binding affinity. Pre-treated TAP1(V288C)/TAP2(wt) (25 μg of total protein) was incubated with increasing concentrations of radiolabeled RRYQKCTEL (plus 1 mM dithiothreitol) for 15 min at 4°C. The amount of specifically bound peptide was plotted against peptide concentration and fitted by a Langmuir (1:1) isotherm. (B) Peptide transport. Pre-treated TAP1(V288C)/TAP2(wt) (150 μg of total protein) was incubated with 1 μM of RRYQNSTC[(F)]L (fluorescein-labeled cysteine) in the presence of 5 mM ATP or ADP for 3 min at 32°C. Transported and glycosylated peptides were purified and detected by fluorescence emission ($\lambda_{ex/em}$ =485/520). ATP-specific transport of trapped (*ADP•AlF$_x$*) and non-trapped (*ATP*) TAP is depicted. The data and errors were derived from triplicate measurements. (C) Oxidative cross-linking. TAP1(V288C)/TAP2(wt) (500 μg of total protein) was trapped in the ADP•AlF$_4^-$ transition state as described above or incubated with either 3 mM ATP, 3 mM ADP, 3 mM AMP-PNP, 3 mM ATPγS, or apyrase (2 units). Afterwards, radiolabeled C6-peptide (1.25 μM) was added in the absence or presence of the competitor peptide RRYQKSTEL (250 μM). Cross-linking was induced by adding copper phenanthroline (1 mM). After metal affinity purification of TAP, cross-linked products were analyzed by non-reducing SDS-PAGE and autoradiography. TAP amount was quantified by immunoblotting. The cross-linking intensities (quantified by ImageQuaNTsoftware) were normalized to TAP amounts, and relative specific cross-linking was related to cross-linking in the presence of apyrase as depicted in the *lower panel* (Herget *et al.,* 2007).

4.2   Architecture of CL1 revealed by fluorescence labeling

4.2.1   Cysteine accessibility using fluorescence labeling

In the previous chapter, I have characterized biochemically the residues of CL1 (TAP1) in respect of protein expression, peptide binding and substrate translocation. Single cysteine mutations in CL1 region have no effect on peptide binding, but in peptide transport, thereby demonstrating their importance in the translocation process.

To characterize the molecular architecture of CL1, a convenient and minimally perturbing approach was used, which combined cysteine substitution in the CL1 region and determination of accessibility to thiol specific compounds with different properties. Therefore, the single cysteine CL1 mutants (TAP1) were co-expressed with TAP2 cysteine less, and the fluorescence labeling has been performed in crude membranes. The thiol specific probes used in this study were: iodoacetamidofluorescein (5-IAF, hydrophilic, negative charged at pH 7.5), coumarin-maleimide (CM, hydrophobic), and BODIPY-maleimide (BM, amphiphilic). The TAP1/TAP2 cysteine less isoform was used as a control for non-specific probe interaction. Similar investigations using cysteine-scanning mutagenesis combined with fluorescence labeling to elucidate the topography of key domains of membrane proteins were applied for P-glycoprotein (Rothnie *et al.,* 2004; Storm *et al.,* 2008).

In order to optimize the labeling reaction, we have tested 5-IAF and determined the effect of time, fluorophore concentration and temperature on the fluorescence labeling in the crude membranes. After labeling, the reaction has been quenched with β-mercaptoethanol and the membranes were solubilized with digitonin (1%) and purified by immunoprecipitation with α-TAP2 antibody (mAb 435.3). Figure 4-8 summarizes the results obtained for in-gel fluorescence measurements and corresponding TAP1 and TAP2 specific immunoblots of C-less (TAP1)/C-less (TAP2), C-less/wt, and Q277C/C-less. Notably, the isoform C-less/wt, which contains 10 cysteines showed the highest fluorescence after 5 min of labeling at 4°C. Interestingly, the cysteine at position 277 (Q277C) was already labeled after 1 min at 50 μM 5-IAF. Minor differences of labeling efficiency after 3 or 5 min were observed. The reaction is site-specific, because C-less TAP shows no labeling (Figure 4-8A). Increasing the 5-IAF concentrations (50 – 200 μM) does not induces a higher labeling efficiency (Figure 4-8B). The optimal temperature for 5-IAF labeling was 4°C, because at this temperature TAP degradation is reduced, thereby facilitating a better labeling efficiency (Figure 4-8C). At higher temperatures TAP is degraded, as observed from the TAP1 and TAP2 specific immunoblots. Taken together, the optimal fluorescence labeling in crude membranes occured

at 50 µM 5-IAF, 4°C, for 3 min. These labeling conditions were used for all fluorophores tested in the present work.
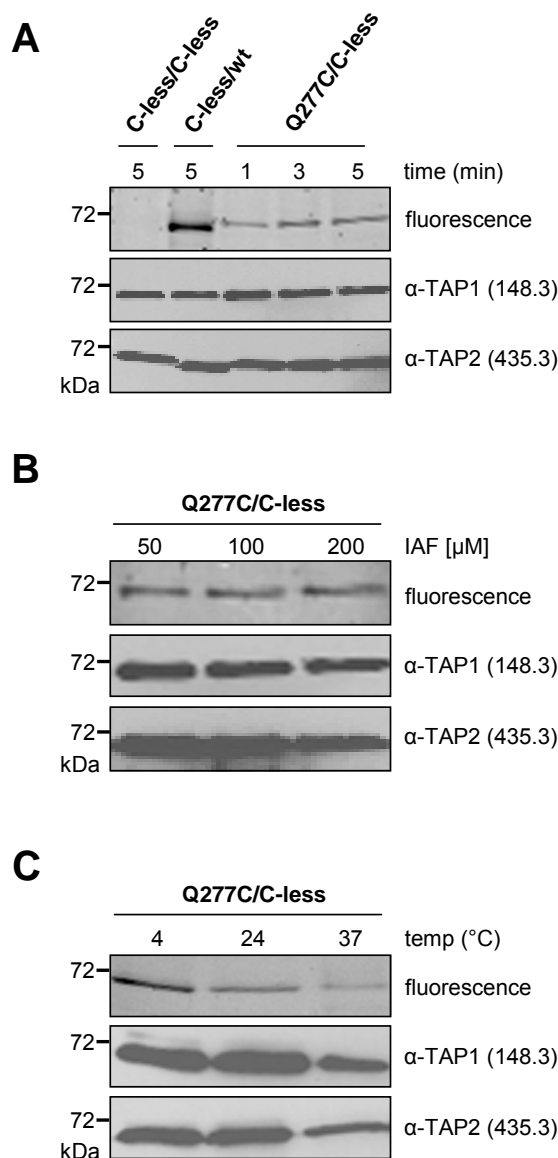
Figure 4-8. Optimization of fluorescence labeling of single-cysteine CL1 mutants.
(A) Influence of time on fluorescence labeling. TAP-containing membranes (0.5 mg of total protein) were labeled with 50 µM thiol-specific probe 5-IAF for 1-5 min at 4°C. (B) Influence of fluorophore concentration. TAP-containing membranes (0.5 mg of total protein) were labeled with 50-200 µM 5-IAF for 3 min at 4°C. (C) Influence of temperature on fluorescence labeling. TAP-containing membranes (0.5 mg of total protein) were labeled with 50 µM 5-IAF for 4 min at 4 - 37°C. The labeling reaction was stopped with β-mercaptoethanol (80 mM). After labeling, the TAP complex was solubilized with digitonin (1%) and purified via immunoprecipitation using Dynabeads M280-Sheep anti mouse IgG coupled with α-TAP2 (435.3) antibody. Co-purification of TAP1 and TAP2 was confirmed by immunoblotting with α-TAP1 and α-TAP2 antibodies, respectively. Cysteine-less TAP was used as negative control in the labeling reaction. The difference in mobility observed for C-less/wt (fluorescence gel and TAP2 immunoblot) are attributed to the absence of histidine tag (His-tag) on this construct, whereas C-less TAP2 had a 10 His-tag on C-terminus.

To determine the topography of CL1, cysteine accessibilities with dyes of different hydrophilic characteristics were studied under the established conditions. To normalize the labeling efficiency to TAP amount, the ratio between fluorescence labeling and TAP1 immunoblot signal has been determined. Importantly, the absolute fluorescence between the thiol-specific probes is not comparabile, because of their different physicochemical properties. The hydrophilic probe 5-IAF labeled with high degree two mutants (Q277C and N283C), and with reduced efficiency three other constructs (G282C, I284C, and V288C; Figure 4-9B). Interestingly, 3 mutants (M285C, S286C, and R287C) were not labeled with 5-IAF. The reaction is cysteine specific, because cys-less TAP shows no labeling. Equal amounts of TAP1 and TAP2 were detected after immunoprecipitation (Figure 4-9B). The amphiphilic probe BM labeled all of the CL1 mutants, however, with different efficiencies. The highest labeling was observed for three mutants (G282C, N283C, and I284C), whereas a reduced efficiency was detected for five other constructs (Q277C, M285C, S286C, R287C, and V288C; Figure 4-9C). The hydrophobic probe CM labeled the single cysteine CL1 mutants in a similar fashion compared with the BM probe. Again, the highest degree of labeling was observed for three constructs (G282C, N283C, and I284C; Figure 4-9D). Interestingly, labeling of the Q277C construct had a low efficiency.

The results are summarized in the Table 4-2, which provides a qualitative assessment of the relative accessibility of the residues to covalent modification. The results are presented as (i) complete labeling during the reaction period (denoted +++), (ii) incomplete, but significantly different from the cysteine-less protein (denoted as + or ++ to enable easier identification of alterations in accessibility), or (iii) unlabeled during the reaction (denoted -). Two striking features are evident from an examination of the data presented in the Table 4-2, namely a good accessibility of the N-terminal residues (Q277C, G282C, N283C, and I284C) for the different fluorescent probes used, whereas the rest of the mutants were less accessible. A second observation is that the C-terminal region of CL1 (M285C, S286C, R287C, and V288C) is accessible for hydrophobic probe (CM), partially labeled by the amphiphilic probe (BM) and poorly labeled by the hydrophilic probe (5-IAF), demonstrating that these amino acid side chains are in a more hydrophobic environment.
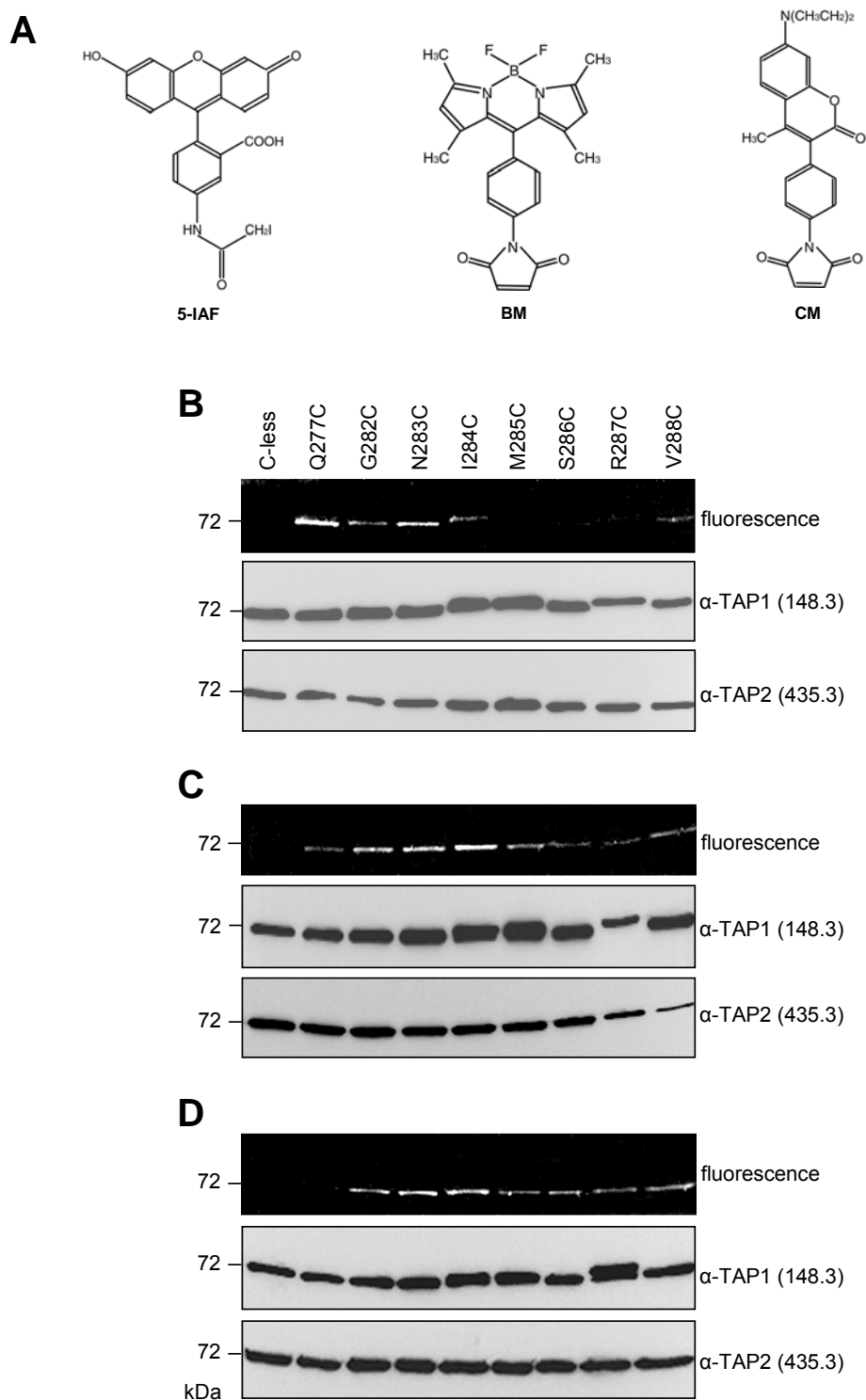
Figure 4-9. Labeling of the single-cysteine CL1 mutants.
(A) Structures of iodoacetamidofluorescein (5-IAF), BODIPY-maleimide (BM), and coumarin-maleimide (CM). TAP-containing membranes (0.5 mg of total protein) were labeled with 50 µM thiol-specific probes 5-IAF (B), BM (C), and CM (D) for 3 min at 4°C. The labeling reaction was stopped with β-mercaptoethanol (80 mM). After labeling, the TAP complex was solubilized with digitonin (1%) and purified via immunoprecipitation using Dynabeads M280-Sheep anti mouse IgG coupled with α-TAP2 antibody. Co-purification of TAP1 and TAP2 was confirmed by immunoblotting with α-TAP1 and α-TAP2 antibodies, respectively. Cysteine-less TAP was used as negative control in the labeling reaction.

Table 4-2. Summary of relative accessibilities of CL1 mutants.
The accessibility of each introduced cysteine residue was determined using 5-IAF, BM or CM, and the ratio between fluorescence labeling and TAP1 immunoblot signal as shown in Fig. 4-9 was quantified. Labeling with a ratio higher than 1.5 was denoted as (+++), whilst incomplete labeling was denoted with either (++) or (+) to enable clear illustration of changes in accessibility. No significant labeling of an isoform with a particular probe is denoted (-). The absolute fluorescence between the thiol-specific probes is not comparabile, because of their different physicochemical properties.

CL1 mutant (TAP1)	5-IAF	BM	CM
Q277C	+++	+	-
G282C	++	+++	++
N283C	+++	+++	+++
I284C	+	+++	+++
M285C	-	+	++
S286C	-	+	++
R287C	-	+	+
V288C	++	++	++
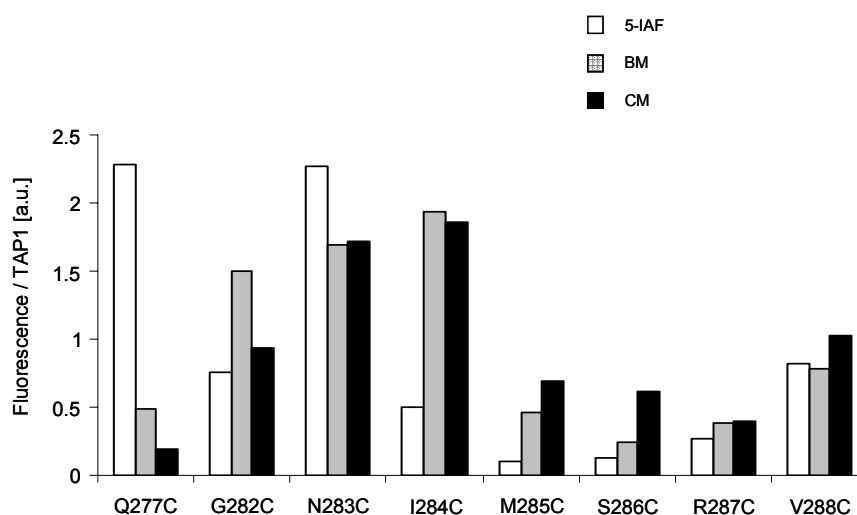
Figure 4-10. TAP labeling efficiency.
TAP containing crude membranes (0.5 mg total protein) were labeled with 50 µM thiol-specific probes 5-IAF (white), BM (grey), and CM (black) as described in Figure 4-9. The ratio between fluorescence labeling and TAP1 immunoblot signal as shown in Figure 4-9 was quantified.

4.2.2   Fluorescence labeling kinetics

From the fluorescence accessibility studies the amphiphatic character of CL1 (TAP1) residues can be suggested. An important question is whether this loop undergoes an conformational change during the transport cycle. In the previous studies (Chapter 4.1) using a crosslinking approach, residues located in CL1 region which are essential for tight coupling of peptide binding and transport were identified. In order to characterize conformational changes of CL1 during the transport cycle, I investigated the kinetics of fluorescence labeling with BM in different states of TAP, such as ATP-, ADP-bound or nucleotide free conformation. The different conformations of TAP were induced by addition/depletion of nucleotides. BM has been the fluorescent probe used in this investigation because it could label all of the CL1 mutants (Figure 4-9). TAP containing membranes were incubated with 3 mM Mg-ATP, Mg-ADP or 1 unit apyrase. Afterwards, the membranes were labeled with 50 µM BM at 4°C, and the reaction was stopped with 80 mM β-mercaptoethanol at different time points (1-30 min). The protein samples were separated by SDS-PAGE (10%) and the TAP-associated fluorescence has been quantified using in-gel fluorescence imaging and normalized by TAP1 amount observed from immunoblotting. To determine 100% labeling, crude membranes containing TAP were solubilized with 2% SDS and then incubated with 150 µM BM for 30 min. Taking a pseudo first order kinetics into account, with a large excess of BM, the data were fitted by a monoexponential equation (see Chapter 3.4.10, equation. 2). Figure 4-11 shows a representative example for the efficiency of labeling Q277C and G282C with BM in different conformations. For Q277C mutant, the highest efficiency of labeling occurred in the ATP bound state (60%), and in the nucleotide free state the efficiency decreased to 50%. Similar labeling efficiencies were observed for G282C construct, for example in the ADP and nucleotide free state. These values were 62% and 60% respectively, whereas in the ATP bound state the efficiency decreased to 54% (Figure 4-11). Higher labeling efficiencies where observed for N283C and I284C mutants. The labeling of N283C with BM in the ADP bound state reached ~ 100%, whereas in the ATP bound conformation the efficiency decreased to 60%. Interestingly, the I284C mutant reached 95% labeling even after 1 min incubation in the nucleotide free state, whereas in the ATP/ADP bound conformations the labeling efficiency reached 95% after 30 min incubation (Figure 4-12). Similar high labeling efficiencies were observed for M285C and S286C mutants (Figure 4-13). The M285C, for example, shows a maximum level of labeling (95%) in the nucleotide free state, and a decreased efficiency (80%) in the ADP bound conformation. The highest labeling efficiency for S286C was observed in the nucleotide-free conformation (58%), whereas in the ATP

bound state the efficiency decreased to 40% (Figure 4-13). The labeling of R287C and V288C with BM in the ADP bound state reached a significant level (90% and 120% respectively), whereas in the ATP bound conformation the efficiencies decreased to 60% (R287C) and 58% (V288C) (Figure 4-14).

A complete graphical representation including the rate constants for BM labeling in different conformational states in shown in Figure 4-15 and Table 4-3. Taken together, the kinetics of fluorescence labeling suggest that the CL1 undergoes nucleotide binding-dependent conformational changes. For example, in the nucleotide free state the I284C mutant is labeled very fast, by reacting very rapidly with the fluorescent probe BM (Figure 4-12). In contrast, in the ATP bound and post-hydrolytic states the rate constant is 100- and 36-fold reduced, respectively. Interestingly, the maximal labeling values are similar for all three conformational states investigated. V288C displayed a significant reduction of the maximal labeling values following the attachement of BM in the ATP bound state (Table 4-3). Regarding the kinetics of fluorescence labeling in different conformational states, we can classify the CL1 mutants in four groups:

> (i) residues which have a slow kinetic of labeling for all conditions tested (N283C, R287C and V288C);
>
> (ii) residues which have higher rate constants for BM labeling in the absence of nucleotide than in the ATP bound state (I284C, M285C and S286C);
>
> (iii) mutants with higher rate constants in the ATP bound state than in the nucleotide free state (G282C);
>
> (iv) mutants with higher rate constants in the nucleotide free/ADP bound state than in the ATP bound conformation (Q277C).

Alternatively, we can classify the CL1 mutants in respect of the maximal labeling values obtained in different conformations:

> (i) mutants which have a higher maximal labeling in the ATP bound conformation (Q277C);
>
> (ii) residues which have a higher maximal labeling in the ADP bound state (N283C, R287C and V288C);
>
> (iii) mutants with a higher maximal labeling in the nucleotide free state (G282C);
>
> (iv) residues with similar maximal labeling in all of the conformational states investigated (I284C, M285C and S286C).

The knowledge that in the presence/absence of nucleotides significant values of the labeling rate constant (k_{on}) are observed, suggests that the nucleotide bound/free state of the NBD induces a conformational change of the CL1 during the transport cycle.

Figure 4-11. Labeling kinetics of the TAP1-single cystein mutants Q277C and G282C.
TAP containing crude membranes (0.5 mg total protein) were labeled with 50 µM BM in the presence of ATP, ADP and apyrase (nucleotide free). The reaction was stopped with β-mercaptoethanol at different time points (1 – 30 min). Aliquotes were applied to SDS-PAGE (10%). BM labeling was monitored by in-gel fluorescence imaging. Fluorescence intensity of TAP1 bands (normalized to TAP1 immunoblot signal) was expressed as percentage of the SDS-denatured TAP labeled with BM and plotted as a function of labeling time. The profiles were fitted using non-linear regression of the exponential association curve, $L = L_{max} \times (1-e^{-kt})$, where L is the percent labeled, L_{max} is the maximum percent labeled, t is time and k is the observed rate constant for labeling.

76

Figure 4-12. Labeling kinetics of the TAP1-single cystein mutants N283C and I284C.
TAP containing crude membranes (0.5 mg total protein) were labeled with 50 µM BM in the presence of ATP, ADP and apyrase (nucleotide free). The reaction was stopped with β-mercaptoethanol at different time points (1 – 30 min). Aliquotes were applied to SDS-PAGE (10%). BM labeling was monitored by in-gel fluorescence imaging. Fluorescence intensity of TAP1 bands (normalized to TAP1 immunoblot signal) was expressed as percentage of the SDS-denatured TAP labeled with BM and plotted as a function of labeling time. The profiles were fitted using non-linear regression of the exponential association curve, $L = L_{max} \times (1-e^{-kt})$, where L is the percent labeled, L_{max} is the maximum percent labeled, t is time and k is the observed rate constant for labeling.

Figure 4-13. Labeling kinetics of the TAP1-single cystein mutants M285C and S286C.
TAP containing crude membranes (0.5 mg total protein) were labeled with 50 µM BM in the presence of ATP, ADP and apyrase (nucleotide free). The reaction was stopped with β-mercaptoethanol at different time points (1 – 30 min). Aliquotes were applied to SDS-PAGE (10%). BM labeling was monitored by in-gel fluorescence imaging. Fluorescence intensity of TAP1 bands (normalized to TAP1 immunoblot signal) was expressed as percentage of the SDS-denatured TAP labeled with BM and plotted as a function of labeling time. The profiles were fitted using non-linear regression of the exponential association curve, $L = L_{max} \times (1-e^{-kt})$, where L is the percent labeled, L_{max} is the maximum percent labeled, t is time and k is the observed rate constant for labeling.
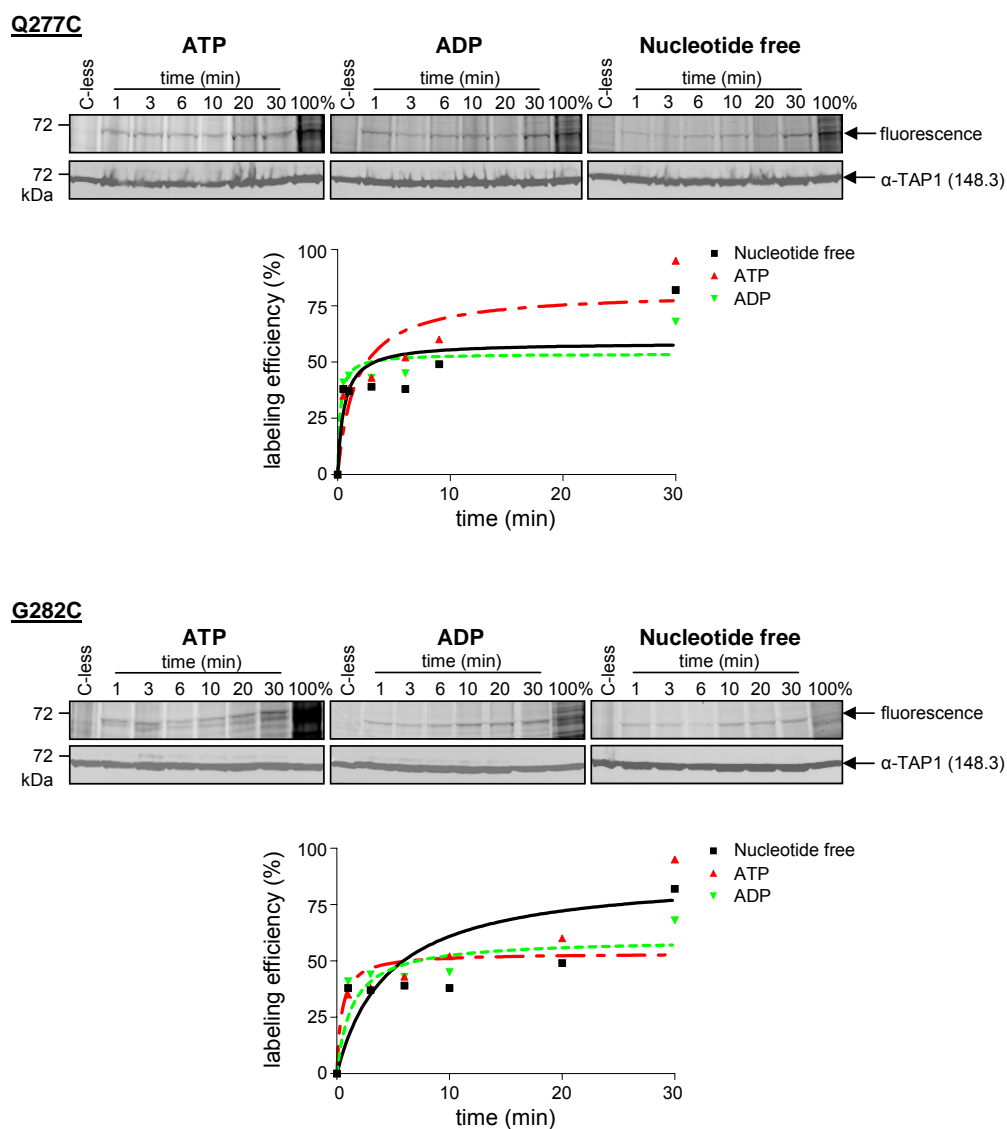
Figure 4-14. Labeling kinetics of the TAP1-single cystein mutants R287C and V288C.
TAP containing crude membranes (0.5 mg total protein) were labeled with 50 µM BM in the presence of ATP, ADP and apyrase (nucleotide free). The reaction was stopped with β-mercaptoethanol at different time points (1 – 30 min). Aliquotes were applied to SDS-PAGE (10%). BM labeling was monitored by in-gel fluorescence imaging. Fluorescence intensity of TAP1 bands (normalized to TAP1 immunoblot signal) was expressed as percentage of the SDS-denatured TAP labeled with BM and plotted as a function of labeling time. The profiles were fitted using non-linear regression of the exponential association curve, $L = L_{max} \times (1 - e^{-kt})$, where L is the percent labeled, L_{max} is the maximum percent labeled, t is time and k is the observed rate constant for labeling.
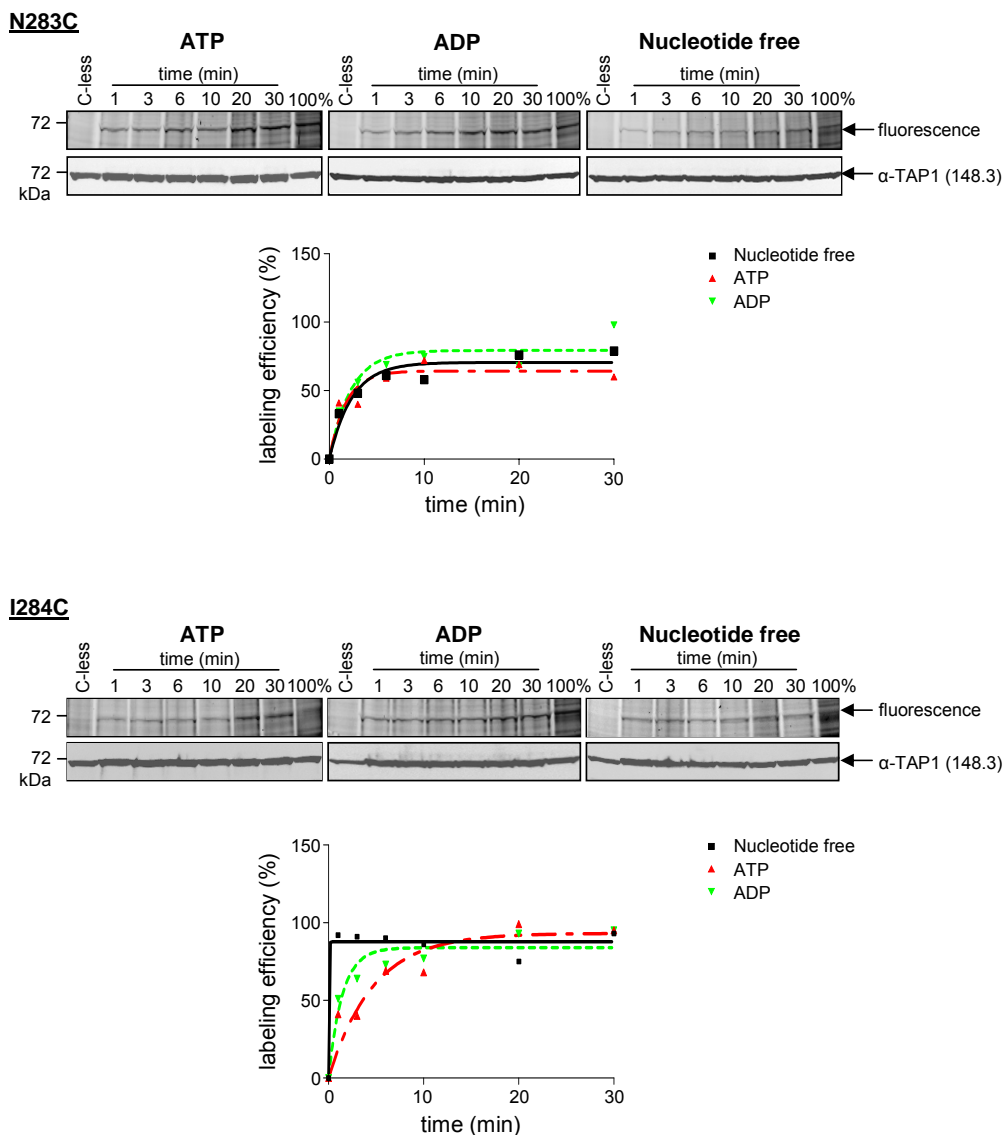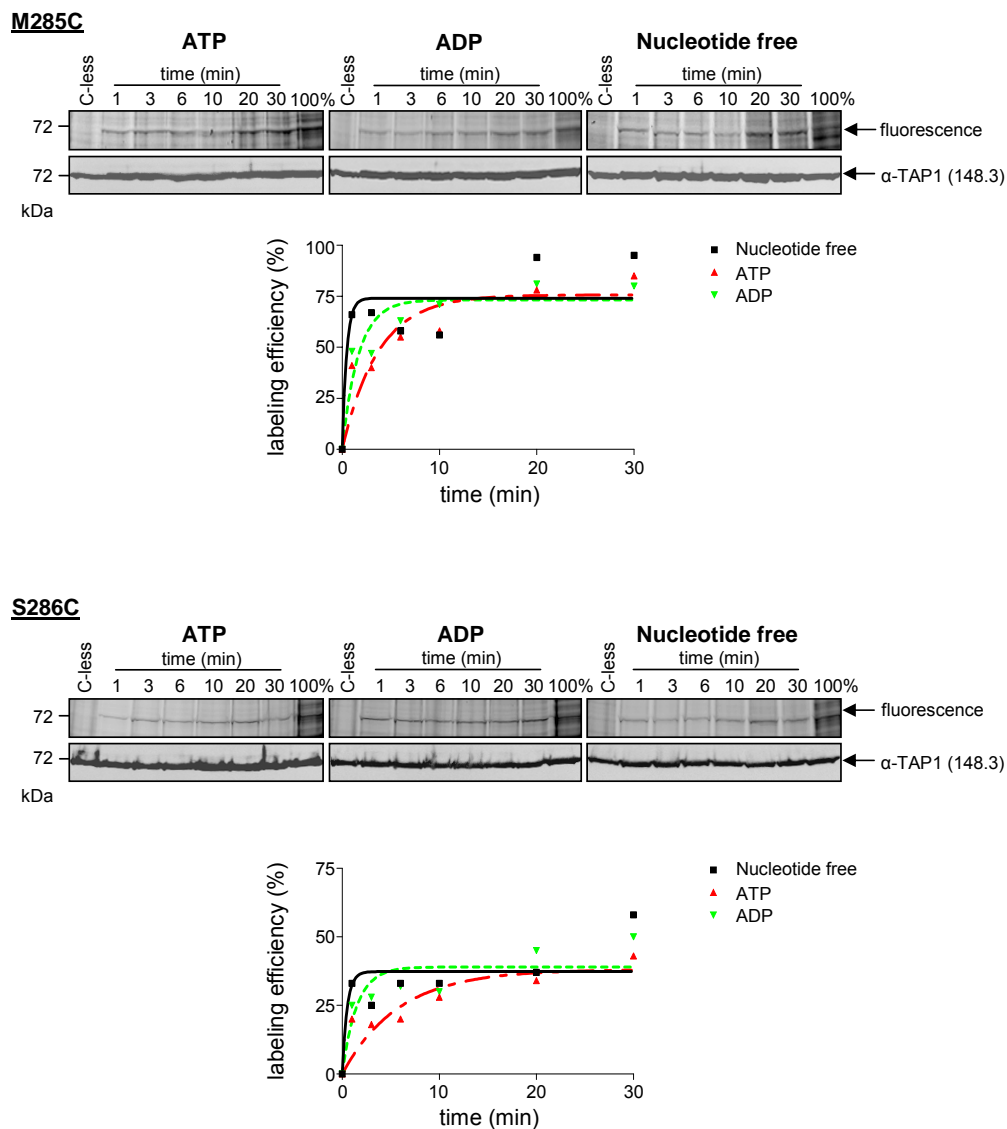
Figure 4-15. Rate constants for BM labeling.
TAP containing membranes (0.5 mg total protein) were labeled with 50 μM BM in the presence of ATP (red), ADP (green) and apyrase (nucleotide free; black) as described above (Figures 4-11 to 4-14). For each single cysteine mutant the rate constant has been determined by a monoexponential function.

Table 4-3. Rate constants (k_{on}) and efficiency of maximal labeling in different conformational states.

CL1 mutants	Nucleotide free		ATP		ADP	
	k_{on} (min^{-1})	Maximal labeling (%)	k_{on} (min^{-1})	Maximal labeling (%)	k_{on} (min^{-1})	Maximal labeling (%)
Q277C	4.84 ± 2.95	41 ± 2.48	1.81 ± 0.59	51 ± 3.91	4.57 ± 1.08	45 ± 1.16
G282C	0.15 ±0.05	65 ± 9.50	1.03 ± 0.52	40 ± 5.41	0.83 ± 0.58	45 ± 7.61
N283C	0.41 ± 0.11	71 ± 4.72	0.57 ± 0.21	64 ± 5.02	0.44 ± 0.14	79 ± 6.03
I284C	25.56 ± 1.13	88 ± 3.05	0.21 ± 0.06	93 ± 9.21	0.69 ± 0.21	84 ± 5.19
M285C	2.18 ± 2.22	74 ± 7.71	0.26 ± 0.10	76 ± 8.51	0.58 ± 0.22	73 ± 5.80
S286C	2.01 ± 2.39	37 ± 5.01	0.17 ± 0.07	38 ± 5.90	0.65 ± 0.36	39 ± 4.29
R287C	0.15 ± 0.04	81 ± 7.64	0.13 ± 0.06	61 ± 9.78	0.10 ± 0.03	96 ± 9.24
V288C	0.42 ± 0.15	90 ± 8.52	0.77 ± 0.27	60 ± 4.09	0.39 ± 0.04	118 ± 3.46

4.2.3   Modification of the CL1 influences the TMD-NBD signaling

We have seen that residues in the CL1 (TAP1) undergo conformational changes during the transport cycle. In the next phase of investigation the functional consequences of perturbing the CL1 topography were assessed. Topographical perturbation was achieved through covalent attachement of BM to the introduced cysteines. BM was chosen since it labels each of the chosen residues. Functional characterization of the covalently modified isoforms was determined by measuring the peptide binding and transport. For this reason we chose five CL1 single cysteine TAP1 mutants which were functional in respect of peptide binding and transport, namely Q277C/C-less, N283C/C-less, M285C/C-less, S286C/C-less, and V288C/C-less. Additional controls for labeling included C-less/C-less and F265C/C-less. The labeling efficiency of these mutants showed values between 36% (M285C) and 66% (N283C) (Table 4-4), which are smaller than the maximal labeling values measured in different conformational states. The maximal labeling values were estimated for a labeling period of 30 min, whereas for studying the effects of fluorescence labeling on TAP function, the labeling period was 10 min only. The peptide binding and transport of the mutant isoforms in the presence or absence of covalent modification by BM are shown in the Figure 4-16. Importantly, for all mutants tested there was no measurable effect of BM labeling on the peptide binding (Figure 4-16B). This suggests that the initial peptide binding is not adversely disrupted by labeling with BM. However, the peptide transport decreased after BM labeling. We identified two single cysteine mutants (N283C, and V288C) that exhibit 33% and 47% decrease in transport activity after BM labeling, respectively (Figure 4-16C). A particular interesting situation is observed for the single cysteine mutant V288C/C-less. Labeling efficiency of this mutant was 51% and the peptide binding after BM labeling was not influenced. However, a significant decrease of 47% of transport activity was observed after BM labeling. This suggests that fluorescence labeling of V288C disrupts completely the ATP-dependent peptide transport. Val-288, together with Ile-284 and Arg-287 are essential in sensing the bound peptide and interdomain signal transmission (Herget *et al.,* 2007).

Overall, the covalent attachment of BM to cysteine residues along the CL1 of TAP1 generated a number of specific effects on peptide transport. The main manifestations were a reduction in the degree of peptide transport after BM labeling. The observation that the covalent modification has no effect on peptide binding, but on the ATP dependent peptide transport, suggests that modifications of the CL1 residues influenced the TMD-NBD signaling.
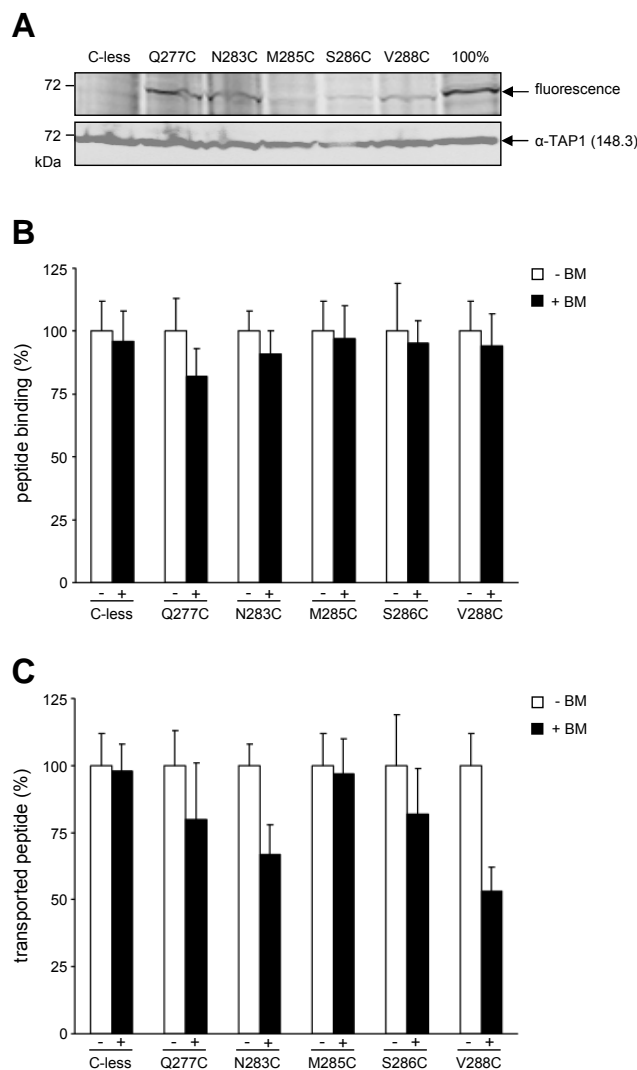
Figure 4-16. The effects of fluorescence labeling with BODIPY-maleimide on TAP function.
TAP containing membranes (0.5 mg total protein) were incubated with (+) or without (-) 50 µM BM in the presence of 10 mM Mg-ATP. After 10 min at 4°C the reaction was stopped with β-mercaptoethanol. Aliquotes were taken for immunoblot analysis and in-gel fluorescence measurements (A), as well as peptide binding (B) and ATP-dependent peptide transport (C), as described in Methods (Chapter 3). For peptide binding, TAP-containing membranes (35 µg of total protein) were incubated with 1 µM radiolabeled RRY(^{125}I)QKSTEL at 4°C for 15 min and the radioactivity was quantified by γ-counting. Specific peptide binding of the not-labeled construct (-BM) was normalized to 100%. For peptide transport, crude membranes (150 µg of total protein) were incubated with radiolabeled (1 µM RRY(^{125}I)QNSTEL) for 3 min at 32°C in the presence or absence of ATP (10 mM). N-core glycosylated and therefore transported peptides were bound to ConA-beads and the radioactivity associated with ConA-Sepharose was quantified by γ-counting. Specific peptide transport of the not-labeled construct (-BM) was normalized to 100%. C-less TAP has been used as negative control of labeling. In order to obtain 100% labeling, the mutant F265C/C-less was labeled with 50 µM BM for 30 min at 4°C, then denaturated in 2% (w/v) SDS for 10 min and additionally labeled with 100 µM BM for 5 min at 4°C. BM labeling was monitored by in-gel fluorescence imaging using the LumiImager software (Roche) and normalized for the TAP1 amount quantified by immunoblot detection. The error bars indicate the deviation of three independent experiments.

Table 4-4 The effects of fluorescence labeling with BODIPY-maleimide on TAP function.
Labeling efficiencies, peptide binding and transport activity (%) were determined from the in-gel fluorescence measurements and immunoblot detection (Figure 4-16).

CL1 mutant	Labeling efficiency (%)	Binding activity (%)	Transport activity (%)
Q277C	64	82 ± 11	80 ± 21
N283C	66	91 ± 9	67 ± 11
M285C	36	97 ± 13	96 ± 11
S286C	45	95 ± 9	82 ± 17
V288C	51	94 ± 13	53 ± 9

4.3   Transmission interface in ABC proteins

4.3.1   The role of the X-loop in the transmission interface of ABC proteins

ATP binding and hydrolysis in the nucleotide binding domain of an ABC transporter generates conformational changes, which are transmitted to the transmembrane domains through non-covalent interactions at the shared interface (Dawson and Locher, 2006). Based on the x-ray structures of ABC transporters, cytoplasmic loops in the TMDs display the interface with the NBDs (Locher *et al*., 2002; Dawson and Locher, 2006). In biochemical studies, the EAA motif in a cytoplasmic loop of the TMD, which is part of the L-loop found in BtuCD, and the Q-loop in the NBD were identified to be important for signal transduction between TMDs and NBDs in ABC importers (Mourez *et al.,* 1997; Hunke *et al.,* 2000). In contrast to the ABC import proteins, the ABC exporters like MsbA and Sav1866 show an enlarged TMD-NBD interface comprising the large cytosolic loops CL1 and CL2 of the TMD and different regions in the NBD (Reyes *et al*., 2006; Dawson and Locher, 2006). Unique for the ABC exporter is the interaction between CL2 in the TMD and the newly identified X-loop of the NBD. Strikingly, most of these interactions are between the TMD of one subunit and the NBD of the second one.

To probe the relevance of the recently identified X-loop in the peptide transporter TAP, I substituted the highly conserved glutamate of the X-loop of TAP2 by different amino acids and analyzed its impact on function. By detailed cysteine scanning combined with biochemical experiments, the physical contact between the X-loop and residues within CL1 and CL2 of an ABC exporter has been investigated. In addition, I identified residues in TAP1, which decouple peptide binding and transport. Trapping TAP by disulfide formation between residues in the TMD and the X-loop induced conformations incapable in peptide binding or transport demonstrating the relevance of structural rearrangements in the domain interface during the transport cycle.

4.3.2 Rational design for the communication between the transmembrane and nucleotide binding domain

During a transport cycle of ABC transporters, there is an intensive communication between the transmembrane and nucleotide binding domains. It is assumed that the binding of substrate is transmitted to the nucleotide binding domains, which subsequently induce conformational changes generated by NBD closure and ATP hydrolysis, allowing substrate translocation. The transmission interface is formed by coupling helices in the intracellular loops of the transmembrane domains and loop regions of the nucleotide binding domains (Locher *et al.*, 2002; Dawson and Locher, 2006). Based on the structure of the ABC exporter Sav1866 and in contrast to the x-ray structures of the importers, the coupling helices of one subunit interact not only with the own but also with the opposite nucleotide binding domain. The coupling helices are short α-helical stretches, which connect the long transmembrane helices and are the most far distant part of the transmembrane domain. Besides the Q-loop of the NBD, the ABC exporter specific X-loop is part of this interdomain network. To identify the interaction site in TAP, a 3D homology model of the core TAP complex based on the x-ray structure of Sav1866 has been constructed (Dawson and Locher, 2006). The CLs of TAP and Sav1866 are of similar length and are clearly distinct from the short intracellular loops of ABC importers. The constructed model is in agreement with experimental data concerning membrane topology, peptide binding pocket and peptide sensor. The NBDs are tightly engaged with distances reflecting the ATP bound state and the transmembrane domain opened to the ER luminal site. The X-loops of TAP1 and TAP2 occupy a central position where the conserved glutamates are surrounded by residues of the coupling helices 1 and 2 of the opposite subunits demonstrating the domain swapping. The X-loop is localized in the α-helical domain of the NBD close by the C-loop suggesting a possible role in transmitting conformational changes generated by ATP binding and hydrolysis. Interestingly, the X-loop of TAP2 shows higher sequence conservation in comparation to TAP1 (Figure 4-1). The function of the X-loop in coupling peptide binding to peptide transport was investigated. To elucidate the functional relevance of the interdomain cross-talk, I performed a cysteine scan of residues in CL1 and CL2 of cysteine-less TAP1 involved in interdomain contacts or identified to be crucial for signal transduction of peptide binding and transport (Herget *et al.*, 2007). By cysteine cross-linking the domain swapping was tested.

4.3.3   Function of the X-loop in coupling peptide binding to peptide transport

Based on the peptide sensor identified in CL1 next to coupling helix 1 of TAP1 (Herget *et al.*, 2007), we focused on the interaction and inter-domain communication with the X-loop of TAP2. The conserved glutamate (E602) was substituted by cysteine, arginine, aspartate, and alanine in a TAP2 variant containing a single cysteine (C213), important for the substrate selection (C. Baldauf, S. Schrodt, J. Koch, and R. Tampé, unpublished results). The X-loop mutants were co-expressed with Cys-less TAP1. Importantly, the X-loop mutations did not affect peptide binding (Figure 4-17B). The slight differences observed are caused by slide variations in the expression level due to co-infection. These results also demonstrate that the X-loop mutations do not interfere with membrane insertion and heterodimer assembly, which is required for peptide binding. Remarkably, all X-loop mutations showed a reduced transport activity, with 50% transport activity for E602C and 20% for E602D or E602A (Figure 4-17C). Complete disruption of peptide transport was observed for the E602R mutant. Thus, the conserved glutamate in the X-loop has a key function in the translocation event, but not in solute binding.

4.3.4   Functional important residues in the TMD (TAP1) - NBD (TAP2) interface

To decipher the transmission interface between the TMD-NBD in the TAP complex, we introduced single cysteines substitution in CL1 and CL2 of cysteine-less TAP1. The positions were identified by homology modeling to be in close contact with the NBDs or to be involved in interdomain signal transduction (Herget *et al*., 2007). All 24 single cysteine TAP1 variants were co-expressed with the TAP2_E602C construct. All TAP mutants showed similar expression (Figure 4-18). Peptide binding of CL1 mutants was not strongly influenced (Figure 4-18A). Minor effects correlate nicely with slight differences in TAP expression. However, all cysteine substitutions in coupling helix 1 besides Q277C interfered with peptide transport (Figure 4-18A). In addition, mutation of G282, I284 and R287 in the peptide sensor decreased transport activity. Surprisingly, in CL2, part of the peptide binding pocket (Nijenhuis *et al*., 1996; Ritz *et al*., 2001), only the mutation of R378C decreased significantly peptide binding, which is also reflected in diminished transport (Figure 4-18B). Furthermore, the cysteine substitution of P375 showed a prominent effect on peptide transport, whereas peptide binding is not disturbed (Figure 4-18B). In conclusion, mutations in CL1 do not interfere with peptide binding but have a strong effect on transport. Therefore, CL1 seems to be the transmission interface between TMDs and NBDs. CL2 is part of the peptide binding

pocket also reflected in the disruption of peptide binding by cysteine substitution of R378. However, this loop has only minor effects in signaling since only the cysteine mutation of P375 disturbs coupling between peptide binding and transport.
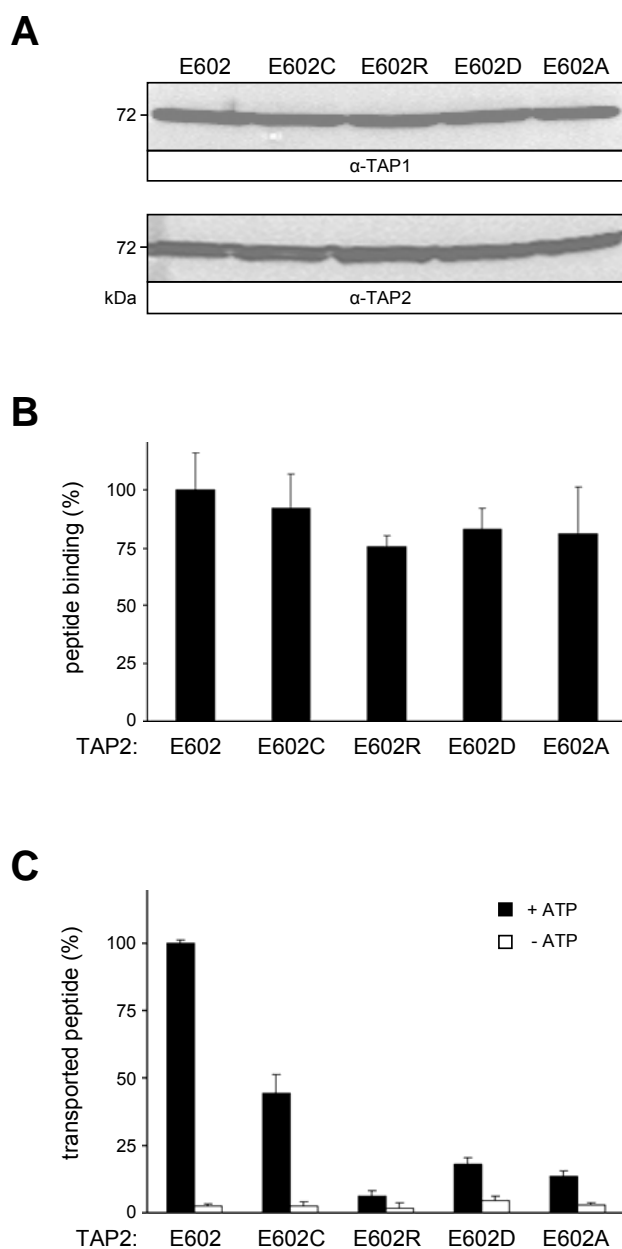
Figure 4-17. Functional importance of the conserved glutamate of the X-loop of TAP2.
(A) Expression of X-loop mutants. Crude membranes from Sf9 insect cells (20 μg protein/lane) were analyzed by SDS-PAGE (10%) followed by immunoblotting against TAP1 (mAb 148.3, α-TAP1) and TAP2 (mAb 435.3, α-TAP2). (B) Peptide binding of X-loop mutants. TAP-containing membranes (35 μg of total protein) were incubated with 1 μM radiolabeled RRYQKSTEL at 4°C for 15 min. Specific peptide binding to TAP1_C-less/TAP2_C213_E602 was normalized to 100%. (C) Peptide transport of X-loop mutants. Crude membranes (150 μg of total protein) were incubated with fluorescein-labeled peptide (1 μM, RRYQNSTC$^{(F)}$L) for 5 min at 32°C in the presence or absence of ATP (3 mM). N-core-glycosylated and therefore transported peptides were bound to ConA-beads and quantified by fluorescence detection after elution with methyl-α-D-mannopyranoside. ATP-specific transport of TAP1_C-less/TAP2_C213_E602 was normalized to 100%. The experiments were performed in triplicate. Error bars show the standard deviation.
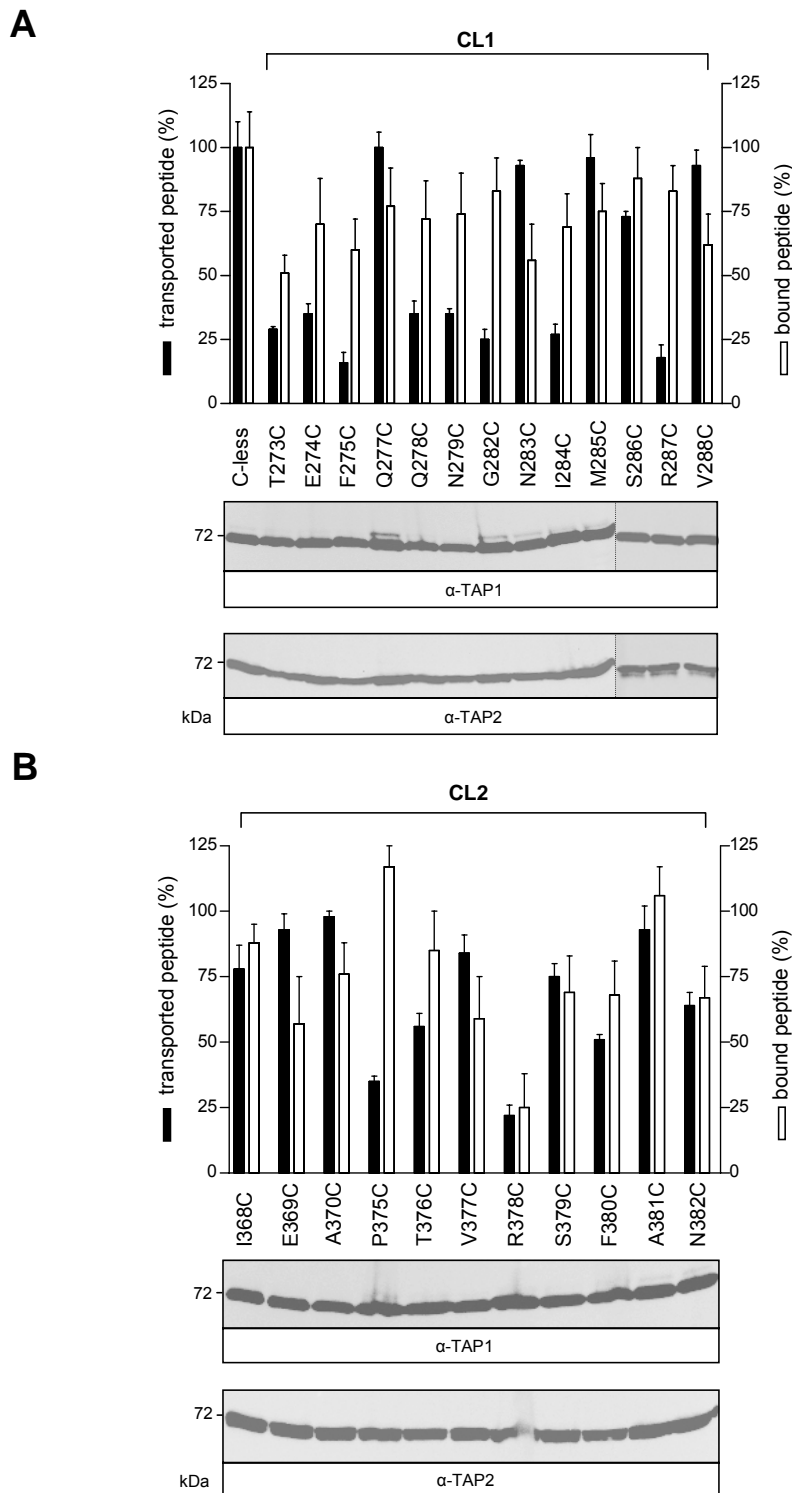
Figure 4-18. CL1 and CL2 of TAP1 have different functions.
Single cysteine TAP1 mutants of CL1 (A) or CL2 (B) in complex with TAP2_E602C were analyzed for peptide binding (open bars) and transport (filled bars). For peptide binding, TAP-containing membranes (35 μg of total protein) were incubated with 1 μM radiolabeled RRYQKSTEL at 4°C for 15 min. Specific peptide binding to TAP1_C-less/TAP2_E602 was normalized to 100%. For peptide transport crude membranes (150 μg of total protein) were incubated with fluorescein-labeled peptide (1 μM RRYQNSTC$^{(F)}$L) for 5 min at 32°C in the presence or absence of ATP (3 mM). N-core-glycosylated and therefore transported peptides were bound to ConA-beads and quantified by fluorescence detection after elution with methyl-α-D-mannopyranoside. ATP-specific transport of TAP1_C-less/TAP2_E602C was normalized to 100%. The experiments were performed in triplicate. Error bars show the standard deviation. Equal amounts of TAP were confirmed by immunoblotting.

4.3.5   Establishing disulfide formation

To investigate the domain swapping, the spatial proximity between residues in the CLs of TAP1 and the X-loop of TAP2 was analyzed by oxidative cysteine cross-linking. To enable disulfide formation even in hydrophobic environment, copper phenanthroline (CuPhen) was used as catalyst. The cross-linking conditions were established with crude membranes containing combinations of TAP1_I368C / TAP2_E602C and TAP1_I381C / TAP2_E602C. Both TAP1 mutations are located in CL2 and do neither influence peptide binding nor transport. Cross-linking was performed at 4°C to minimize thermal denaturation of TAP and to decrease structural fluctuations within the TAP complex. The reaction time was restricted to 1 min, in which on one hand to reach maximal disulfide formation but on the other hand with minimal site reactions (oxidation of thiols to sulfite). After incubation with CuPhen, reaction was stopped by complexing copper by EDTA. After oxidative crosslinking, disulfide formation was inhibited by blocking free sulfhydryl groups by N-ethylmaleimide. Subsequently, samples were separated by SDS-PAGE and analyzed by immunoblotting using monoclonal antibodies against human TAP1 and TAP2. In addition to monomeric TAP1 and TAP2 (75 kDa), also higher molecular weight species of TAP1 and TAP2 were observed under oxidizing conditions (Figure 4-19A, B). Immunoblotts probed with anti-TAP1 antibody showed high molecular weight bands with a molecular weight of 174 kDa and 162 kDa, whereas stained with anti-TAP2 antibody bands at 162 kDa and 150 kDa occurred. Notably, all three high molecular weight bands were visible if immunoblotts stained with both antibodies simultaneously. Remarkably, single expressed TAP1 or TAP2 cysteine containing subunits showed bands at 174 kDa and 150 kDa, respectively, indicating the formation of homodimeric complexes, reported also previously (Antoniou *et al*., 2002). In conclusion, the upper band resembles TAP1 homodimers (174 kDa), the middle of the three bands indicate TAP1/2 heterodimers (162 kDa), whereas the lower band reflects TAP2 cross-linked homodimers (150 kDa). Interestingly, for TAP1 constructs with a single cysteine in CL1 a cross-linked homodimeric TAP1 species was only observed for single expressed TAP1 but not in combination with TAP2 probably reflecting the different expression levels. The cross-linking is cysteine specific since cysteine-less constructs of TAP show no higher molecular weight bands. In addition, disulfide bond formation is CuPhen dependent and reversible by reducing with DTT (Figure 4-19A). Cross-link efficiency could not be enhanced by increasing concentrations of CuPhen or elongation of the reaction time most probably due to unproductive sulfhydryl oxidation either to sulfinic or sulfonic acid (Careaga and Falke, 1992).

Since the TAP2 construct used for cysteine cross-linking studies contained in addition to the cysteine in the X-loop also the functional important cysteine at position 213, the contribution of this region in subunit contacts was analyzed. Therefore, TAP2 variants with single natural occurring cysteines, all located in transmembrane helix two of the TAP2 core complex, were expressed in combination with cysteine-less TAP1 or with TAP1_A381C. All of these cysteines are shielded or spatially separated since none of these cysteines are capable to form covalently linked neither homodimeric nor heterodimeric complexes (Figure 4-19C). In contrast, the TAP2 variant containing C213 and E602C form homodimeric as well as heterodimeric cross-linked complexes. In conclusion, we have evolved conditions, under which TAP subunits can be specifically cross-linked by cysteines located in the CLs of TAP1 and the X-loop of TAP2.
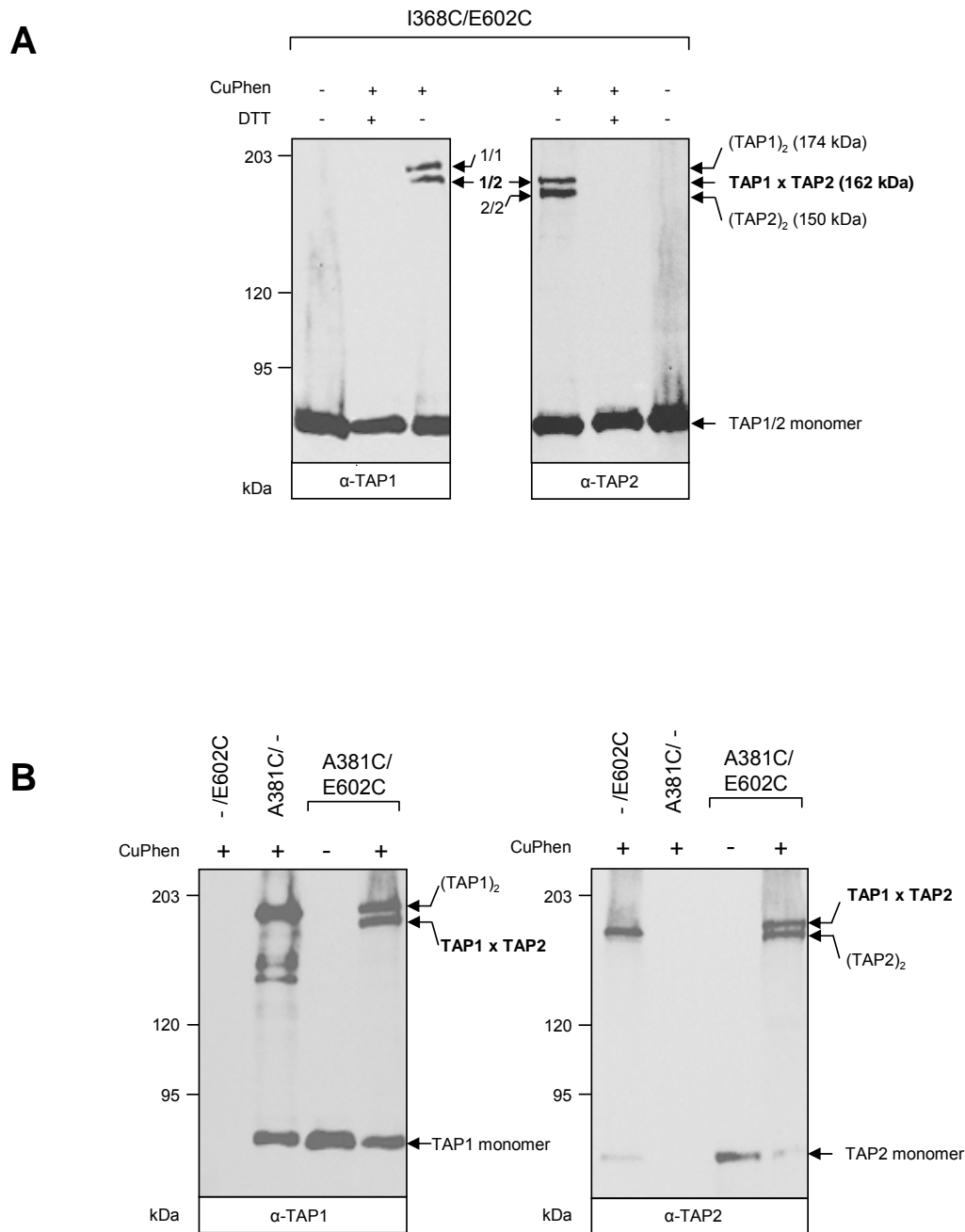
Figure 4-19. Oxidative cross-linking between TAP1 and TAP2.
Crude membranes containing different TAP1 and TAP2 constructs (500 μg of total protein) were incubated in the presence or absence of copper phenanthroline (1 mM Cu^{2+}) for 1 min at 4°C. Oxidative cross-linking was terminated by NEM and EDTA, 10 mM each. Samples (20 μg of total protein per lane) were subjected to non-reducing SDS-PAGE (6%) followed by immunoblotting against TAP1 (mAb 148.3, α-TAP1) and TAP2 (mAb 435.3, α-TAP2). The positions of the cross-linked TAP1/TAP2 (highlighted in bold), homodimeric $(TAP1)_2$ and $(TAP2)_2$ and monomeric TAP1 and TAP2 are indicated. (A) Disulfide formation under oxidative conditions. Copper phenanthroline dependent intermolecular disulfide formation was tested with TAP1_I368C/TAP2_E602C. To show reversibility of disulfide cross-linking, 100 mM DTT were added in the sample buffer. (B) Identification of TAP oligomers. To assign the high molecular weight bands to hetero- and homooligomeric TAP complexes, crude membranes containing TAP1_A381C, TAP2_E602C or both subunits were cross-linked and analyzed by immunoblotting. (C) C213 of TAP2 is not involved in disulfide formation. Crude membranes of different TAP variants were cross-linked and immunoblotted.

C
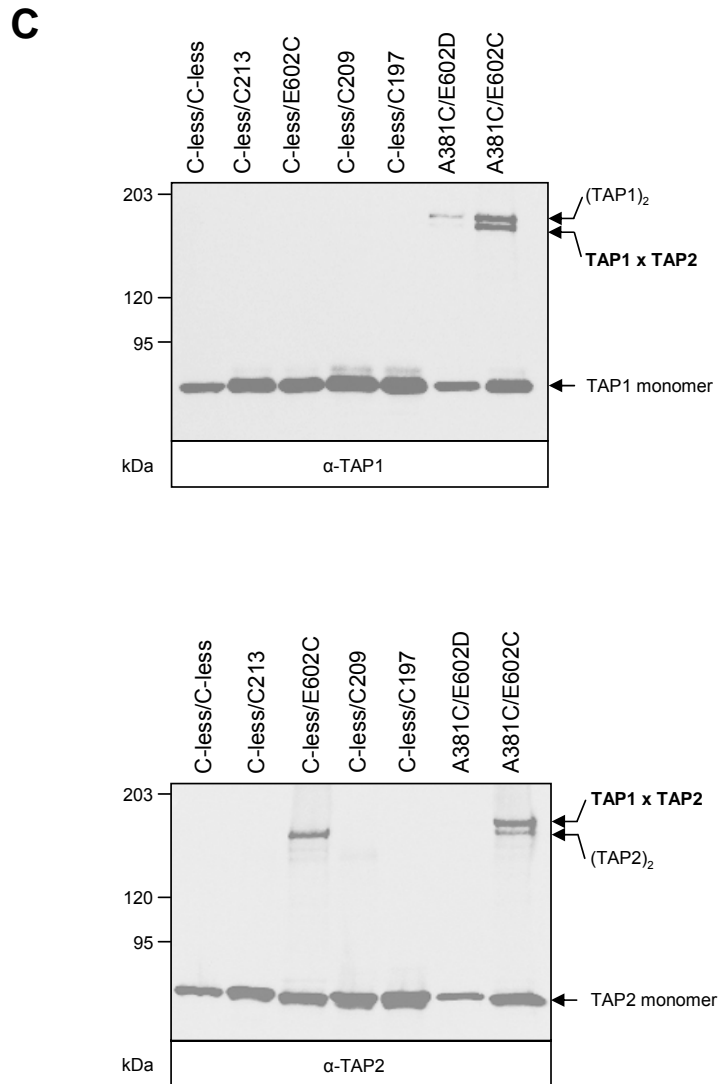
Figure 4-19. continued

4.3.6   Domain swapping within the TAP complex

To investigate the spatial proximity of the CLs of TAP1 and the X-loop of TAP2 and therefore proof the domain swapping, we performed oxidative cross-linking with all described mutants. Interestingly, all cysteine mutants in CL1 of TAP1 are in physical contact with the X-loop (Figure 4-20). However, gradual differences exist. Strongest cross-linking was observed for residues covering the C-terminal half of the coupling helix 1 and the N-terminal half of the peptide sensor. Cross-linking of residues within CL2 with the X-loop are less efficient. Pronounced interaction was detected only for residues 380 and 381 (Figure 4-21). Similar cross-linking for all mutants was obtained between 4°C and 37°C. Moreover, cross-linking with bifunctional cysteine-specific reagent MTS-2-MTS gave the same picture. In addition, disulfide formation did not change in different states of the transport cycle. Therefore, CL1 appears to be highly dynamic since contacts can form even between residues

more than 1.5 nm apart as deduced from the 3D homology model (see Figure 4-1). Similar rotational and translational freedom of cysteine residues was also reported for other proteins such as D-galactose chemosensory receptor (Careaga and Falke, 1992). In conclusion, the CLs from TAP1 interact with the X-loop of TAP2, proofing the domain swapping. In addition, CL1 seems to be more involved in this interaction than CL2.
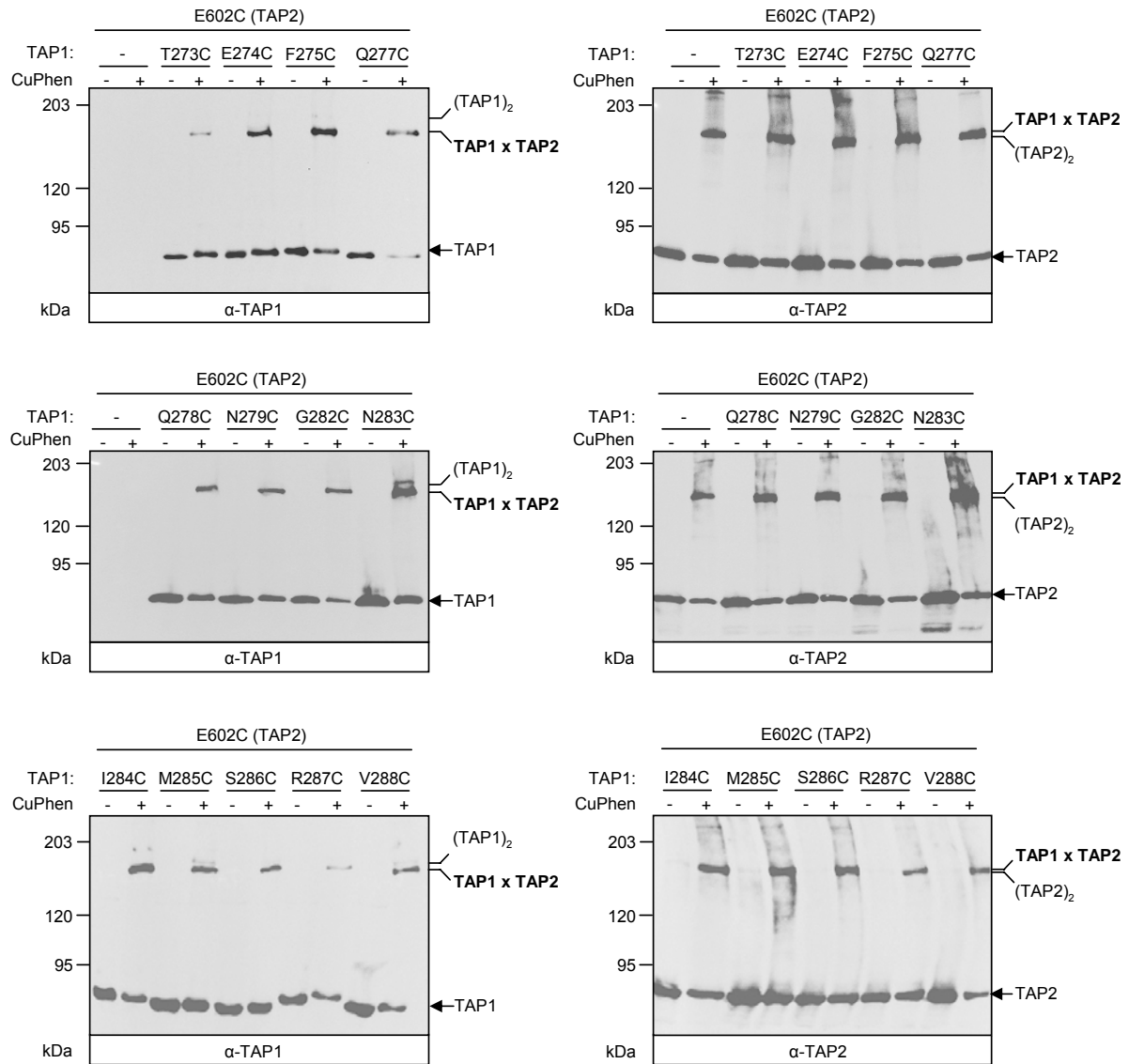
Figure 4-20. Physical interaction between CL1 of TAP1 and X-loop of TAP2.
Crude membranes containing different single cysteine variants of the CL1 of TAP1 and TAP2_E602C (500 µg of total protein) were incubated in the presence or absence of copper phenanthroline (1 mM Cu^{2+}) for 1 min at 4°C. Oxidative cross-linking was terminated by NEM and EDTA, 10 mM each. Samples (20 µg of total protein per lane) were subjected to non-reducing SDS-PAGE (6%) followed by immunoblotting against TAP1 (mAb 148.3, α-TAP1) and TAP2 (mAb 435.3, α-TAP2).
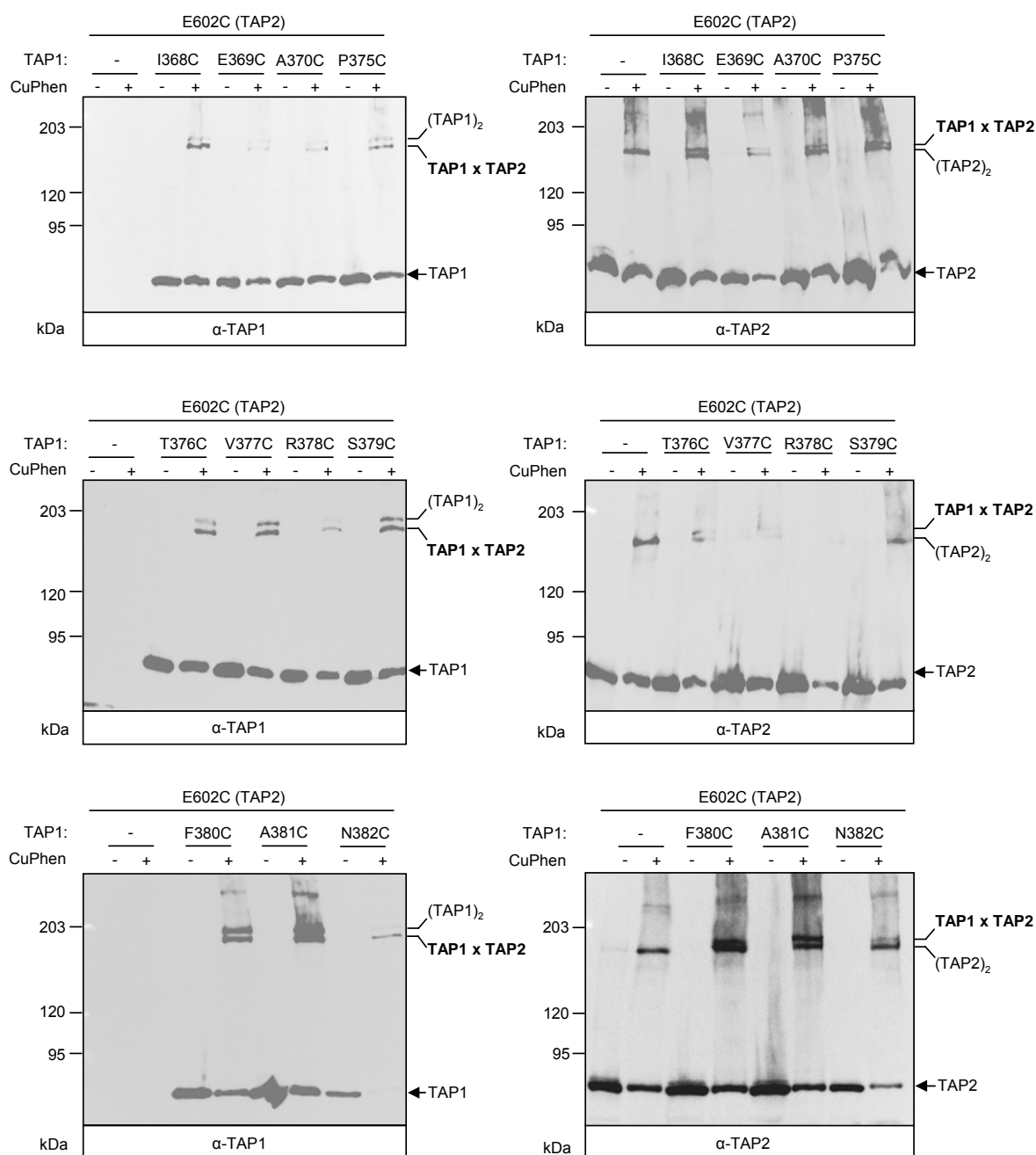
Figure 4-21. Physical interaction between CL2 of TAP1 and X-loop of TAP2.
Crude membranes containing different single cysteine variants of the CL2 of TAP1 and TAP2_E602C (500 μg of total protein) were incubated in the presence or absence of copper phenanthroline (1 mM Cu^{2+}) for 1 min at 4°C. Oxidative cross-linking was terminated by NEM and EDTA, 10 mM each. Samples (20 μg of total protein per lane) were subjected to non-reducing SDS-PAGE (6%) followed by immunoblotting against TAP1 (mAb 148.3, α-TAP1) and TAP2 (mAb 435.3, α-TAP2).

4.3.7   Arresting TAP in a transport incompetent state

Due to the motional freedom of the loops investigated herein, transport state dependent differences in cysteine cross-linking were not observed. However, TAP undergoes multiple conformational changes during peptide transport, in which the CLs seems to be involved (Reits *et al.,* 2000; Neumann *et al.,* 2002; Herget *et al.,* 2007). Therefore, we addressed the interdomain cross-talk by restricting the structural rearrangement by disulfide formation between the X-loop and CL1 or CL2. For cysteine cross-linking, we choose TAP1_Q277C/TAP2_E602C and TAP1_A381C/TAP2_E602C. These mutations had no influence on peptide binding and transport but showed high cross-linking efficiency (Figure 4-22A). Disulfide formation reduced peptide binding of TAP1_A381C/TAP2_E602C to 5% of the reduced state, whereas it had no influence on TAP1_Q277C/TAP2_E602C as well as TAP1_Cys-less/TAP2_E602C (Figure 4-22B). However, in the presence of CuPhen, peptide transport was decreased by cysteine cross-linking of TAP1_Q277C/TAP2_E602C and TAP1_A381C/TAP2_E602C to 10% in comparasion to the absence of CuPhen (Figure 4-22C). Transport inhibition relies on disulfide formation since transport activity of TAP1_Cys-less/TAP2_E602C was only slightly reduced under oxidizing conditions. In addition, transport inhibition was reversed by reducing disulfide bridges with β-mercaptoethanol. In conclusion, cross-linking between CL2 and the X-loop seems to change the structure of the peptide binding pocket, whereas the disulfide bridge between CL1 and X-loop destroys the interdomain communication most likely by impeding structural rearrangements.

A
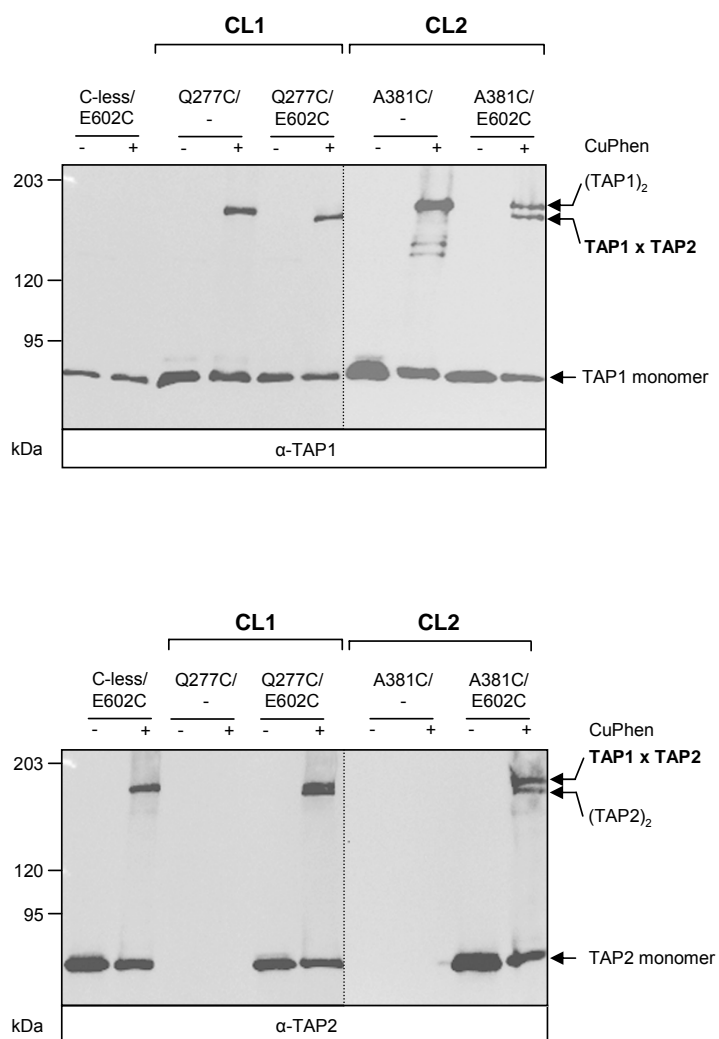
Figure 4-22. Differential effects of disulfide bridges on TAP function.
Crude membranes containing different single cysteine variants of the CL1 and CL2 of TAP1 and TAP2_E602C (500 µg) were incubated in the presence or absence of copper phenanthroline (1 mM Cu^{2+}) for 1 min at 4°C and washed twice. (A) Identification of disulfide formation. After cross-linking, samples (20 µg of total protein per lane) were analyzed by SDS-PAGE (6%) and immunoblotting. (B) Peptide binding. TAP-containing membranes (35 µg of total protein) were incubated with 1 µM radiolabeled RRYQKSTEL at 4°C for 15 min. Specific peptide binding to TAP constructs, which were incubated in the absence of copper phenanthroline, were normalized to 100%. (C) Peptide transport. Crude membranes (150 µg of total protein) were incubated with fluorescein-labeled peptide (1 µM, RRYQNSTC$^{(F)}$L) for 5 min at 32°C in the presence or absence of ATP (3 mM). ATP-specific transport of TAP constructs not incubated with copper phenanthroline were normalized to 100%. To proof reversibility, cross-linked samples were reduced with 100 mM β-mercaptoethanol for 5 min at 4°C. The experiments were performed in triplicate. Error bars show the standard deviation.

B

C
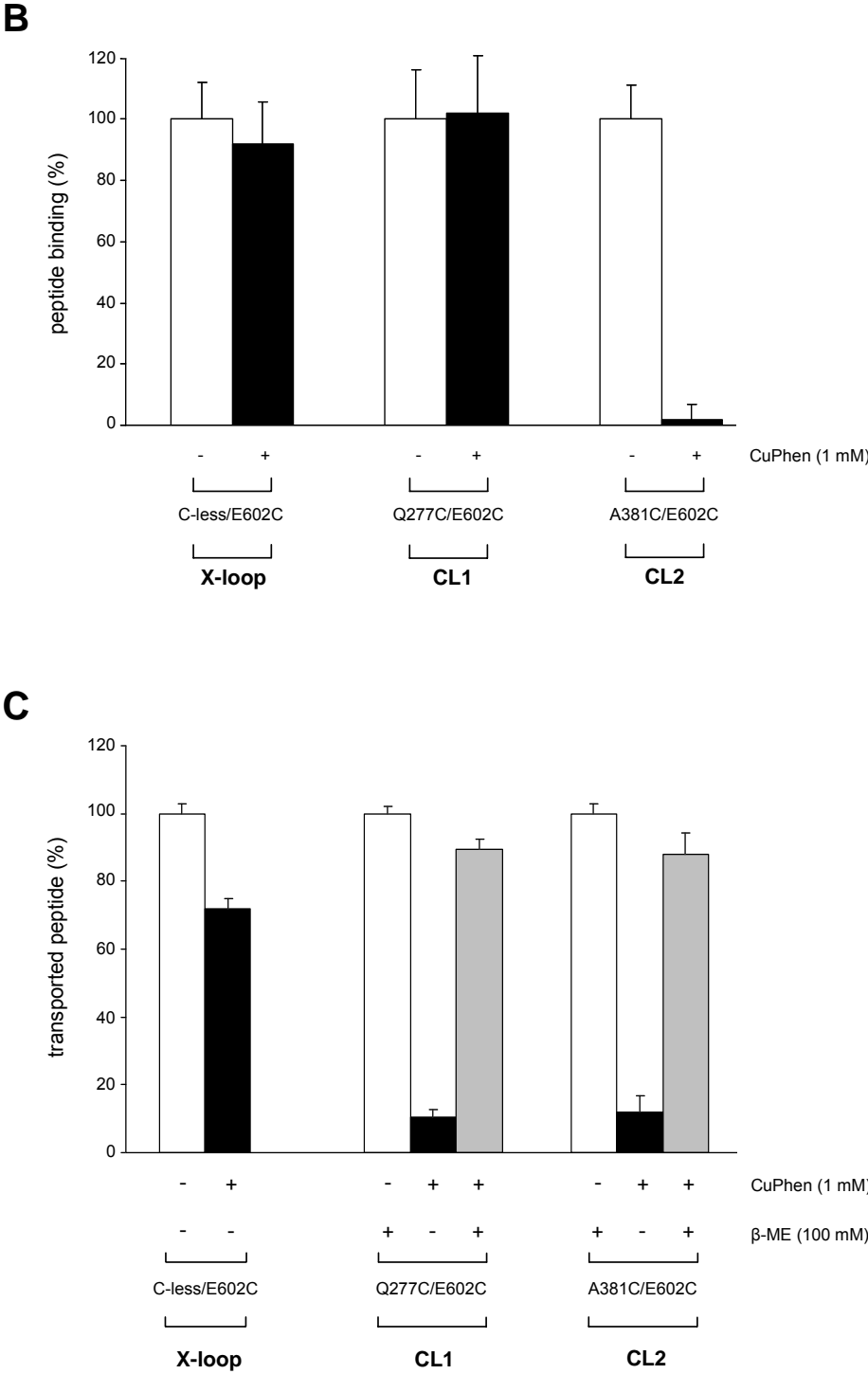
Figure 4-22. continued

96

5.   Discussion

5.1.   CL1 of TAP1 has an important role in substate sensing and signal transmission

As the key component of the MHC class I peptide-loading complex, TAP translocates proteasomal degradation products into the lumen of the endoplasmic reticulum. Peptide binding is a key step in the overall TAP transport mechanism and in the selection of epitopes presented by MHC class I molecules (Uebel and Tampé, 1999; van Endert *et al.*, 2002). ATP hydrolysis by the NBDs is tightly coupled to peptide binding to the transmembrane domains of TAP (Gorbulev *et al.*, 2001; Chen *et al.*, 2003). However, sterically restricted peptides bound to TAP do not trigger ATP hydrolysis and are not transported (Gorbulev *et al.,* 2001). It is an open question how the quality of incoming peptides is checked and transmitted to the ATPase domains to drive peptide translocation.

The identified peptide sensor and transmission interface aligns with the cytosolic loop 1 of MsbA or the CL1 of the Sav1866. Biochemical and structural studies showed that these transmembrane loops are in close contact with the Q-loop and the α-helical domain of the NBD (Locher *et al.*, 2002; Dalmas *et al.*, 2005, Ward *et al.*, 2007). Derived from x-ray structures, the Q-loop connects the catalytic domain with the α-helical domain of the NBDs and is involved in structural rearrangement by sensing bound ATP, which is the initial step for dimerization of the NBDs (Smith *et al.,* 2002). The cysteine-scanning approach support the function of the CL1 as signal transducer in ABC exporters, because it does not interfere with substrate binding but with substrate transport. Interestingly, the most severe effects in disrupting the tight coupling between peptide binding and transport and the inter-domain communication were found for the most conserved residues in the sensor loop, comprising Gly-282, which seems to function as a helix breaker, as well as Ile-284 and Arg-287 of TAP1. The later two residues are separated by three residues and therefore face the same site of an α-helix. Together with Val-288, these residues are essential in sensing the bound peptide and interdomain signal transmission. Interestingly, the dual function can also be structurally separated to the sensor region at the C-terminal end and the transmission site upstream of the α-helix.

The peptide contact site is restructured during the ATP hydrolysis cycle. In the nucleotide-free state, the strongest cross-linking between peptide and sensor loop is detected. Binding of nucleotide weakens this interaction, which could resemble a structural

rearrangement. For P-glycoprotein such a conformational change by binding AMP-PNP could be shown by cryo-electron microscopy (cryo-EM) of two-dimensional crystals (Rosenberg *et al.,* 2003). Trapping P-glycoprotein in the ATP hydrolysis state by ortho-vanadate, which resembles the same trapped state as AlF_x in myosin (Fisher *et al.,* 1995*;* Smith and Rayment, 1996), induced a further change in structure. Also TAP showed a structural change trapped in the ATP hydrolysis transition state, because direct contact between peptide and the sensor and transmission loop is abolished.

5.2.   Cross-talk between TMD/NBD revealed by fluorescence accessibility studies

We have demonstrated that the CL1 is involved in the tight coupling of peptide binding and transport (Herget *et al.*, 2007). Further data support the idea that this sensor and transmission interface is restructured during the ATP hydrolysis cycle, emphasizing its important function in the cross-talk between the transmembrane and nucleotide binding domains (Herget *et al.*, 2007). Our *modus operandi* involves introducing unique cysteine residues along the CL1 of TAP1 and the subsequent covalent attachment of fluorescent probes to these. The fluorescence labeling has been applied to CL1 in order to decipher the topography and to observe whether this region is involved in the cross-talk between TMD–NBD. Following labeling, two residues (N283C and V288C) were associated with a reduction of the ATP-dependent peptide transport activity. Interestingly, the covalent attachment of fluorescent probes has no effect on peptide binding.

What is the mechanism underlying the effect of covalent modification of CL1 on the coupling of peptide binding in the TMDs to ATP hydrolysis by the NBDs? The data demonstrated that the perturbation of the ATP-dependent peptide transport process caused by covalent attachment of BODIPY-maleimide to CL1 is most likely due to the modification of the communication pathway that links the peptide binding event in the TMDs to the progression of the catalytic cycle in the NBDs. The communication pathway clearly involves CL1, given that mutations or covalent modification within this helix impairs the peptide transport activity.

What is the nature of involvement of CL1 in the TMD–NBD communication pathway? To address this question, the topography of the CL1 was examined in distinct conformations of TAP. The conformations reflected the progression of the protein through the catalytic cycle and was visualized by the accessibility of engineered cysteines to covalent modification by iodoacetamidofluorescein and maleimide probes. This loop region was highly

accessible to covalent modification, regardless of the physicochemical properties of the different probes. In addition, the CL1 displayed different accessibility to probes when the protein undergoes distinct conformations (e.g., nucleotide-free state), thereby reflecting conformational transitions.

The kinetics of fluorescence labeling showed that, except for Q277C, all of the residues reflected similar rate constants (k_{on}) for BM labeling in the presence of ATP (Table 4-3). However, significant differences of the rate constants for BM labeling were observed in the absence of nucleotide or in the presence of ADP (Table 4-3). The highest rate constant observed was for I284C in the nucleotide-free state, $k_{on} = 26 \pm 1$ (min^{-1}). Interestingly, in the ADP-bound state the highest rate constant was observed for Q277C mutant. The communication pathway clearly involves CL1, given that mutations or covalent modification within this helix impairs the ATP-dependent peptide transport. On the basis of the observations in the present investigation, it appears that CL1 undergoes distinct changes in conformation in response to events occurring in the NBDs. A general view along the CL1 region, indicates important conserved residues which are essential in peptide transport (Gly-282, Ile-284 and Arg-287; Figure 5-1). Interestingly, among these residues, the mutant I284C displayed the greatest propensity for changes in accessibility, indicating important conformational changes in this region of the helix. Covalent modification of CL1 induces severe effects on peptide transport. For example, BM labeling of V288C mutant induces a lost of ATP-dependent peptide translocation. The N- and C-terminal regions of CL1 are oriented in different local environments. The N-terminal region has an hydrophilic character, whereas the C-terminus is accessible for amphiphilic and hydrophobic probes.
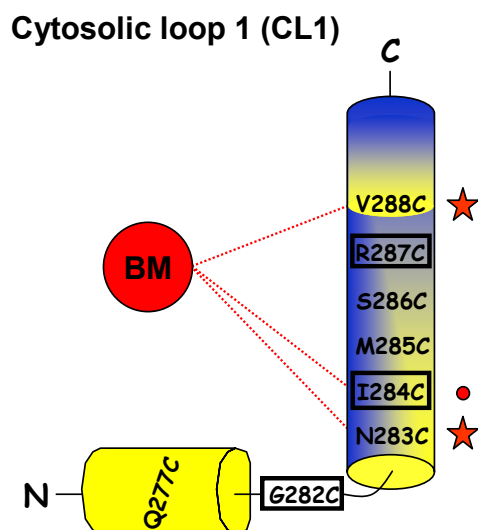
Figure 5-1. Residues of CL1 (TAP1) important in TMD-NBD signal transduction.
Along the CL1 region, conserved residues are required for transport at a step downstream of binding (Gly-282, Ile-284 and Arg-287; labeled in squares). The covalent attachment of BM (highlighted in red circle) to cysteine residues along the CL1 generated a lost of transport for V288C mutant and a 33% decrease in transport activity for N283C (marked by red stars). In the nucleotide-free state the I284C mutant (marked by red circle) is labeled very fast, by reacting very rapidly with the fluorescent probe BM. In contrast, in the ATP-bound and post-hydrolytic states the rate constant is 100- and 36-fold reduced, respectively. The N-terminal region of CL1 is accessible for hydrophilic probe (IAF, highlighted in yellow cylinder), whereas the C-terminal region is accessible for hydrophobic probe (CM, highlighted in blue cylinder).

In the absence of a high-resolution structure of TAP, homology models may assist in the interpretation of these experimental data. Such an homology model for TAP based on the crystal structure of Sav1866 (Dawson and Locher, 2006) has been generated in the group of Peter Tieleman (Department of Biological Sciences, University of Calgary). According to this model the CL1 residues investigated in the present work are located in the cellular loop 1 of TAP1. Along this region, a short helix oriented roughly parallel to the membrane plane, named coupling helix 1 (CH1), provides a bulk of contacts to the NBDs of both subunits. From this homology model, a *trans*-contact between Q277-TAP1 and E602-TAP2, as well as a *cis*-contact between E274-TAP1 and Y555-TAP1 is observed (Figure 5-2). The amino acid side chains of cysteine, glutamine (Q277C) or glutamate (E274C) in the CL1 of TAP1 can build hydrogen bonds, and alternatively, drastical mutagenesis along the CL1 can be investigated, and on the other side, the single cysteine mutations could be derivatized with methanethiosulfonate reagents (MTS) in order to simulate a positive, negative and hydrophobic side chain. From the accessibility studies we can draw the conclusion that the CL1 of TAP1 has an amphiphatic character. The putative interaction partners in the NBD are Q- and X-loop as well as the vicinity of Walker A motifs, which is supported by a significant

structural and biochemical amount of data (Dalmas *et al.*, 2005; Dawson and Locher, 2006; Zolnerciks *et al.*, 2007).
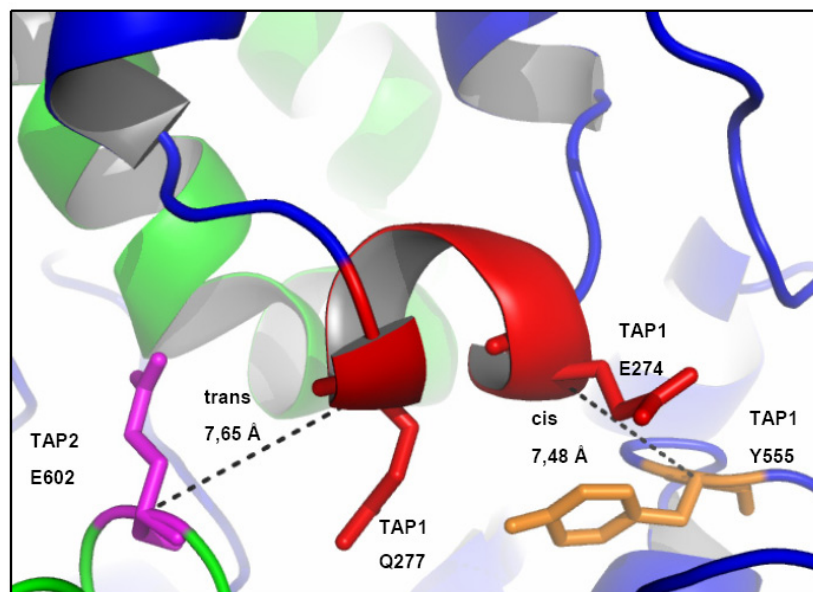
Figure 5-2. Putative TMD-NBD transmission interface of TAP1.
Amino acid residues of CH1 (red) are highlighted as stick representation. The putative interaction partners E602 (TAP2, *trans*-contact, magenta) and Y555 (TAP1, *cis*-contact, orange), which are located in the vicinity of CH1, are illustrated. The C_α-atom distances between Q277:E602 and E274:Y555 are shown. The presented structure is an homology model based on the crystal structure of Sav1866 (Dawson and Locher, 2006), modeled in the group of Peter Tieleman (Department of Biological Sciences, University of Calgary).

In summary, our data support the hypothesis that CL1 is likely involved in the bi-directional communication between TMDs and NBDs of TAP that is essential for a coupled transport process. The present work demonstrates that the topography of CL1 undergoes significant reconfiguration between the nucleotide-free, nucleotide-bound and post-hydrolytic states of TAP. These results are in good agreement with data of Loo *et al.*, which suggests that the binding of ATP to the NBDs can induce long-range conformational changes to alter the structure of the TMDs of human P-glycoprotein (Loo *et al.*, 2007). Similar fluorescence labeling studies show that nucleotide binding can affect the conformation of TMDs in P-glycoprotein (Rothnie *et al.*, 2004). Different cysteine crosslinking approaches have shown that in the ATP bound state the CL1 and Q-loop are moved away from each other; however, crosslinking between these two domains could still be achieved in the presence of ATP-Mg plus vanadate when homobifunctional crosslinkers with a length of 13Å were used (Dalmas *et al.,* 2005; Daus *et al.,* 2007).

5.3. The role of the X-loop in the transmission interface of TAP

Peptide binding, ATP hydrolysis and peptide transport are tightly coupled within the peptide transporter TAP implying signal transduction between TMD and NBD (Gorbulev *et al.*, 2001; Herget *et al.*, 2007). In addition to the Q-loop, the newly identified X-loop, present in ABC exporters only, was proposed from the X-ray structure of Sav1866 to be involved in cross-talk between TMD and NBD (Dawson and Locher, 2006). By substitution of the conserved glutamate of the X-loop in TAP2, we first demonstrated that this loop is indeed essential for coupling of peptide binding to the subsequent translocation step. We next identified critical residues for this event in CL1 and CL2. By using both cysteine scanning and cross-linking, we mapped the contact sites of the CLs of TAP1 with the X-loop of TAP2, thereby providing direct evidence for domain intertwining in a heterodimeric ABC transport complex. It is remarkable that mutations in CL1 almost exclusively disrupt TAP function in a step downstream of peptide binding. The inter-domain cross-talk involves structural rearrangements, since conformational trapping of TAP by disulfide formation reversibly interrupts peptide transport.

The X-loop is a motif solely found in the NBD of ABC exporters. Substitution of the conserved glutamate E602 in the X-loop of TAP2 had no effect on TAP expression and peptide binding, demonstrating further that these mutations do not affect membrane insertion, folding, and heterodimer assembly. However, peptide transport is impaired by substitution with a positively charged residue. The introduction of a short hydrophobic side chain or the conservative mutation to aspartate reduced transport activity to 20%, while substitution to cysteine decreased transport activity by only 50%. The reduced side chain of aspartate may position the negative charge in an unfavored environment. The sulfhydryl group of cysteine is largely tolerated. The X-loop appears very flexible since it shows a high B-factor in the X-ray structure of ABC exporters as well as of isolated NBDs (Zaitseva *et al.,* 2005; Lewis *et al.,* 2004). Moreover, this region may be involved in transmitting ATP binding and hydrolysis of the NBDs to the TMDs via structural changes because of its close proximity to the C-loop, which senses the γ-phosphate of the bound ATP in the NBD-NBD interface. Remarkably, in the nucleotide-free and the ATP-bound state of HlyB-NBD (Zaitseva *et al.,* 2005; Schmitt *et al.,* 2003) the root-mean-square deviation of the C_α atom of the X-loop glutamate is three-fold higher than the entire NBD. However, it should be pointed out that the X-loop is conserved only in subfamily B and C of eukaryotic ABC transporters. Whether this region is also part of the transmission interface in the other subfamilies, remains to be addressed in future studies.

A surprising finding of this study was that each of the CLs of core TAP1 had different functions. None of the mutations in CL1 influenced peptide binding, whereas most substitutions interfered with the translocation step. These residues are located in coupling helix 1 and the peptide sensor (Figure 4-1). The 3D model suggests that the bulky hydrophobic phenylalanine residues of the coupling helix (F275 and F276) point into a hydrophobic core, thus stabilizing CL1, and substitution of these residues may collapse coupling helix 1. Mutations of hydrophilic and charged residues probably affect the orientation of CL1 or disrupt inter-domain contacts. The function of CL1 in peptide sensing and signaling during the ATP-hydrolysis cycle was proposed recently, with residue 288 of TAP1 found to be in direct contact with the bound peptide (Herget *et al.,* 2007). In addition, this sensor region is structurally reorganized during the transport cycle. Thus the presence of bound peptide may be signaled via the adjacent coupling helix 1 to other parts of the protein responsible for downstream events in the transport cycle.

Surprisingly, substitutions in CL2 of TAP1 only had minor impacts on TAP function. By peptide photo-crosslinking and deletion studies, the region comprising CL2 was previously identified as part of an overlapping peptide-binding region (Nijenhuis *et al*., 1996; Ritz *et al*., 2001). Here, we could demonstrate that arginine 378 in TAP1 is essential for peptide binding. The 3D model indicates that this residue is part of coupling helix 2. Its side chain points into the opposite direction of the X-loop and might stay in direct contact with the peptide. It is tempting to speculate that the positive guanidinium group forms a salt bridge with the C-terminal carboxyl group of the peptide, which is essential for recognition. Interestingly, the P375C substitution disrupted the transport function of TAP leaving peptide binding unaffected. Proline 375 caps the coupling helix 2 by a kink, which may be important for signal transmission.

By oxidative cysteine cross-linking, we verified direct contacts between the CLs and the X-loop, thus providing evidence for domain swapping and dynamic transmission interface in the TAP complex. Based on the number of efficiently cross-linked residues, CL1 was found to be more flexible than CL2. However, it should be mentioned that CL1 is in close proximity not only to the X-loop of the opposite NBD but also to the Q-loop of the NBD in "*cis*" as demonstrated by chemical cross-linking studies using the multidrug exporter BmrA of *B. subtilis* (Dalmas *et al*., 2005). On the other hand, CL2 does not exclusively form contacts with the X-loop but also with the Q-loop of the "*trans*" NBD as shown by chemical cross-linking for P-glycoprotein and CFTR (Zolnerciks *et al*., 2007; Serohijos *et al*., 2008; He

et al., 2008). A similar Sav1866-like inter-domain organization was recently found for the yeast ABC exporter Yor1p (Pagant *et al.,* 2008).

The transmission interface, framed by two CLs and the NBDs, showed considerable flexibility as we detected a similar cross-linking pattern in the presence of ATP, ADP or ATP plus vanadate or BeF_x. A highly dynamic arrangement of the transmission interface was also observed for CFTR (Dawson and Locher, 2006; Serohijos *et al.,* 2008; He *et al.,* 2008). The need for conformational changes in the transmission interface during the transport cycle is supported by transport inhibition through cross-linking of the CLs with the NBDs. In the bacterial exporter BmrA, cross-linking of CL1 with the Q-loop of the NBD in "*cis*" disrupted ATP hydrolysis and substrate transport (Dalmas *et al.,* 2005). Arresting CFTR by chemical cross-linking of CL2 or CL4 with residues near the Q-loop of the "*trans*" NBD impaired channel activity (Serohijos *et al.,* 2008; He *et al.,* 2008). Furthermore, also the maltose permease is fixed by disulfide formation between the "EAA"-motif of the TMD and a surface exposed residue in the "*cis*" NBD in an inactive state (Daus *et al*., 2007). Here, we demonstrate that cross-linking of CL1 with the X-loop in "*trans*" arrested the TAP complex in a transport-incompetent state, which was still able to bind peptides. The transmission interface is not restricted to a narrow region of the polypeptide chain but rather is distributed among the NBDs and CLs of the TMDs. Notably, cross-linking of CL2 in TAP1 and the X-loop in TAP2, impaired not only transport but also peptide binding. Since CL2 is part of the peptide-binding pocket, it is likely that the disulfide bridge induces a binding-incompetent conformation. Thus, the CLs have different functions in substrate recognition, signaling and transport binding.

Besides cross-linked heterodimers of TAP1 and TAP2, covalent coupled homodimers of TAP1 and TAP2 were detected under oxidative conditions. TAP2 homodimers were also observed by chemical cross-linking using activated NHS esters (Antoniou *et al*., 2002). In addition, TAP1 or TAP2 homodimers are inactive in respect of peptide binding and subsequently peptide transport. We believe that the homodimer formation occurs only in cells, in which one subunit is in excess. This conclusion is supported by the fact that the homodimeric signal in single infected cells was much stronger than in double infected cells. Since we coinfected the insect cells by two separate viruses coding for TAP1 and TAP2, single infected cells will be present. Importantly, oxidative cross-linking was observed only for a few residues. Residues in CL1 and CL2 of TAP1 as well as residue 602 in TAP2 seems to be in appropriate conformation for cross-linking of homodimeric as well as heterodimeric complexes. However, the natural occurring cysteines at position 197, 209 and 213 of TAP are

not involved in any disulfide formation although they are accessible for cysteine reactive compounds (Baldauf *et al*., manuscript in preparation).

5.4.   **Different models of coupling mechanisms for importers and exporters**

Different models of how ABC transporters might work can be found in the literature. Because their substrates and even the direction of transport are distinct, it might seem unreasonable to suggest that importers and exporters operate on a similar mechanism. However, the structures of full ABC transporters suggest that they indeed share a common way of converting ATP binding and hydrolysis to essentially unidirectional transport (Dawson *et al*., 2007).

In the absence of nucleotide, the NBDs adopt an open conformation, as visualized by ModBC-A or HI1470/71 (Hollenstein *et al*., 2007; Pinkett *et al*., 2007). Upon binding ATP, the NBDs adopt a "closed" conformation, with bound nucleotide sandwiched between the Walker A and the LSGGQ motifs, as observed in Sav1866. A comparision of ModBC and Sav1866 reveals that the distance between their coupling helices decreases substantially (by some 10-15 Å) upon ATP binding (Dawson *et al*., 2007). In other words, binding of ATP brings the two coupling helices closer together (Figure 5-3A). As the coupling helices approach, the TMDs flip from the inward-facing to the outward-facing conformation. After hydrolysis and dissociation of inorganic phosphate and ADP, the NBDs assume an "open" conformation. This increases the distance between coupling helices and flips the transporters into an inward-facing conformation. Such a conversion is reminiscent of the "alternating access and release" mechanism, postulated half a century ago (Jardetzky, 1966) and still providing a useful framework for understanding the mechanism of transporters such as major facilitators (Lemieux *et al*., 2004; Guan and Kaback, 2006).

However, domain-swapped interactions do not appear to be universal among ABC transporters. The structures of bacterial ABC importers reveal that the dimer interface forms from the two separate monomers and likely involves a distinct mechanism of transport. One limitation of these structural studies is that the full transporters have been crystallized in the absence of substrate, making the interpretation of how substrate binding influences interdomain interaction and transport difficult. Another key question is how nucleotide binding and/or hydrolysis influences domain arrangement and facilitates transport. Although a number of different crystal structures have been solved for transporters stabilized by the presence of different nucleotides, three structures of ABC exporters in different states, MsbA-AMP-PNP, MsbA-ADP·Vi, and Sav1866-ADP do not show any striking conformational

differences (Dawson and Locher, 2006; Dawson and Locher, 2007; Ward *et al.,* 2007). Moreover, *in vitro* characterization of the domain-domain interactions in CFTR suggests that the CL4-NBD1 and CL2-NBD2 interfaces do not change in the presence of ATP, ADP, or AMP-PNP, suggesting that the formation of these two modules is not influenced by ATP binding/hydrolysis.

On contrary, our results examining the nucleotide dependence of substrate binding to CL1 of the TAP complex were suggestive of structural rearrangements during ATP hydrolysis (Herget *et al.,* 2007). Recently, biochemical studies on the eukaryotic drug pump Yor1p revealed relatively weak NBD-NBD and CL-CL interactions that may correspond to transient sites of crosstalk between domains required for coupling of ATP hydrolysis with substrate translocation (Pagant *et al.,* 2008). Based on the data presented in the PhD thesis, a new adapted putative model of transmission interface in the TAP complex can be drawn (Figure 5-3B):

1. The peptide transporter is in the "open" conformation. The peptide and nucleotide are not bound, therefore the CHs are not in direct contact with the NBD.

2. Peptide and ATP bind independently to TAP (van Endert *et al.,* 1994; Tomazin *et al.,* 1996).

3. TAP is loaded always with ATP, because of the high intracellular ATP concentration (Lapinski *et al.,* 2003). During the ATP binding, the CL1 adopts a "pre-peptide binding conformation".

4. After peptide binding, the peptide sensor V288 recognizes the peptide binding conformation (Herget *et al.,* 2007), which subsequently induces a structural change of the side chain of R287 (see Chapter 5.1 and Neumann *et al.,* 2002).

5. The conformational change of R287 allows formation of the cation-π-complex with the aromatic aminoacids of CH1, which induces a conformational change of the CL1.

6. This conformational change of CL1 facilitates a direct contact between CH1 and NBD. The side chains of E274 and Q277 build a TMD-NBD "signal transduction bridge" with their interaction partners in the NBD, that induces NBD dimerization.

7. The conformational change of NBD act as a power stroke, that will be communicated to the TMD via TMD-NBD "signal transduction bridge". This leads to a change of the TMD conformation (Loo *et al.,* 2007) and subsequently the peptide will be released in the ER-lumen.

8. After ATP hydrolysis, the TMD-NBD "signal transduction bridge" will be disconnected and the transporter will return to the "open" conformation.
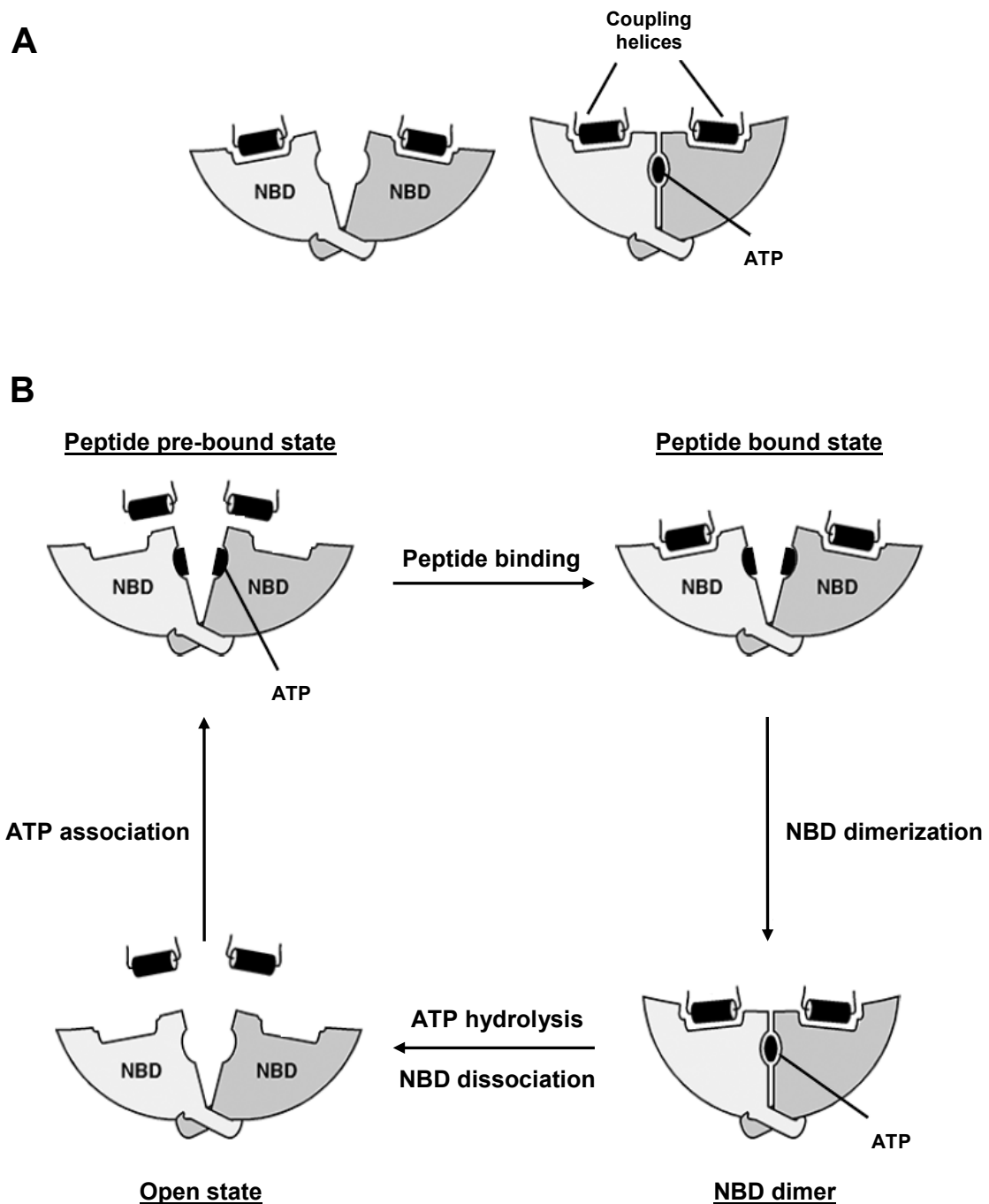
Figure 5-3. Dynamic interactions between CHs and NBDs during the translocation cycle.
(A) Model of interaction based on structural data. According to this model, the CHs stay in contact with the NBDs during the translocation cycle (Dawson *et al.,* 2007). (B) Model of interaction based on biochemical studies of the present PhD thesis.

6.   Literature

Abele, R. and Tampé, R. (1999) Function of the transport complex TAP in cellular immune recognition. *Biochim. Biophys. Acta.* **1461,** 405-419.

Abele, R. and Tampé, R. (2004) The ABCs of immunology: structure and function of TAP, the transporter associated with antigen processing. *Physiology (Bethesda)* **19**, 216-224.

Albrecht, C., McVey, J. H., Elliott, J. I., Sardini, A., Kasza, I., Mumford, A. D., Naoumova, R. P., Tuddenham, E. G., Szabo, K. and Higgins, C. F. (2005) A novel missense mutation in ABCA1 results in altered protein trafficking and reduced phosphatidylserine translocation in a patient with Scott syndrome. *Blood* **196**, 542-549.

Androlewicz, M. J., Anderson, K. S. and Cresswell, P. (1993) Evidence that transporters associated with antigen processing translocate a major histocompatibility complex class I binding peptide into the endoplasmic reticulum in an ATP-dependent manner. *Proc. Natl. Acad. Sci. U. S. A.* **90,** 9130-9134.

Androlewicz, M. J. and Cresswell, P. (1994) Human transporters associated with antigen processing possess a promiscuous peptide-binding site. *Immunity* **1,** 7-14.

Antoniou, A. N., Ford, S., Pilley, E. S., Blake, N. and Powis, S. J. (2002) Interactions formed by individually expressed TAP1 and TAP2 polypeptide subunits. *Immunology* **106,** 182-189.

Arora, S., Lapinski, P. E. and Raghavan, M. (2001) Use of chimeric proteins to investigate the role of transporter associated with antigen processing (TAP) structural domains in peptide binding and translocation. *Proc. Natl. Acad. Sci. U. S. A.* **98,** 7241-7246.

Attaya, M., Jameson, S., Martinez, C. K., Hermel, E., Aldrich, C., Forman, J., Lindahl, K. F., Bevan, M. J. and Monaco, J. J. (1992) Ham-2 corrects the class I antigen-processing defect in RMA-S cells. *Nature* **355,** 647-649.

Baumeister, W., Walz, J., Zühl, F. and Seemüller, E. (1998) The proteasome: paradigm of a self-compartmentalizing protease. *Cell* **92,** 367-380.

Beismann-Driemeyer, S. and Tampé, R. (2004) Function of the antigen transport complex TAP in cellular immunity. *Angew. Chem. Int. Ed.* **43,** 4014-4031.

Beninga, J., Rock, K. L. and Goldberg, A. L. (1998) Interferon-gamma can stimulate post-proteasomal trimming of the N terminus of an antigenic peptide by inducing leucine aminopeptidase. *J. Biol. Chem.* **273,** 18734-18742.

Brown, M. G., Driscoll, J. and Monaco, J. J. (1991) Structural and serological similarity of MHC-linked LMP and proteasome (multicatalytic proteinase) complexes. *Nature* **353,** 355-357.

Browne, B. L., McClendon, V. and Bedwell, D. M. (1996) Mutations within the first LSGGQ motif of Ste6p cause defects in a-factor transport and mating in *Saccharomyces cerevisiae*. *J. Bacteriol.* **178,** 1712-1719.

Careaga, C. L. and Falke, J. J. (1992a) Themal motions of surface α-helices in the D-Galactose chemosensory receptor. *J. Mol. Biol.* **226,** 1219-1235.

Careaga, C. L. and Falke, J. J. (1992b) Structure and dynamics of *E. coli* chemosensory receptors: engineered sulfhydryl studies. *Biophys. J.* **62,** 209-219.

Chen, H. L., Gabrilovich, D., Tampé, R., Girgis, K. R., Nadaf, S. and Carbone, D. P. (1996) A functionally defective allele of TAP1 results in loss of MHC class I antigen presentation in a human lung cancer. *Nat. Genet.* **13,** 210-213.

Chen, J., Lu, G., Lin, J., Davidson, A. L. and Quiocho, F. A. (2003a) A tweezers-like motion of the ATP-binding cassette dimer in an ABC transport cycle. *Mol. Cell* **12**, 651-661.

Chen, M., Abele, R. and Tampé, R. (2003b) Peptides induce ATP hydrolysis at both subunits of the transporter associated with antigen processing. *J. Biol. Chem.* **278**, 29686-29692.

Chen, M., Abele, R. and Tampé, R. (2004) Functional non-equivalence of ATP-binding cassette signature motifs in the transporter associated with antigen processing (TAP). *J. Biol. Chem.* **279,** 46073-46081.

Coux, O., Tanaka, K. and Goldberg, A. L. (1996) Structure and functions of the 20S and 26S proteasomes. *Annu. Rev. Biochem.* **65,** 801-847.

Dalmas, O., Orelle, C., Foucher, A. E., Geourjon, C., Crouzy. S., Di Pietro, A. and Jault, J. M. (2005) The Q-loop disengages from the first intracellular loop during the catalytic cycle of the multidrug ABC transporter BmrA. *J. Biol. Chem.* **280,** 36857-36864.

Daumke, O. and Knittler, M. R. (2001) Functional asymmetry of the ATP-binding-cassettes of the ABC transporter TAP is determined by intrinsic properties of the nucleotide binding domains. *Eur. J. Biochem.* **268,** 4776-4786.

Daus, M. L., Grote, M., Mueller, P., Doebber, M., Herrmann, A., Steinhoff, H. J., Dassa, E. and Schneider, E. (2007) ATP-driven MalK dimer closure and reopening and conformational changes of the "EAA" motifs are crucial for function of the maltose ATP-binding cassette transporter (MalFGK2). *J. Biol. Chem.* **282,** 22387-22396.

Davidson, A. L. and Chen, J. (2004) ATP-binding cassette transporters in bacteria. *Annu. Rev. Biochem.* **73,** 241-268.

Dawson, R. J. P. and Locher, K. P. (2006) Structure of a bacterial multidrug ABC transporter. *Nature* **443,** 180-185.

Dawson, R. J. P. and Locher, K. P. (2007) Structure of the multidrug ABC transporter Sav1866 from Staphylococcus aureus in complex with AMP-PNP. *FEBS Lett.* **581,** 935-938.

Dawson, R. J. P., Hollenstein, K. and Locher, K. P. (2007) Uptake or extrusion: crystal structures of full ABC transporters suggest a common mechanism. *Mol. Microbiol.* **65,** 250-257.

Dean, M., Rzhetsky, A. and Allikmets, R. (2001) The human ATP-binding cassette (ABC) transporter superfamily. *Genome Res.* **11,** 1156-1166.

De la Salle, H., Hanau, D., Fricker, D., Urlacher, A., Kelly, A., Salamero, J., Powis, S. H., Donato, L., Bausinger, H., Laforet, M., Jeras, M., Spehner, D., Bieber, T., Falkenrodt, A., Cazenave, J. P., Trowsdale, J. and Tongio, M. M. (1994) Homozygous human TAP peptide transporter mutation in HLA class I deficiency. *Science* **265,** 237-241.

DeMars, R., Rudersdorf, R., Chang, C., Petersen, J., Strandtmann, J., Korn, N., Sidwell, B. and Orr, H. T. (1985) Mutations that impair a posttranscriptional step in expression of HLA-A and -B antigens. *Proc. Natl. Acad. Sci. U. S. A*. **82**, 8183-8187.

Ehring, B., Meyer, T. H., Eckerskorn, C., Lottspeich, F., and Tampé, R. (1996) Effects of major-histocompatibility-complex-encoded subunits on the peptidase and proteolytic activities of human 20S proteasomes. Cleavage of proteins and antigenic peptides. *Eur. J. Biochem.* **235,** 404-415.

Falk, K., Rotzschke, O., Stevanovic, S., Jung, G. and Rammensee, H. G. (1991) Allele-specific motifs revealed by sequencing of self-peptides eluted from MHC molecules. *Nature* **351,** 290-296.

Fenteany, G., Standaert, R. F., Lane, W. S., Choi, S., Corey, E. J., and Schreiber, S. L. (1995) Inhibition of proteasome activities and subunit-specific amino-terminal threonine modification by lactacystin. *Science* **268,** 726-731.

Fisher, A. J., Smith, C. A., Thoden, J. B., Smith, R., Sutoh, K., Holden, H. M. and Rayment, I. (1995) X-ray structures of the myosin motor domain of *Dictyostelium discoideum* complexed with MgADP·BeF$_x$ and MgADP·AlF$_4^-$. *Biochemistry* **34,** 8960-8972.

Flajnik, M. F. and Kasahara, M. (2001) Comparative genomics of the MHC: glimpses into the evolution of the adaptive immune system. *Immunity* **15,** 351-362.

Früh, K. and Yang, Y. (1999) Antigen presentation by MHC class I and its regulation by interferon gamma. *Curr. Opin. Immunol.* **11,** 76-81.

Garboczi, D. N., Ghosh, P., Utz, U., Fan, Q. R., Biddison, W. E. and Wiley, D. C. (1996) Structure of the complex between human T-cell receptor, viral peptide and HLA-A2. *Nature* **384**, 134-141.

Garcia, K. C., Degano, M., Stanfield, R. L., Brunmark, A., Jackson, M. R., Peterson, P. A., Teyton, L. and Wilson, I. A. (1996) An alphabeta T cell receptor structure at 2.5 Å and its orientation in the TCR-MHC complex. *Science* **274**, 209-219.

Geier, E., Pfeifer, G., Wilm, M., Lucchiari-Hartz, M., Baumeister, W., Eichmann, K. and Niedermann, G. (1999) A giant protease with potential to substitute for some functions of the proteasome. *Science* **283,** 978-981.

Glas, R., Bogyo, M., McAster, J. S., Gaczynska, M. and Ploegh, H. L. (1998) A proteolytic system that compensates for loss of proteasome function. *Nature* **392,** 618-622.

Glynne, R., Powis, S. H., Beck, S., Kelly, A., Kerr, L. A. and Trowsdale, J. A. (1991) A proteasome-related gene between the two ABC transporter loci in the class II region of the human MHC. *Nature* **353,** 357-360.

Goldberg, A. L. and St. John, A. C. (1976) Intracellular protein degradation in mammalian and bacterial cells: part 2. *Annu. Rev. Biochem.* **45,** 747-803.

Gorbulev, S., Abele, R. and Tampé, R. (2001) Allosteric crosstalk between peptide-binding, transport, and ATP hydrolysis of the ABC transporter TAP. *Proc. Natl. Acad. Sci. U. S. A.* **98,** 3732-3737.

Gromme, M., van der Valk, R., Sliedregt, K., Vernie, L., Liskamp, R., Hämmerling, G., Koopmann, J. O., Momburg, F. and Neefjes, J. (1997) The rational design of TAP inhibitors using peptide substrate modifications and peptidomimetics. *Eur. J. Immunol.* **28,** 898-904.

Guan, L. and Kaback, H. R. (2006) Lessons from lactose permease. *Annu. Rev. Biophys. Biomol. Struct.* **35,** 67-91.

Guex, N. and Peitsch, M. C. (1997) SWISS-MODEL and the Swiss-PdbViewer: an environment for comparative protein modeling. *Electrophoresis* **18,** 2714-2723.

He, L., Aleksandrov, A. A., Serohijos, A. W. R., Hegedus, Aleksandrov, L. A., Cui, L., Dokholyan, N. V. and Riordan, J. R. (2008) Multiple membrane-cytoplasmic domain contacts in the Cystic Fibrosis Transmembrane Conductance Regulator (CFTR) mediate regulation of channel gating. *J. Biol. Chem.* **283,** 26383-26390.

Heintke, S., Chen, M., Ritz, U., Lankat-Buttgereit, B., Koch, J., Abele, R., Seliger, B. and Tampé, R. (2003) Functional cysteine-less subunits of the transporter associated with antigen processing (TAP1 and TAP2) by de novo gene assembly. *FEBS Lett.* **533,** 42-46.

Herget, M., Oancea, G., Schrodt, S., Karas, M., Tampé, R. and Abele, R. (2007) Mechanism of substrate sensing and signal transmission within an ABC transporter: use of a Trojan horse strategy. *J. Biol. Chem.* **282,** 3871-3880.

Higgins, C. F. (1992) ABC transporters: from microorganisms to man. *Annu. Rev. Cell. Bio.* **8**, 67-113.

Higgins, C. F. and Linton, K. J. (2004) The ATP switch model for ABC transporters. *Nat. Struct. Mol. Biol.* **11,** 918-926.

Hilton, C. J., Dahl, A. M. and Rock, K. L. (2001) Anti-peptide antibody blocks peptide binding to MHC class I molecules in the endoplasmic reticulum. *J. Immunol.* **166,** 3952-3956.

Hirano, T. (2006) At the heart of the chromosome: SMC proteins in action. *Nat. Rev. Mol. Cell. Biol.* **7,** 311-322.

Holland, I. B., Cole, S. P. C., Kuchler, K. and Higgins, C. F. (2003) ABC proteins: From Bacteria to Man. London, Academic Press.

Hollenstein, K., Frei, D. C. and Locher, K. P. (2007) Structure of an ABC transporter in complex with its binding protein. *Nature* **446,** 213-216.

Hoof, T., Demmer, A., Hadam, M. R., Riordan, J. R. and Tummler, B. (1994) Cystic fibrosis-type mutational analysis in the ATP-binding cassette transporter signature of human P-glycoprotein MDR1. *J. Biol. Chem.* **269,** 20575-20583.

Hopfner, K. P., Karcher, A., Shin, D. S., Craig, L., Arthur, L. M., Carney, J. P. and Tainer, J. A. (2000) Structural biology of Rad50 ATPase: ATP-driven conformational control in DNA double-strand break repair and the ABC-ATPase superfamily. *Cell* **101,** 789-800.

Horn, C., Bremer, E. and Schmitt, L. (2003) Nucleotide dependent monomer/dimer equilibrium of OpuAA, the nucleotide-binding protein of the osmotically regulated ABC transporter OpuA from *Bacillus subtilis. J. Mol. Biol.* **334,** 403-419.

Hung, L. W., Wang, I. X., Nikaido, K., Liu, P. Q., Ames G. F. and Kim, S. H. (1998) Crystal structure of the ATP-binding subunit of an ABC transporter. *Nature* **396**, 703-707.

Hunke, S., Mourez, M., Jehanno, M., Dassa, E. and Schneider, E. (2000) ATP modulates subunit-subunit interactions in an ATP-binding cassette transporter (MalF-GK2) determined by site-directed chemical cross-linking. *J. Biol. Chem.* **275,** 15526-15534.

Hunter, W. M. and Greenwood, F. C. (1964) A radio-immunoelectrophoretic assay for human growth hormone. *Biochem. J.* **91,** 43-56.

Inagaki, N., Gonoi, T., Clement, J. P., Namba, N., Inazawa, J., Gonzalez, G., Aguilar-Bryan, L., Seino, S. and Bryan, J. (1995) Reconstitution of IKATP: an inward rectifier subunit plus the sulfonylurea receptor. *Science* **270**, 1166-1170.

Jacquemin, E. (2000) Progressive familial intrahepatic cholestasis. Genetic basis and treatment. *Clin. Liver Dis.* **4,** 753-763.

Janas, E., Hofacker, M., Chen, M., Gompf, S., van der Does, C. and Tampé, R. (2003) The ATP hydrolysis cycle of the nucleotide-binding domain of the mitochondrial ATP-binding cassette transporter Mdl1p. *J. Biol. Chem.* **278,** 26862-26869.

Jardetzky, O. (1966) Simple allosteric model for membrane pumps. *Nature,* **211,** 969-970.

Jones, P. M. and George, A. M. (2004) The ABC transporter structure and mechanism: perspectives on recent research. *Cell. Mol. Life Sci.* **61,** 682-699.

Jonker, J. W., Smit, J. W., Brinkhuis, R. F., Maliepaard, M., Beijnen, J. H., Schellens, J. H. and Schinkel, A. H. (2000) Role of breast cancer resistance protein in the bioavailability and fetal penetration of topotecan. *J. Natl. Cancer Inst.* **92,** 1651-1656.

Johnsen, A. K., Templeton, D. J., Sy, M. and Harding, C. V. (1999) Deficiency of transporter for antigen presentation (TAP) in tumor cells allows evasion of immune surveillance and increases tumorigenesis. *J. Immunol.* **163,** 4224-4231.

Kadaba, N. S., Kaiser, J. T., Johnson, E., Lee, A. and Rees, D. C. (2008) The high-affinity E. coli methionine ABC transporter: structure and allosteric regulation. *Science* **321,** 250-253.

Karpowich, N., Martsinkevich, O., Millen, L., Yuan, Y. R., Dai, P. L., MacVey, K., Thomas, P. J. and Hunt, J. F. (2001) Crystal structures of the MJ1267 ATP binding cassette reveal an induced-fit effect at the ATPase active site of an ABC transporter. *Structure* **9**, 571-586.

Karttunen, J. T., Lehner, P. J., Gupta, S. S., Hewitt, E. W. and Cresswell, P. (2001) Distinct functions and cooperative interaction of the subunits of the transporter associated with antigen processing (TAP). *Proc. Natl. Acad. Sci. U. S. A.* **98,** 7431-7436.

Kelly, A. P., Powis, S. H., Kerr, L.-A., Mockridge, I., Elliot, T., Bastin, J., Uchanska-Ziegler, B., Ziegler, A., Trowsdale, J. and Townsend, A. (1992) Assembly and function of the two ABC transporter proteins encoded in the human major histocompatibility complex. *Nature* **355,** 641-644.

Kisselev, A. F., Akopian, T. N., Woo, K. M. and Goldberg, A. L. (1999) The sizes of peptides generated from protein by mammalian 26 and 20 S proteasomes. Implications for understanding the degradative mechanism and antigen presentation. *J. Biol. Chem.* **274,** 3363-3371.

Kleijmeer, M., Kelly, A., Geuze, H. J., Slot, J. W., Townsend, A. and Trowsdale, J. (1992) Location of MHC-encoded transporters in the endoplasmic reticulum and *cis*-Golgi. *Nature* **357,** 342-344.

Koch, J., Guntrum, R., Heintke, S., Kyritsis, C. and Tampé, R. (2004) Functional dissection of the transmembrane domains of the transporter associated with antigen processing (TAP). *J. Biol. Chem.* **279,** 10142-10147.

Koch, J., Guntrum, R. and Tampé, R. (2005) Exploring the minimal functional unit of the transporter associated with antigen processing. *FEBS Lett.* **579,** 4413-4416.

Kozak, L., Gopal, G., Yoon, J. H., Sauna, S. E., Ambudkar, S. V., Thakurta, A. G. and Dhar, R. (2002) Elf1p, a member of the ABC class of ATPases, functions as a mRNA export factor in *Schizosacchromyces pombe*. *J. Biol. Chem.* **277,** 33580-33589.

Laemmli, U. K. (1970) Cleavage of structural proteins during the assembly of the head of bacteriophage T4. *Nature* **227**, 680-685.

Lankat-Buttgereit, B. and Tampé, R. (1999) The transporter associated with antigen processing TAP: structure and function. *FEBS Lett.* **464,** 108-112.

Lankat-Buttgereit, B. and Tampé, R. (2002) The transporter associated with antigen processing: function and implications in human diseases. *Physiol. Rev.* **82,** 187-204.

Lankat-Buttgereit, B. and Tampé, R. (2003) The transporter associated with antigen processing (TAP): a peptide transport and loading complex essential for cellular immune response. In *ABC proteins: From Bacteria to Man. London, Academic Press,* 533-550.

Lapinski, P. E., Neubig, R. R. and Raghavan, M. (2001) Walker A lysine mutations of TAP1 and TAP2 interfere with peptide translocation but not peptide binding. *J. Biol. Chem.* **276,** 7526-7533.

Lemieux, M. J., Huang, Y. and Wang, D. N. (2004) Glycerol-3-phosphate transporter of *Escherichia coli*: structure, function and regulation. *Res. Microbiol.* **155**, 623-629.

Lewis, H. A., Buchanan, S. G., Burley, S. K., Conners, K., Dickey, M., Dorwart, M., Fowler, R., Gao, X., Guggino, W. B., Hendrickson, W. A., Hunt, J. F., Kearins, MC., Lorimer, D., Maloney, P. C., Post, K. W., Rajashankar, K. R., Rutter, M. E., Sauder, J. M., Shriver, S., Thibodeau, P. H., Thomas, P. J., Zhang, M., Zhao, X. and Emtage, S. (2004) Structure of nucleotide-binding domain 1 of the cystic fibrosis transmembrane conductance regulator. *EMBO J.* **23,** 282-293.

Linton, K. J. (2007) Structure and function of ABC transporters. *Physiology* **22,** 122-130.

Liu, Y. and Eisenberg, D. (2002) 3D domain swapping: as domains continue to swap. *Protein Sci.* **11,** 1285-1299.

Locher, K. P., Lee, A. T. and Rees, D. C. (2002) The *E. coli* BtuCD structure: a framework for ABC transporter architecture and mechanism. *Science* **296,** 1091-1098.

Loo, T. W., Bartlett, M. C. and Clarke, D. M. (2007) Nucleotide binding, ATP hydrolysis, and mutation of the catalytic carboxylates of human P-glycoprotein cause distinct conformational changes in the transmembrane segments. *Biochemistry* **46,** 9328-9336.

Löwe, J., Stock, D., Jap, B., Zwickl, P., Baumeister, W. and Huber, R. (1995) Crystal structure of the 20S proteasome from the archaeon *T. acidophilum* at 34 Å resolution. *Science* **268,** 533-539.

Lunardi, J., Dupuis, A., Garin, J., Issartel, J. P., Michel, L., Chabre, M. and Vignais, P. V. (1988) Inhibition of H^+-transporting ATPase by formation of a tight nucleoside diphosphate-fluoroaluminate complex at the catalytic site. *Proc. Natl. Acad. Sci. U. S. A.* **85,** 8958-8962.

Manavalan, P., Dearborn, D. G., McPherson, J. M. and Smith, A. E. (1995) Sequence homologies between nucleotide binding regions of CFTR and G-proteins suggest structural and functional similarities. *FEBS Lett.* **366,** 87-91.

Martinez, C. K. and Monaco, J. J. (1991) Homology of proteasome subunits to a major histocompatibility complex-linked LMP gene. *Nature* **353,** 664-667.

Martinez-Mir, A., Paloma, E., Allikmets, R., Ayuso, C., del Rio, T., Dean, M., Vilageliu, L., Gonzalez-Duarte, R. and Balcells, S. (1998) Retinitis pigmentosa caused by a homozygous mutation in the Stargardt disease gene ABCR. *Nat. Genet.* **18,** 11-12.

Meyer, T. H., van Endert, P. M., Uebel, S., Ehring, B. and Tampé, R. (1994) Functional expression and purification of the ABC transporter complex associated with antigen processing (TAP) in insect cells. *FEBS Lett.* **351,** 443-447.

Moody, J. E., Millen, L., Binns, D., Hunt, J. F. and Thomas, P. J. (2002) Cooperative, ATP-dependent association of the nucleotide binding cassettes during the catalytic cycle of ATP-binding cassette transporters. *J. Biol. Chem.* **277,** 21111-21114.

Moore, M. W., Carbone, F. R. and Bevan, M. J. (1988) Introduction of soluble protein into class I pathway of antigen processing and presentation. *Cell* **54,** 777-785.

Mourez, M., Hofnung, M. and Dassa, E. (1997) Subunit interactions in ABC transporters: a conserved sequence in hydrophobic membrane proteins of periplasmic permeases defines an important site of interaction with the ATPase subunits. *EMBO J.* **16,** 3066-3077.

Müller, K. M., Ebensperger, C. and Tampé, R. (1994) Nucleotide binding to the hydrophilic C-terminal domain of the transporter associated with antigen processing (TAP). *J. Biol. Chem.* **269,** 14032-14037.

Neefjes, J. J., Momburg, F. and Hämmerling, G. J. (1993) Selective and ATP-dependent translocation of peptides by the MHC-encoded transporter. *Science* **261,** 769-771.

Neumann, L. and Tampé, R. (1999) Kinetic analysis of peptide binding to the TAP transport complex: evidence for structural rearrangements induced by substrate binding. *J. Mol. Biol.* **294**, 1203-1213.

Neumann, L., Abele, R. and Tampé, R. (2002) Thermodynamics of peptide binding to the transporter associated with antigen processing (TAP). *J. Mol. Biol.* **324**, 965-973.

Nijenhuis, M. and Hämmerling, G. J. (1996) Multiple regions of the transporter associated with antigen processing (TAP) contribute to its peptide binding site. *J. Immunol.* **157,** 5467-5477.

Nijenhuis, M., Schmitt, S., Armandola, E. A., Obst, R., Brunner, J. and Hämmerling, G. J. (1996) Identification of a contact region for peptide on the TAP1 chain of the transporter associated with antigen processing. *J. Immunol.* **156,** 2186-2195.

Obmolova, G., Ban, C., Hsieh, P. and Yang, W. (2000) Crystal structures of mismatch repair protein MutS and its complex with a substrate DNA. *Nature* **407,** 703-710.

Oldham, M. L., Khare, D., Quiocho, F. A., Davidson, A. L. and Chen, J. (2007) Crystal structure of a catalytic intermediate of the maltose transporter. *Nature* **450,** 515-521.

O'Mara, M. L. and Tieleman, D. P. (2007) P-glycoprotein models of the apo and ATP-bound states based on homology with Sav1866 and MalK. *FEBS Lett.* **581,** 4217-4222.

Ortmann, B., Copeman, J., Lehner, P. J., Sadasivan, B., Herberg, J. A., Grandea, A. G., Riddell, S. R., Tampé, R., Spies, T., Trowsdale, J. and Cresswell, P. (1997) A critical role for tapasin in the assembly and function of multimeric MHC class I-TAP complexes. *Science* **277,** 1306-1309.

Pagant, S., Brovman, E. Y., Halliday, J. J. and Miller, E. A. (2008) Mapping of interdomain interfaces required for the functional architecture of Yor1p, a eukaryotic ATP-binding cassette (ABC) transporter. *J. Biol. Chem.* **283,** 26444-26451.

Peters, J. M. (1994) Proteasomes. Protein degradation machines of the cell. *Trends Biochem. Sci.* **19,** 377-382.

Pinkett, H. W., Lee, A. T., Lum, P., Locher, K. P. and Rees, D. C. (2007) An inward-facing conformation of a putative metal-chelate-type ABC transporter. *Science* **315,** 373-377.

Powis, S. J., Townsend, A. R., Deverson, E. V., Bastin, J., Butcher, G. W. and Howard, J. C. (1991) Restoration of antigen presentation to the mutant cell line RMA-S by an MHC-linked transporter. *Nature* **354**, 528-531.

Qu, Q., Chu, J. W. and Sharom, F. J. (2003) Transition state P-glycoprotein binds drugs and modulators with unchanged affinity, suggesting a concerted transport mechanism. *Biochemistry* **42,** 1345-1353.

Ramachandra, M., Ambudkar, S. V., Chen, D., Hrycyna, C. A., Dey, S., Gottesman, M. M. and Pastan, I. (1998) Human P-glycoprotein exhibits reduced affinity for substrates during a catalytic transition state. *Biochemistry* **37**, 5010-5019.

Rechsteiner, M., Hoffman, L. and Dubiel, W. (1993) The multicatalytic and 26S proteases. *J. Biol. Chem.* **268,** 6065-6068.

Reits, E. A., Vos, J. C., Gromme, M. and Neefjes, J. (2000) The major substrates for TAP in vivo are derived from newly synthesized proteins. *Nature* **404,** 774-778.

Reits, E., Neijssen, J., Herberts, C., Benckhuijsen, W., Janssen, L., Drijfhout, J. W. and Neefjes, J. (2004) A major role for TPPII in trimming proteasomal degradation products for MHC class I antigen presentation. *Immunity* **20,** 495-506.

Reyes, C. L., Ward, A., Yu, J. and Chang, G. (2006) The structures of MsbA: Insight into ABC transporter-mediated multidrug efflux. *FEBS Lett.* **580,** 1042-1048.

Ritz, U., Momburg, F., Pircher, H. P., Strand, D., Huber, C. and Seliger, B. (2001) Identification of sequences in the human peptide transporter subunit TAP1 required for transporter associated with antigen processing (TAP) function. *Int. Immunol.* **13,** 31-41.

Rock, K. L., Gramm, C., Rothstein, L., Clark, K., Stein, R., Dick, L., Hwang, D. and Goldberg, A. L. (1994) Inhibitors of the proteasome block the degradation of most cell proteins and the generation of peptides presented on MHC class I molecules. *Cell* **78,** 761-771.

Rock, K. L. and Goldberg, A. L. (1999) Degradation of cell proteins and the generation of MHC class I-presented peptides. *Annu. Rev. Immunol.* **17,** 739-779.

Rosenberg, M. F., Kamis, A. B., Callaghan, R., Higgins, C. F. and Ford, R. C. (2003) Three-dimensional structures of the mammalian multidrug resistance P-glycoprotein demonstrate major conformational changes in the transmembrane domains upon nucleotide binding. *J. Biol. Chem.* **278,** 8294-8299.

Rost, B., Yachdav, G., and Liu J. (2004) The PredictProtein server. *Nucleic Acids Res.* **32,** W321-W326.

Rothnie, A., Storm, J., Campbell, J., Linton, K. J., Kerr, I. D. and Callaghan, R. (2004) The topography of transmembrane six is altered during the catalytic cycle of P-glycoprotein. *J. Biol. Chem.* **279,** 34913-34921.

Russell, P. L. and Sharom, F. J. (2006) Conformational and functional characterization of trapped complexes of the P-glycoprotein multidrug transporter. *Biochem. J.* **399,** 315-323.

Sali, A. and Blundell T. L. (1993) Comparative protein modeling by satisfaction of spatial restraints. *J. Mol. Biol.* **234,** 779-815.

Sambrook, J. and Russell, D. W. (2001) Molecular cloning, 3rd edition, Cold Spring Harbor Laboratory Press, Cold Spring Harbor, NY, USA.

Sankaran, B., Bhagat, S. and Senior, A. E. (1997) Inhibition of P-glycoprotein ATPase activity by procedures involving trapping of nucleotide in catalytic sites. *Arch. Biochem. Biophys.* **341,** 160-169.

Saric, T., Chang, S. C., Hattori, A., York, I. A., Markant, S., Rock, K. L., Tsujimoto, M. and Goldberg, A. L. (2002) An IFN-gamma-induced aminopeptidase in the ER, ERAP1, trims precursors to MHC class I-presented peptides. *Nat. Immunol.* **3,** 1169-1176.

Sarkadi, B., Homolya, L., Szakacs, G. and Varadi, A. (2006) Human multidrug resistance ABCB and ABCG transporters: participation in a chemoimmunity defense system. *Physiol. Rev.* **86,** 1179-1236.

Saveanu, L., Daniel, S. and van Endert, P. M. (2001) Distinct functions of the ATP binding cassettes of transporters associated with antigen processing: a mutational analysis of Walker A and B sequences. *J. Biol. Chem.* **276,** 22107-22113.

Saveanu, L., Carroll, O., Lindo, V., Del Val, M., Lopez, D., Lepelletier, Y., Greer, F., Schomburg, L., Fruci, D., Niedermann, G. and van Endert, P. M. (2005) Concerted peptide trimming by human ERAP1 and ERAP2 aminopeptidase complexes in the endoplasmic reticulum. *Nat. Immunol.* **6,** 689-697.

Schinkel, A. H., Mol, C. A., Wagenaar, E., van Deemter, L., Smit, J. J. and Borst, P. (1995) Multidrug resistance and the role of P-glycoprotein knockout mice. *Eur. J. Cancer* **31A,** 1295-1298.

Schmitt, L. and Tampé, R. (2002) Structure and mechanism of ABC transporters. *Curr. Opin. Struct. Biol.* **12,** 754-760.

Schmitt, L., Benabdelhak, H., Blight, M. A., Holland, I. B. and Stubbs, M. T. (2003) Crystal structure of the nucleotide-binding domain of the ABC transporter haemolysin B: identification of a variable region within ABC helical domains. *J. Mol. Biol.* **330**, 333-342.

Schneider, E. and Hunke, S. (1998) ATP-binding-cassette (ABC) transport systems: functional and structural aspects of the ATP-hydrolyzing subunits/domains. *FEMS Microbiol. Rev.* **22,** 1-20.

Schölz, C., and Tampé, R. (2005) The intracellular antigen transport machinery TAP in adaptive immunity and virus escape mechanisms. *J. Bioenerg. Biomembr.* **37,** 509-515.

Schrodt, S., Koch, J. and Tampé, R. (2006) Membrane topology of the transporter associated with antigen processing (TAP1) within an assembled functional peptide-loading complex. *J. Biol. Chem.* **281,** 6455-6462.

Schubert, U., Antón, L. C., Gibbs, J., Norbury, C. C., Yewdell, J. W., Turner, G. C. and Varshavski, A. (2000) Detecting and measuring cotranslational protein degradation in vivo. *Science* **289,** 2117-2120.

Seemüller, E., Lupas, A., Stock, D., Löwe, J. Huber, R. and Baumeister W. (1995) Proteasome from *Thermoplasma acidophilum*: a threonine protease. *Science* **268,** 579-582.

Self, W. T., Grunden, A. M., Hasona, A. and Schanmugam, K. T. (2001) Molybdate transport. *Res. Microbiol.* **152,** 311-321.

Seliger, B., Maeurer, M. J. and Ferrone, S. (2000) Antigen-processing machinery breakdown and tumor growth. *Immunol. Today* **21,** 455-464.

Seliger, B., Ritz, U., Abele, R., Bock, M., Tampé, R., Sutter, G., Drexler, I., Huber, C. and Ferrone, S. (2001) Immune escape of melanoma: first evidence of structural alterations in two distinct components of the MHC class I antigen processing pathway. *Cancer Res.* **61,** 8647-8650.

Serohijos, A. W., Hegedus, T., Aleksandrov, A. A., He, L., Cui, L., Dokholyan, N. V. and Riordan, J. R. (2008) Phenylalanine-508 mediates a cytoplasmic membrane domain contact in the CFTR 3D structure crucial to assembly and channel function. *Proc. Natl. Acad. Sci. U. S. A.* **105,** 3256-3261.

Serwold, T., Gonzalez, F., Kim, J., Jacob, R. and Shastri, N. (2002) ERAAP customizes peptides for MHC class I molecules in the endoplasmic reticulum. *Nature* **419,** 480-483.

Smith, C. A. and Rayment, I. (1996) X-ray structure of the Magnesium(II)·ADP·Vanadate complex of the *Dictyostelium discoideum* myosin motor domain to 1.9 Å resolution. *Biochemistry* **35,** 5404-5417.

Smith, P. C., Karpowich, N., Millen, L., Moody, J. E., Rosen, J., Thomas, P. J. and Hunt, J. F. (2002) ATP binding to the motor domain from an ABC transporter drives formation of a nucleotide sandwich dimer. *Mol. Cell* **10,** 139-149.

Spies, T., Cerundolo, V., Colonna, M., Cresswell, P., Townsend, A. and DeMars, R. (1992) Presentation of viral antigen by MHC class I molecules is dependent on a putative peptide transporter heterodimer. *Nature* **355**, 644-646.

Spies, T. and DeMars, R. (1991) Restored expression of major histocompatibility class I molecules by gene transfer of a putative peptide transporter. *Nature* **351**, 323-324.

Stoltze, L., Schirle, M., Schwarz, G., Schröter, C., Thompson, M. W., Hersh, L. B., Kalbacher, H., Stevanovic, S., Rammensee, H. G. and Schild, H. (2000) Two new proteases in the MHC class I processing pathway. *Nat. Immunol.* **1,** 413-418.

Storm, J., Modok, S., O'Mara, M. L., Tieleman, D. P., Kerr, I. D. and Callaghan, R. (2008) Cytosolic region of TM6 in P-glycoprotein: topographical analysis and functional perturbation by site directed labeling. *Biochemistry* **47,** 3615-3624.

Tabcharani, J. A., Chang, X. B., Riordan, J. R. and Hanrahan, J. W. (1991) Phosphorylation-regulated Cl⁻ channel in CHO cells stably expressing the cystic fibrosis gene. *Nature* **352**, 628-631.

Tampé, R., Urlinger, S., Pawlitschko, K. and Uebel, S. (1997) in *Unusual Secretory Pathways: From Bacteria to Man* (Kuchler, K., Rubartelli, A. and Holland, B., eds) pp.115-136, Springer, New York.

Thompson, J. D., Higgins, D. G. and Gibson, T. J. (1994) CLUSTAL W: improving the sensitivity of progressive multiple sequence alignment through sequence weighting, position-specific gap penalties and weight matrix choice. *Nucleic Acids Res.* **22,** 4673-4680.

Tomazin, R., Hill, A. B., Jugovic, P., York, I., van Endert, P., Ploegh, H. L., Andrews, A. B. and Johnson, D. C. (1996). Stable binding of the herpes simplex virus ICP47 protein to the peptide binding site of TAP. *EMBO J.* **15**, 3256-3266.

Townsend, A. R., Bastin, J., Gould, K. and Brownlee, G. G. (1986) Cytotoxic T-lymphocytes recognize influenza haemagglutinin that lacks a signal sequence. *Nature* **324,** 575-577.

Trowsdale, J., Hanson, I., Mockridge, I., Beck, S., Townsend, A. and Kelly, A. (1990) Sequences encoded in the class II region of the MHC related to the 'ABC' superfamily of transporters. *Nature* **348,** 741-744.

Trowsdale, J., Ragoussis, J. and Campbell, R. D. (1991) Map of the human MHC. *Immunol. Today* **12**, 443-446.

Turner, G. C. and Varshavski, A. (2000) Detecting and measuring cotranslational protein degradation in vivo. *Science* **289,** 2117-2120.

Uebel, S., Meyer, T. H., Kraas, W., Kienle, S., Jung, G., Wiesmüller, K. H. and Tampé, R. (1995) Requirements for peptide binding to the human transporter associated with antigen processing revealed by peptide scans and complex peptide libraries. *J. Biol. Chem.* **270,** 18512-18516.

Uebel, S., Kraas, W., Kienle, S., Wiesmüller, K. H., Jung, G. and Tampé, R. (1997) Recognition principle of the TAP transporter dissclosed by combinatorial peptide libraries. *Proc. Natl. Acad. Sci. U. S. A.* **94,** 8976-8981.

Uebel, S. and Tampé, R. (1999) Specificity of the proteasome and the TAP transporter. *Curr. Opin. Immunol.* **11,** 203-208.

Urlinger, S., Kuchler, K., Meyer, T. H., Uebel, S. and Tampé, R. (1997) Intracellular location, complex formation, and function of the transporter associated with antigen processing in yeast. *Eur. J. Biochem.* **245,** 266-272.

van der Does, C. and Tampé, R. (2004). How do ABC transporters drive transport? *Biol. Chem.* **385,** 927-933.

van Endert, P. M., Tampé, R., Meyer, T. H., Tisch, R., Bach, J. F. and McDevitt, H. O. (1994). A sequential model for peptide binding and transport by the transporter associated with antigen processing. *Immunity* **1**, 491-500.

van Endert, P. M., Saveanu, L., Hewitt, E. W. and Lehner, P. (2002) Powering the peptide pump: TAP crosstalk with energetic nucleotides. *Trends Biochem. Sci.* **27,** 454-461.

van Veen, H. W., Margolles, A., Muller, M., Higgins, C. F. and Konings, W. N. (2000) The homodimeric ATP-binding cassette transporter LmrA mediates multidrug transport by an alternating two-site (two-cylinder engine) mechanism. *EMBO J.* **19,** 2503-2514.

Walker, J. E., Saraste, M., Runswick, M. J. and Gay, N. J. (1982) Distantly related sequences in the alpha- and beta-subunits of ATP synthase, myosin, kinases and other ATP-requiring enzymes and a common nucleotide binding fold. *EMBO J.* **1**, 945-951.

Wang, K. N., Früh, K., Peterson, P. A. and Yang, Y. (1994) nucleotide binding of the C-terminal domains of the major histocompatibility complex-encoded transporter expressed in *Drosophila melanogaster* cells. *FEBS Lett.* **350,** 337-341.

Ward, A., Reyes, C. L., Yu, J., Roth, C. B. and Chang, G. (2007) Flexibility in the ABC transporter MsbA: Alternating access with a twist. *Proc. Natl. Acad. Sci. U. S. A.* **104,** 19005-19010.

Wu, J. and Kaback, H. R., (1996) A general method for determining helix packing in membrane proteins in situ: helices I and II are close to helix VII in the lactose permease of *Escherichia coli. Proc. Natl. Acad. Sci. U. S. A.* **93,** 14498-14402.

Zaitseva, J., Jenewein, S., Jumpertz, T., Holland, I. B. and Schmitt, L. (2005) H662 is the linchpin of ATP hydrolysis in the nucleotide-binding domain of the ABC transporter HlyB. *EMBO J.* **24**, 1901-1910.

Zaitseva, J., Oswald, C., Jumpertz, T., Jenewein, S., Wiedenmann, A., Holland, I. B. and Schmitt, L. (2006) A structural analysis of asymmetry required for catalytic activity of an ABC-ATPase domain dimer. *EMBO J.* **25,** 3432-3443.

Zhou, S., Schuetz, J. D., Bunting, K. D., Colapietro, A. M., Sampath, J., Morris, J. J., Lagutina, I., Grosveld, G. C., Osawa, M., Nakauchi, H. and Sorrentino, B. P. (2001) The ABC transporter Bcrp1/ABCG2 is expressed in a wide variety of stem cells and is a molecular determinant of the side-population phenotype. *Nat. Med.* **7,** 1028-1034.

Zolnerciks, J. K., Wooding, C. and Linton, K. J. (2007) Evidence for a Sav1866-like architecture for the human multidrug transporter P-glycoprotein. *FASEB J.* **21,** 3937-3948.

Yang, T., McNally, B. A., Ferrone, S., Liu, Y. and Zheng, P. (2003) A single-nucleotide deletion leads to rapid degradation of TAP1-mRNA in a melanoma cell line. *J. Biol. Chem.* **278,** 15291-15296.

Yewdell, J. W., Benninck, J. R. and Osaka, Y. H. (1988) Cells process exogenous proteins for recognition by cytotoxic T-lymphocytes. *Science* **239,** 637-640.

York, I. A., Goldberg, A. L., Mo, X. Y., and Rock, K. L. (1999) Proteolysis and class I major histocompatibility complex antigen presentation. *Immunol. Rev.* **172,** 49-66.

York, I. A., Chang, S. C., Saric, T., Keys, J. A., Favreau, J. M., Goldberg, A. L. and Rock, K. L. (2002) The ER aminopeptidase ERAP1 enhances or limits antigen presentation by trimming epitopes to 8-9 residues. *Nat. Immunol.* **3,** 1177-1184.

Abbreviations

Code	Identification
ABC	ATP binding cassette
ABCA	ABC transporter subfamily A
ABCB	ABC transporter subfamily B
ABCC	ABC transporter subfamily C
ABCD	ABC transporter subfamily D
ABCG	ABC transporter subfamily G
ABCR	ABC transporter subfamily R
ADP	Adenosine-5'-diphosphate
$AlCl_3$	Aluminium chloride
ALD	Adrenoleukodystrophy
AlF_x	Aluminium fluoride
AMP-PNP	5'-Adenylyl-β, γ-imidodiphosphate
APS	Ammonium peroxydisulfate
ATP	Adenosine-5'-triphosphate
ATPγS	Adenosine -5'-O-(thiotriphosphate)
BCA	Bicinchoninic acid assay
BCRP	Breast cancer resistance protein
BiP	Immunoglobulin binding protein
Bluo-gal	5-Bromo-3-indolyl-D-galactoside
BM	BODIPY maleimide
B_{max}	Maximal peptide-binding capacity
$BM(PEO)_3$	1,8-Bis-maleimidotriethylene glycol
BmrA	*Bacillus* multidrug resistance ATP
BSA	Bovine serum albumin
BSEP	Bile salt export pump
BtuCD	Vitamin B_{12} import system permease
$CaCl_2$	Calcium chloride
CD4/8	Cluster of differentiation
CFTR	Cystic fibrosis transmembrane conductance regulator
CHs	Coupling helices

CIAP	Calf intestine
CLs	Cytosolic loops
CM	Coumarin maleimide
ConA	Concanavalin A
Crio-EM	Cryo-electron microscopy
CTL	Cytotoxic T-lymphocyte
CuPhen	Copper phenanthroline
CuSO$_4$	Copper sulphate
Cys-less	Cysteine free
Da	Dalton
D-J syndrome	Dubin-Johnson syndrome
DMF	N,N-Dimethylformamide
DMSO	Dimethylsulfoxide
DNA	Desoxyribonucleic acid
dNTP	Dinucleotide 5'-triphosphate
DTT	1,4-Dithiothreitol
E. coli	*Escherichia coli*
ECL	Enhanced chemiluminescence
ECLs	Extracellular loops
EDTA	Ethylendiamine-tetraacetic acid
Elf1p	Elongation-like factor protein
ER	Endoplasmic reticulum
ERp57	Protein disulphide isomerase-associated 3
FC-14	Tetradecylphosphocholine
FCS	Fetal calf serum
h	Hours
HEPES	N-(2-Hydroxyethyl)-piperazine-N'-2-ethansulfonic acid
HI1470/71	Putative metal-chelate-type transporter ABC complex
His-tag	Histidine tag
HlyA/B	α-Hemolysin ATP permease
IAF	Iodoacetamidofluorescein
ICLs	Intracellular loops
IgG	Immunoglobulin G
INF-γ	Interferon γ

IP	Immunoprecipitation
IPTG	Isopropyl-β-D-thiogalactopyranoside
KCl	Potassium chloride
K_d	Dissociation constant
KH_2PO_4	Potassium dihydrogen phosphate
Km	Kanamycin
k_{on}	Labeling rate constant
L	Percent of fluorescence labeling
LB	Luria-Bertani medium
LCR	Ligase Chain Reaction
L_{max}	Maximum percent of fluorescence labeling
LMP	Low-molecular-mass polypeptides
mAb	Monoclonal antibody
$MalFGK_2$	Maltose transporter ABC complex
MDR	Multidrug resistance
MetNI	Methionine transporter ABC complex
$MgCl_2$	Magnesium chloride
$MgSO_4$	Magnesium sulfate
MHC	Major histocompatibility complex
min	Minutes
MJ0796	Methanococcus jannaschii ABC transporter
$MnCl_2$	Manganese chloride
ModBC-A	Molybdate/tungstate transporter ABC complex
MOI	Multiplicity of infection
MOPS	3-(N-morpholino)propanesulfonic acid
MRP	Multidrug resistance protein
MsbA	Lipid A flippase ABC transporter
MTS	Methanethiosulfonate
MTS-2-MTS	1,2-Ethanediyl-bis-methanethiosulfonate
MTS-5-MTS	1,5-Pentanediyl-bis-methanethiosulfonate
NaCl	Sodium chloride
NaF	Sodium fluoride
Na_2HPO_4	Disodium hydrogen phosphate
$Na^{125}I$	Sodium iodide

NaN$_3$	Sodium azide
NaOH	Sodium hydroxide
Na$_2$S$_2$O$_5$	Sodium disulfite
NBD	Nucleotide binding domain
NEM	N-Ethylmaleimide
NHS	N-Hydroxysuccinimide
Ni-NTA	Nickel-Nitrilotriacetic acid
NP-40	Igepal
OC	Obstetric cholestasis
PAGE	Polyacrylamide gelelectrophoresis
PBS	Phosphate-buffered saline
PCR	Polymerase chain reaction
PEI	Polyethylimine
PFIC3	Progressive familial intrahepatic cholestasis type 3
Pgp	P-glycoprotein
pH	*Potentia hydrogenii*
PHHI	Persistent hyperinsulinemic hypoglycaemia of infancy
Pi	Inorganic phosphate
Pi-Mix	Protease-inhibitor mix
PLC	Peptide loading complex
PMSF	Phenylmethanesulfonyl fluoride
POPE	1-Palmitoyl-2-oleoyl-phosphatidyl ethanolamine
PVDF	Polyvinylidene fluoride
Rad50	Recombination mediator associated with DNA repair
RbCl	Rubidium chloride
RMSD	Root-mean-square deviation
Sav1866	Homologue of multidrug ABC transporters
SDS	Sodium dodecyl sulphate
Sf9	*Spodoptera frugiperda*
SMC1-6	Structural-maintenance-of-chromosome proteins
SPDBV	Swiss-Protein Data Bank Viewer
SUR	Sulphonyl urea receptor
t	Time
TAE	Tris-acetate EDTA buffer

TAP	Transporter associated with antigen processing
TAPL	Transporter associated with antigen processing (TAP)-like
TBS-T	Tris-buffered saline – Triton X-100
TEMED	N,N,N',N'-Tetramethyl-ethylendiamine
TFB	Transformation buffer
TMD	Transmembrane domain
TMD0	TMHs of each unique N-domain
TMHs	Transmembrane helices
UV	Ultraviolet light
V_{max}	Maximal rate constant
v/v	volume per volume
V	Volt
XLSA	X-linked sideroblastic anemia with ataxia
W	Watt
WHATIF	Molecular modeling software
wt	Wild type
w/v	Weight per volume
Yor1p	Plasma membrane ABC transporter

Acknowledgements

My very special thanks go to my mentor (doctor father) Prof. Dr. Robert Tampé for the chance and the possibility to achieve this work at Institute of Biochemistry, for the supervision of the present Thesis and for precious ideas and suggestions.

I would like to thank particularly to Dr. Rupert Abele for helpful advices and discussions and for the critical review of this work, which helped me much in elaborating this Thesis.

I particularly wish to thank to Prof. Dr. Bernd Ludwig and Prof. Dr. Werner Kühlbrandt for helpful discussions and support of the present work. The precious ideas and suggestions of the PhD Thesis Committee during the International Max-Planck-Research School Program helped me significantly to develop my scientific career, allowing me to accomplish successfully the PhD Program.

I would like to thank to our collaborators Megan L. O'Mara, W. F. Drew Bennett and D. Peter Tieleman (Department of Biological Sciences, University of Calgary, Canada) who constructed the 3D homology model of the core TAP complex.

I would like to thank Eckhard Linker and Gudrun Illig for excellent technical assistance.

I thank to all colleagues of the Institute of Biochemistry for real support and understanding, especially to Min Chen, Meike Herget, Susanne Heintke, Chenguang Zhao and Christoph Baldauf.

I thank to International Max-Planck-Research School and Center for Membrane Proteomics for support.

I thank to my family for support and patience.

E R K L Ä R U N G

Ich erkläre hiermit, dass ich mich bisher keiner Doktorprüfung unterzogen habe.

Frankfurt am Main, den 04.12.2008

....

(Unterschrift)

Eidesstattliche Versicherung

Ich erkläre hiermit an Eides Statt, dass ich die vorgelegte Dissertation über

On the crosstalk between transmembrane and nucleotide binding domains of the ABC

transport complex TAP

selbständig angefertigt und mich anderer Hilfsmittel als der in ihr angegebenen nicht bedient habe, insbesondere, dass aus Schriften Entlehnungen, soweit sie in der Dissertation nicht ausdrücklich als solche mit Angabe der betreffenden Schrift bezeichnet sind, nicht stattgefunden haben.

Frankfurt am Main, den 04.12.2008   ....
                                                                (Unterschrift)

XXIII

Publications

- Herget M*, **Oancea G***, Schrodt S, Karas M, Tampé R, Abele R
  Mechanism of substrate sensing and signal transmission within an ABC transporter: use of a Trojan horse strategy.
  J Biol Chem. 2007 Feb 9;282(6):3871-3880.
  * Both authors contributed equally to this work.

- **Oancea G**, O'Mara M L, Bennett W F D, Tieleman D P, Abele R, Tampé R
  Structural arrangement of the transmission interface in the ABC transporter TAP critical for antigen binding and translocation.
  PNAS 2009 Mar 18 [Epub ahead of print].

Curriculum Vitae

Personal data

Name: Giani Oancea
Date of birth: 07.02.1975
Place of birth: Onesti
Nationality: Romanian
Marrital status: Married, one child (6)

Education

Since 02/04	PhD work at the Institute of Biochemistry, of the J.W. Goethe-University, Frankfurt am Main with the title: "On the crosstalk between transmembrane and nucleotide binding domains of the ABC transport complex TAP" Doctoral thesis supervisor: Prof. Dr. Robert Tampé
08/01 – 04/02	Martin Luther-University Halle/Saale, Institute of Microbiology Researcher Supervisor: Prof. Dr. Jan Remer Andreesen
06/00 – 05/01	Technical University Berlin, Institute of Biotechnology Trainee student Supervisor: Prof. Dr. Rainer Buchholz
10/98 – 02/00	Al. I. Cuza-University Iasi (Romania), Institute of Microbiology Master of Science – Biotechnology Supervisor: Prof. Dr. Octavita Ailiesei Degree: 9.80 (very good)
10/94 – 06/98	Al. I. Cuza-University Iasi, Faculty of Biology University Diploma in Biology (second major: Ecology and Environment Protection) Supervisor: Prof. Dr. Gheorghe Acatrinei Degree: 9.80 (very good)

Employment History

05/02 – 01/04	Robert Koch Institute Wernigerode, Department of Nosokomial Infections Biolog Supervisor: Prof. Dr. Wolfgang Witte
11/99 – 03/00	Antibiotics Industries, Biosynthesis Department, Iasi (Romania) Biolog Supervisor: Dr.-Ing. Vasile Capraru

Publications

Herget M*, **Oancea G***, Schrodt S, Karas M, Tampé R, Abele R

Mechanism of substrate sensing and signal transmission within an ABC transporter: use of a Trojan horse strategy.

J Biol Chem 2007 Feb 9;282(6):3871-3880.

* Both authors contributed equally to this work.

Oancea G, O'Mara M L, Bennett W F D, Tieleman D P, Abele R, Tampé R

Structural arrangement of the transmission interface in the ABC transporter TAP critical for antigen binding and translocation.

PNAS 2009 Mar 18 [Epub ahead of print].

Practical courses

21.06.04 – 12.06.04   2D crystallisation, electron cryo-microscopy and image processing
(Prof. Dr. Werner Kühlbrandt, Dr. Janet Vonck)

01.11.04 – 12.02.05   B-cell hybridoma technology and monoclonal antibodies production:
practical and theoretical approaches
(Prof. Dr. Jürgen Bereiter-Hahn, Dr. Mihail Moisenovich)

08.05.05 – 19.05.05   Site directed mutagenesis
(Prof. Dr. Bernd Ludwig, Dr. Oliver-Matthias Richter)